AD-A126 199 INVESTIGATION OF CREW RESTRAINT SYSTEM BIOMECHANICS(U) 1/2
DAYTON UNIV OH RESEARCH INST N S PHILLIPS ET AL.
MAY 82 AFAMRL-TR-81-103 F33615-79-C-0525

UNCLASSIFIED F/G 5/5 NL

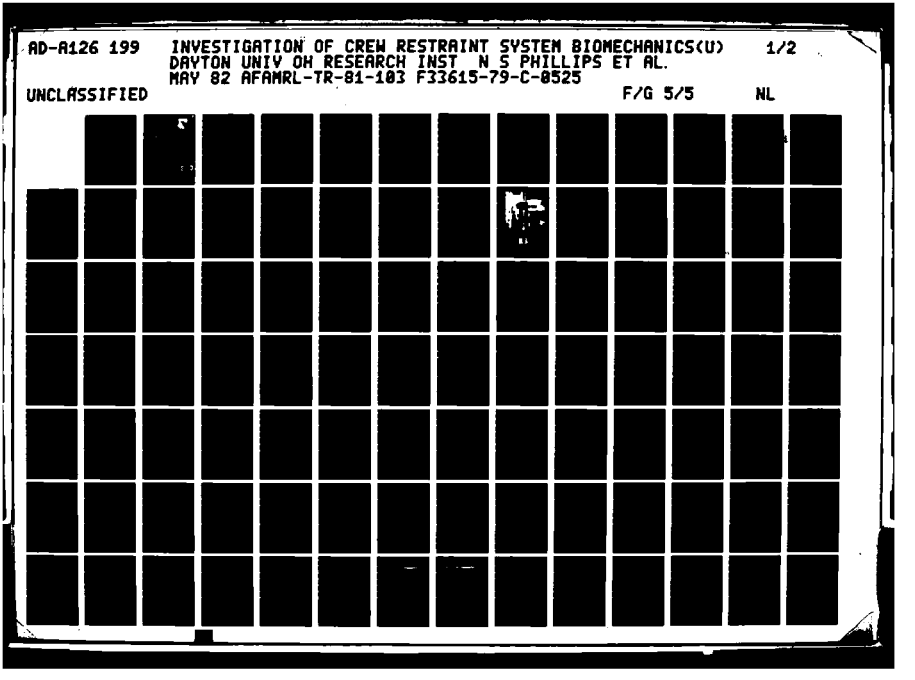

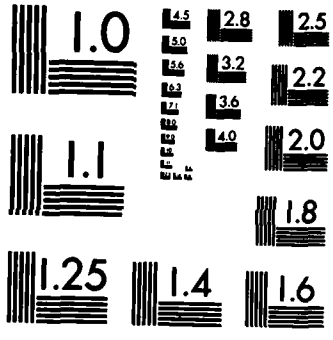

AFAMRL-TR-81-103

AD A126199

INVESTIGATION OF CREW RESTRAINT SYSTEM BIOMECHANICS

NORMAN S. PHILLIPS
ROBERT A. THOMSON
IRA B. FISCUS

UNIVERSITY OF DAYTON RESEARCH INSTITUTE
300 COLLEGE PARK AVENUE
DAYTON, OHIO 45469

DTIC FILE COPY

Approved for public release; distribution unlimited.

AIR FORCE AEROSPACE MEDICAL RESEARCH LABORATORY
AEROSPACE MEDICAL DIVISION
AIR FORCE SYSTEMS COMMAND
WRIGHT-PATTERSON AIR FORCE BASE, OHIO

NOTICES

When US Government drawings, specifications, or other data are used for any purpose other than a definitely related Government procurement operation, the Government thereby incurs no responsibility nor any obligation whatsoever, and the fact that the Government may have formulated, furnished, or in any way supplied the said drawings, specifications, or other data, is not to be regarded by implication or otherwise, as in any manner licensing the holder or any other person or corporation, or conveying any rights or permission to manufacture, use, or sell any patented invention that may in any way be related thereto.

Please do not request copies of this report from Air Force Aerospace Medical Research Laboratory. Additional copies may be purchased from:

National Technical Information Service
5285 Port Royal Road
Springfield, Virginia 22161

Federal Government agencies and their contractors registered with Defense Technical Information Center should direct requests for copies of this report to:

Defense Technical Information Center
Cameron Station
Alexandria, Virginia 22314

TECHNICAL REVIEW AND APPROVAL

AFAMRL-TR-81-103

The voluntary informed consent of the subjects used in this research was obtained as required by Air Force Regulation 169-3.

This report has been reviewed by the Office of Public Affairs (PA) and is releasable to the National Technical Information Service (NTIS). At NTIS, it will be available to the general public, including foreign nations.

This technical report has been reviewed and is approved for publication.

FOR THE COMMANDER

HENNING E. VON GIERKE, Dr Ing
Director
Biodynamics and Bioengineering Division
Air Force Aerospace Medical Research Laboratory

SECURITY CLASSIFICATION OF THIS PAGE *(When Data Entered)*

REPORT DOCUMENTATION PAGE

READ INSTRUCTIONS BEFORE COMPLETING FORM

1. REPORT NUMBER: AFAMRL-TR-81-103	2. GOVT ACCESSION NO.: AD-A126 199
3. RECIPIENT'S CATALOG NUMBER:	
4. TITLE *(and Subtitle)*: INVESTIGATION OF CREW RESTRAINT SYSTEM BIOMECHANICS	5. TYPE OF REPORT & PERIOD COVERED: May 1979-March 1981
	6. PERFORMING ORG. REPORT NUMBER:
7. AUTHOR(s): Norman S. Phillips, Robert A. Thomson, Ira B. Fiscus	8. CONTRACT OR GRANT NUMBER(s): F33615-79-C-0525
9. PERFORMING ORGANIZATION NAME AND ADDRESS: University of Dayton Research Institute, 300 College Park Avenue, Dayton, Ohio 45469	10. PROGRAM ELEMENT, PROJECT, TASK AREA & WORK UNIT NUMBERS: 62202F-7231-16-16
11. CONTROLLING OFFICE NAME AND ADDRESS: Air Force Aerospace Medical Research Lab, Aerospace Medical Division, AF Systems Command, Wright-Patterson AFB, OH 45433	12. REPORT DATE: May 1982
	13. NUMBER OF PAGES: 173
14. MONITORING AGENCY NAME & ADDRESS *(if different from Controlling Office)*:	15. SECURITY CLASS. *(of this report)*: Unclassified
	15a. DECLASSIFICATION/DOWNGRADING SCHEDULE:

16. DISTRIBUTION STATEMENT *(of this Report)*

Approved for public release; distribution unlimited.

17. DISTRIBUTION STATEMENT *(of the abstract entered in Block 20, if different from Report)*

18. SUPPLEMENTARY NOTES

Contact: James Brinkley
AFAMRL/BBP(255-3931)
WPAFB, OH 45433

19. KEY WORDS *(Continue on reverse side if necessary and identify by block number)*

Restraint
Inertia Reel
Escape System
Biomechanics
Impact Protection
Restraint Models

20. ABSTRACT *(Continue on reverse side if necessary and identify by block number)*

Experimental data were collected and analyses were performed to study the influence of the dynamic mechanical properties of restraint system components on human response to impact and restraint system haulback. Tests were accomplished to isolate the characteristics of the restraint system and the human body. Three restraint webbing materials were studied at varied strain rates. A pyrotechnically-powered inertia reel was tested, but could not be analytically modeled successfully. Analytical models of the human and restraint system were used to

DD FORM 1 JAN 73 1473 EDITION OF 1 NOV 65 IS OBSOLETE

SECURITY CLASSIFICATION OF THIS PAGE *(When Data Entered)*

Block 20. (continued)

study the influence of restraint material properties changes on human response parameters. An analytical model of a rhesus monkey was also used to study the efficacy of animal tests and scaling techniques to evaluate restraint systems for human use applications.

SUMMARY

Research was accomplished to provide experimental data and analytical methods that could be used in the development of future aircraft restraint systems. Data were collected and analyzed to isolate characteristics of the restraint system and human. Once this was accomplished, the mechanical properties of the elements were varied analytically to study their effects and guide future testing.

Three webbing materials currently used in USAF restraint systems were tested at strain rates comparable to those encountered during torso retraction. The resulting stress-strain diagrams were matched reasonably well in the linear range by a four-element viscoelastic fluid model. The element coefficients were establihsed for all three materials.

A pyrotechnic inertia reel used as part of ejection seat restraint systems was investigated but could not be successfully modeled. Only limited experimental data were available. The problem was aggravated by the lack of well-defined dimensional data, differences found between design data and hardware, and difficulties in interpreting physical phenomena as inferred by measured data.

A rigid torso model was designed and fabricated to duplicate the size, mass, and mass moment of inertia in pitch of the 95th percentile man. The rigid model was used with the Body Positioning and Restraint Device (BPRD) to study the effects of a standard PCU-15/P torso restraint harness.

An analytical model of a human with torso, head, neck, chest, and harness elements was evolved using the rigid torso test data and existing human test data collected using the same harness and instrumentation. Restraint material properties and harness characteristics were included in the model.

The analytical model was also used with biomechanical data for the rhesus monkey to examine the response of an assumed restrained rhesus configuration. For this particular model, computed responses to selected input acceleration levels indicate that kinetic response and measures of injury response are not linearly related to variations in the input acceleration. Hence, in scaling the human input environment by altering the restraint harness or acceleration waveform in order to test primates it may not be possible to study the same injury mechanism in both human and rhesus. The critical injury parameter for the human in a particular environment may not be critical for the primate in the scaled environment. Limited analyses using the model indicate that scaling may be impractical or impossible if primate duplication of a particular human injury mechanism is required. A more detailed model may indicate a particular injury mechanism common to both species. A proposed methodology for evolving future scaling attempts is included.

TABLE OF CONTENTS

TABLE OF CONTENTS (continued)

LIST OF FIGURES

LIST OF FIGURES (continued)

LIST OF FIGURES (continued)

LIST OF TABLES

SECTION 1

INTRODUCTION

USAF restraint systems are designed, procured, and evaluated using static load criteria only. Powered inertia reels are evaluated using rigid torso dummies. These are adequate approaches only if the effects of the dynamic impact environments and biodynamic responses encountered during emergency escape and aircraft crash are understood and can be accounted for using dynamic load factors. Unfortunately, the technology data base that is available is not adequate for the development of these dynamic load factors. The dynamic inertial response of the human body and its interaction with the mechanical response characteristics of restraint systems and system components must be quantified to provide this technology base. The development of mathematical analogs of the human body and restraint systems offers a method that can be used to analytically determine optimum material properties for given operational conditions and a foundation for test and evaluation criteria. However, such models must be based upon adequate experimental data. Applicable experimental data is limited. One of the primary goals of this research effort was to provide experimental data and methods that could be used to acquire additional data required to develop and validate these mathematical analogs.

As the maneuvering capability of aircraft increases with improved control technology, the operating environment of the aircrewman becomes more hazardous during ejection. The probability of poor body position prior to ejection is increased and this places a greater technical burden on the designer of the restraint system. How can the restraint system be improved to permit faster torso retraction and ejection during more severe maneuvering environments?

If a system is to be improved it is necessary to understand the function and capability of each of the elements of the system. In order for torso retraction to occur, an automatic restraint haulback device must be activated. Shoulder harness retraction devices that are currently used "wind-up" the straps running from the retraction spool to a restraint harness attachment point. The retraction device is not a large device of infinite power and hence its response to the force that builds up in the strap influences the performance of the reel. Similarly, the straps are materials with viscoelastic properties which respond to the motion between reel and torso as functions of relative velocity. The restraint harness is also constructed of viscoelastic material, but in addition it is not several straight elements but rather a configuration of elements with the capability to rotate over the torso while elongation occurs within elements. Simultaneously with the occurrence of material elongation and configuration changes, the chest is compressed, the torso rotates against its own inertia and joint stiffness, and the lower torso deforms against the seat belt and harness, depending upon the

restraint configuration. Additionally, the torso "drives" the head and neck system which creates another inertial subsystem. Clearly, the response of the aircrewman to the retraction initiated by the haulback device is complex. If the response is to be evaluated in terms of injury protection provided by variations in all restraint system elements then either a monumental testing program is required, or a valid analytical technique is necessary to select the properties that are most promising. The objective of this research effort is to create the latter choice so that testing can be focused on restraint configurations that are likely to be most effective.

The research conducted presupposes that it is possible to select parameters and test conditions in such a manner that it will be possible to analytically isolate the characteristics of each subsystem of the restraint system. Specifically, the objectives of the research were:

- (1) To quantify pertinent dynamic properties of restraint materials,

- (2) To provide test data and mathematical models of ballistically activated restraint haulback devices,

- (3) To develop experimental designs to investigate the effects of the restraint harness loading on the human body,

- (4) To provide guidelines for subhuman primate testing using dimensional scaling relationships, and

- (5) To develop restraint system evaluation techniques using both experimental and analytical approaches.

The objectives generated several specific technical approaches.

Tests were to be conducted to determine the dynamic response characteristics of USAF operational restraint systems under $-G_x$ impacts and rapid haulback of the restraint system shoulder straps. By conducting tests with a rigid body simulator and comparing the result with data collected using humans subjected to similar environments, we hoped to be able to isolate human inertial response from restraint system response.

Testing of pyrotechnically activated restraint haulback and tensioning devices was required in order to develop a performance predicting mathematical model. By testing with selected materials, strap lengths and resisting forces, a model was to be evaluated which could predict the mechanical performance under varied loading conditions.

Test hardware were to be designed for use with highspeed testing machines in order to measure restraint material response at selected strain rates. By testing at various lengths and strain rates data were to be collected to characterize the viscoelastic nature of the material.

From the data collected and analyzed, all model representations were to be included into a restraint system dynamic model for use by equipment designers. By having representations for the ballistic reel, restraint material, harness and human, one system model was to be synthesized which could reflect all significant elements of the system, without incorporating any unnecessary elements. Inherent in the ultimate use of the model was the inclusion of some injury criteria.

Finally, having developed a model with both mechanical and injury prediction capability, the model was to be used in the study of experimental designs using primates. Problem areas to be addressed were restraint hardware scaling and selection of impact environments in order to test primates and correlate the results with predicted human response.

In summary, the effort required was directed toward quantitatively describing all of the effects described in the opening paragraphs of this section. With careful selection of test conditions, fabrication of unique test hardware, utilization of existing data, and collection of more data, the results were to be incorporated into an analytical model capable of predicting human or primate response for selected parameter values of each subsystem. The model was to reflect all necessary and sufficient aspects of the system but no more.

SECTION 2

RESTRAINT MATERIALS TESTING

INTRODUCTION

Of all of the elements of the restraint system, the easest to analyze are the straps that attach the harness to the retraction device, or the retraction device directly to lap belt attachment. Although the straps have a particular configuration which must be eventually considered, the area of primary emphasis of this section is that of determining material properties.

Restraint webbing has been tested for many years to determine that it conforms to the requirements of Federal Standard-191-Textile Test Methods. This assures the buyer that the material has a certain ultimate breaking strength but doesn't specify other material properties. Test data collected many years ago, shown in Figure 1, indicate that the force-displacement characteristics of webbing are not typical of what would normally be called an "engineering" material. A material that demonstrates two different stress-strain curves if tested at two different strain (or stress) rates cannot be called a Hookean solid. This was, of course, the reason that the testing and the characterization of restraint materials were included in the restraint system research. How can you describe the material in terms of material properties, and how do you include these descriptions into usable restraint system models?

Selection of an Analytical Representation

There are many ways to represent the mechanical properties of a material with a spectrum of idealization beginning with the inelastic solid and ending with the inviscid fluid. Clearly from curves such as Figure 1, the restraint material is not a Hookean solid. Also, it is not a fluid since straps do not continue to elongate (appreciably) under sustained reasonable forces. Consequently, the material must be idealized as a viscoleastic material which will enable the investigator to select as many elements for the representation as necessary.

Viscoelastic phenomena are discussed in many references, Flugge [1] and Nielsen [2] for example, and can be presented analytically in terms of mathematical expressions not related to analytical models as in Gross [3], or primarily in terms of discrete element models as presented in Flugge [1]. The following discussions of viscoelastic response are related to a discrete element representation of the restraint material. This has the advantage of a better visuilization of material response (engineers "see" viscous dashpots and elastic springs) while providing the same results as could be found using other approaches. Those preferring frequency domain analysis or use of Hereditary Integral may refer to the classic work by Gross [3].

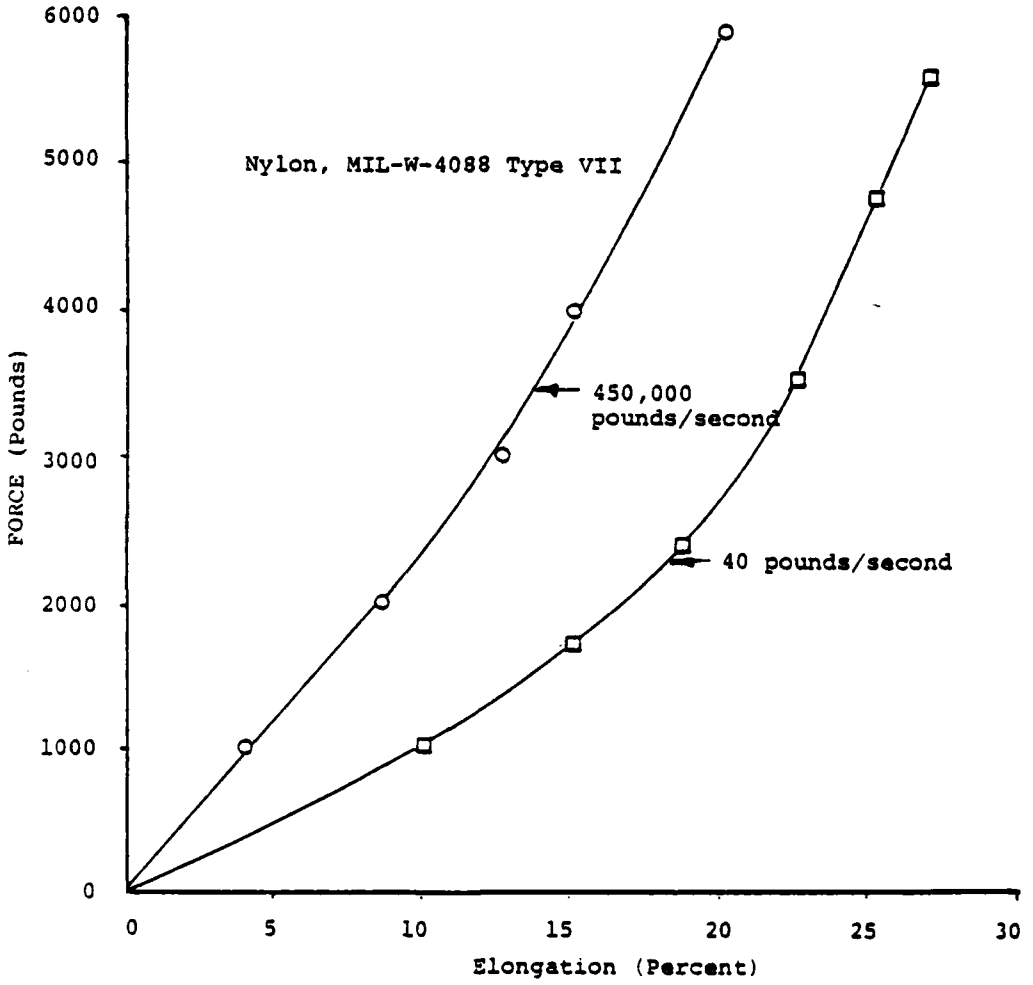

Figure 1 Nylon Webbing Tested at Two Stress Rates. (Redrawn from Beta Industries Report BII-2203 dated August 1971.)

Several viscoelastic models and their responses to given strain rates are shown in Figure 2. By comparing with the curves of Figure 1, it is apparent that the closest possible representation apparent is that of the spring and dashpot in series, a Maxwell fluid. However, for a restraint webbing it is known that ultimately the material is a "solid" and hence the viscous elements should have some very large value of viscosity if it is to carry a force over large finite periods of time. If a high viscosity element is in series with other elements, and yet the variation of stress with strain rate is desired, then at least a three-element model is required. If instantaneous elasticity capability is desired, an elastic element in series is required. Consequently, the simplest model capable of having the instantaneous elasticity of a solid, long-term creep of a fluid, and the strain rate sensitivity "in between" is the visoelastic model referred to as a four-element fluid. The representation assumed is as shown below.

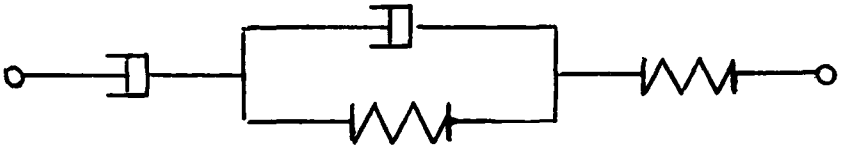

The model has a transfer function which can be used to determine its response to any input condition. The differential equation is of the form [1]:

$$p_2\ddot{\sigma} + p_1\dot{\sigma} + \sigma = q_1\dot{\varepsilon} + q_2\ddot{\varepsilon}$$

where p's and q's are constants, σ's and ε's are stresses and strains respectively, and the dot superscripts are Newtonian notation for time differentation.

With the model selected and the describing function available, the next step was the selection of a test methodology that permitted model coefficient determination from test data.

In summary, the interpretation of the term "material properties" has been defined by assuming a particular viscoelastic model. The material properties to be found are the two viscous and two elastic coefficients of the four-element model. The model is a linear viscoelastic four-element fluid which has the capability to provide stress-strain curves of the form shown in Figure 1 [2].

Development of a Test Program for Restraint Materials

Three materials were to be tested. The material types were selected because of their use in USAF restraint systems and because the materials were used in previous human testing programs. Hence, in subsequent studies of restrained human response we hoped that one element of the system would be quantitatively defined.

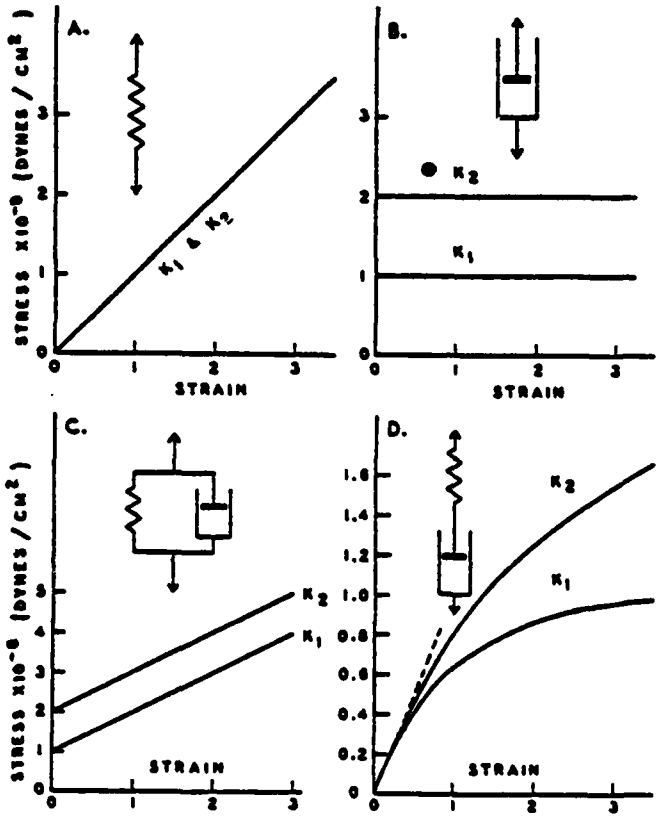

Figure 2. Stress-Strain Curves for Four Simple Viscoelastic Models at Two Strain Rates $K_2 = 2K_1$.

Several cursory examinations of available test data from restrained human tests indicated that the relative velocity between torso and input device was approximately 100 inches/second. This compared favorably with the requirement that retraction of the torso must be accomplished within 0.3 seconds, and with the published capability of the Body Positioning and Retraction Device (BPRD) at AFAMRL. Therefore, it was reasonable to assume that material testing should be conducted in the range of 5 to 10 inches/inch/second in order to collect data at strain rates indicative of operational requirements.

The materials selected for testing were:

(1) Type III polyester low elongation, of 1-23/32 inch width MIL-W-25361 C.

(2) Type VIII nylon of 1-23/32 inch width as described in MIL-W-4088H.

(3) Type XIII nylon of 1-23/32 inch width as also described in MIL-W-0488H.

Ample material was provided by AFAMRL.

The tests required were selected by consideration of several parameters. The testing should be conducted for all materials from "static" through the desired 5 to 10 inch per inch per second strain rate. The tests should be conducted to failure to establish the linearly viscoelastic range. Test coupons should be at several lengths in order to study length effects, if they exist, and as required to generate the proper strain rates.

The test device selected was an MTS universal test machine capable of 35 inch per second crosshead speed. The initial test matrix that was established specifies the strap lengths and the strain rates to be tested. These are shown in Table 1.

STRAP LENGTH (inches)	STRAIN RATES (in/in/sec)					
	0	2	4	8	16	
17.5	3				3	
8.750	3			3	3	
4.375	3	3	3	3	3	
2.188	3	3	3	3	3	

Table 1 Initial Test Matrix With Number of Tests Shown in Each Cell.

Test grips, shown in Figure 3, were designed to support twice the strength capability of the strongest strap. The intention was that the strap would pass down the side of one jaw, wrap around a pin and pass out the inside of the other jaw. The design assumed that the forces on the pin would wedge the pin into the webbing and lock the webbing in place. The first tests of this design showed that the concept did not work and had to be modified by inserting a true wedge between pin and webbing. The wedge, with rough surfaces, was a standard machine file which when preloaded with only 20 pounds locked the webbing in place. Because of the size of the grips between pin and jaw edge, it was not possible to use strap samples of less than 3.00 inch gage length. Consequently, the finalized tests for all samples were collected under the following test conditions.

Table 2. Final Test Conditions

Sample Length (inches)	Crosshead Speed (inches/min)	Strain Rate in/in/sec
17.5	2.1	0.002 (static)
17.5	1000	0.952
17.5	2000	1.904
8.75	1.05	0.002 (static)
8.75	500	0.952
8.75	1000	1.904
8.75	2000	3.808
4.50	0.54	0.002 (static)
4.50	514	1.904
4.50	1028	3.809
4.50	1500	5.555
3.00	0.36	0.002 (static)
3.00	342	1.904
3.00	684	3.809
3.00	1000	5.555
3.00	2000	11.111

The values specified in Table 2 were nominal values desired for each test and the processed data indicated little deviation from those values. All tests were repeated twice. From the tabulated data it was possible to conduct multiple tests at the same strain rates for different lengths. This was in addition to variations in strain rate for a fixed length.

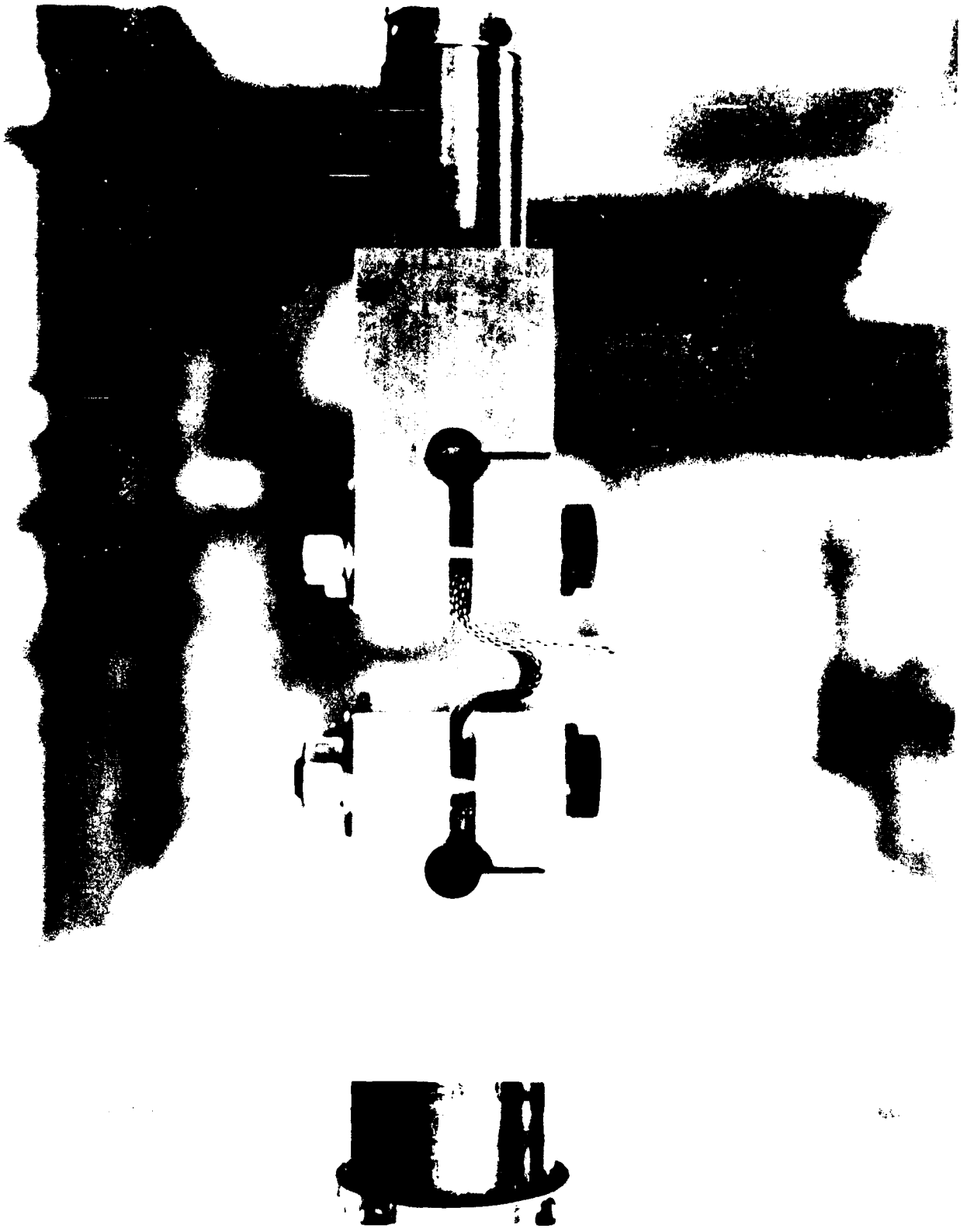

Figure 3. Test Grips Designed for Restraint Materials Testing.

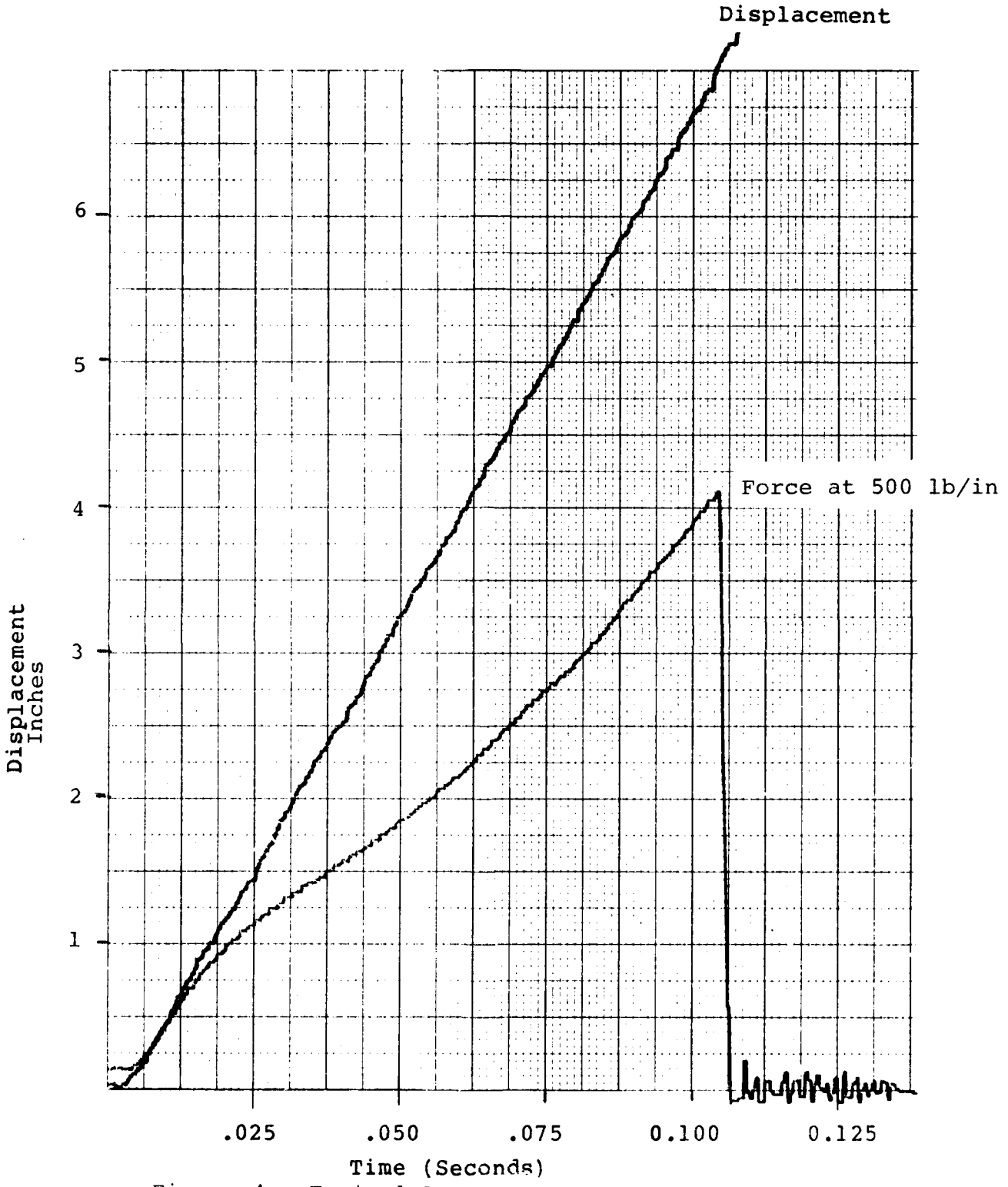

Figure 4. Typical Test Data as Recorded.

Data from the testing machines were available as shown in Figure 4. Each test generated a plot of load versus displacement of the cross head, and load and displacement versus time.

DATA COMPILATION AND DATA ANALYSIS

The data collected and shown in Figure 4, were compiled in sets by type of material and the load-displacement was recalculated to present stress-strain curves. The load was converted to stress by using the nominal dimensions given in the material specifications, and the strain was calculated based upon the coupon length between the locking wedges.

Figure 5 presents the data processed for the Type III polyester webbing. The figure shows a spectrum of curves for the shortest samples, the longest sample, and the static and highest strain rates. From the curve it is apparent that for the static testing, the stress-strain curve is dependent upon the length of the sample. However, if the data are indicative of material "properties," the stress-strain curve for a given strain rate should be the same. Assuming that the measured crosshead speeds are correct, and that the sample lengths were correct to begin with, the differences must then be functions of the end effects, whether due to local strain effects or jaw motion. Because of the rigidity of the jaws relative to the compressibility of the webbing within the jaws, it was assumed that any crosshead motion would generate true strain as well as extraneous strain due to wedge motion against the webbing within the jaws. Consequently, the strain can be represented as:

$$\varepsilon_T = \varepsilon_W + \varepsilon_B$$

where ε_T is the total strain, crosshead motion divided by length,

ε_W is the strain due to wedge motion, and

ε_B is the strain of the belt.

Since the "strain" of the wedge is a function of the force being carried by the webbing and is constant for a given force, data collected for a given force level should have the same wedge motion even though the length of the webbing and the strain rate changes. Therefore, the strain desired is:

$$\varepsilon_B = \frac{(\varepsilon_T L)_1 - (\varepsilon_T L)_2}{L_1 - L_2}$$

where the subscripts imply two different tested strap lengths at the same strain rate at a given force level.

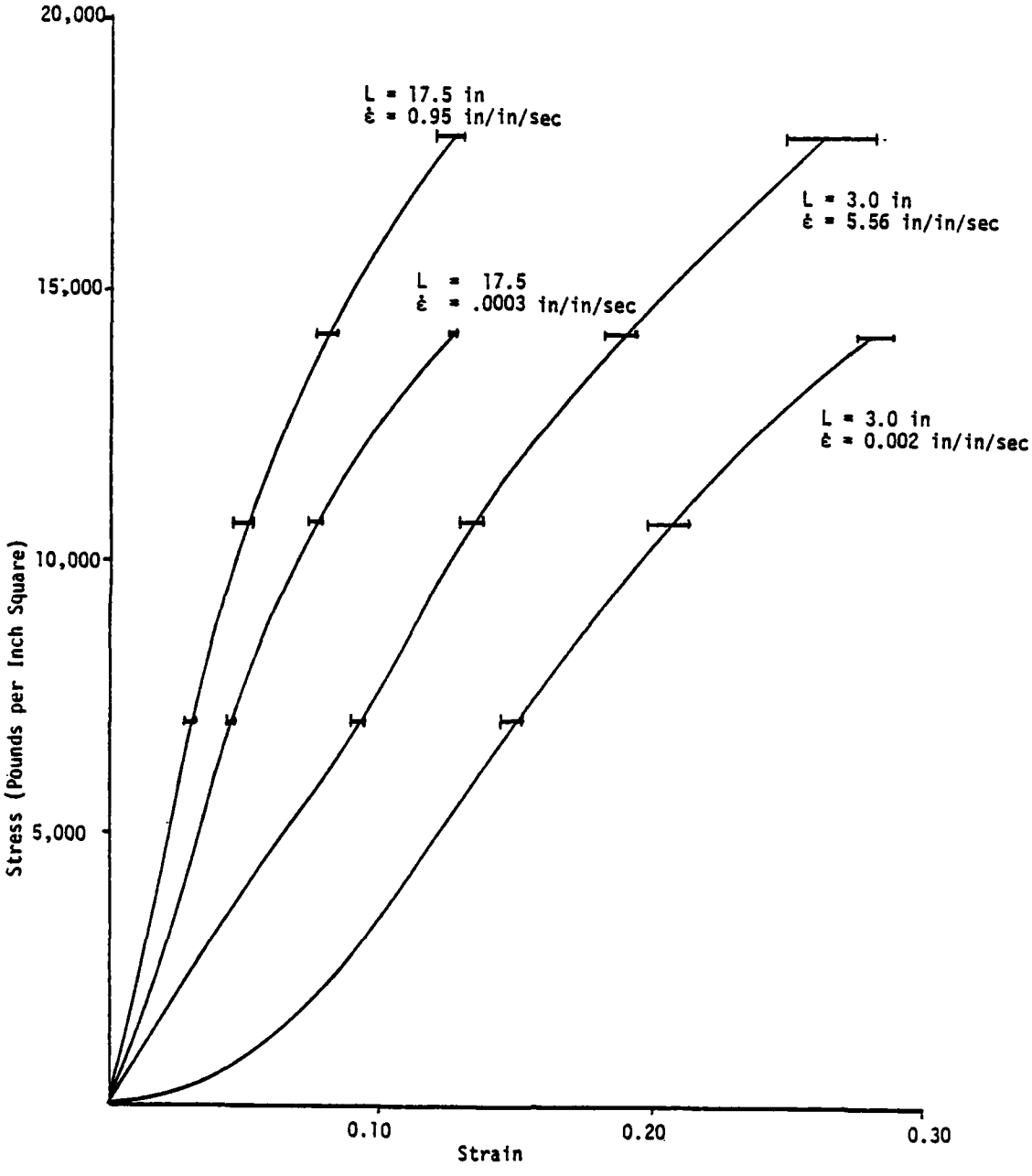

Figure 5 Stress-Strain Curves for Type III Polyester.

By examining the curves of Figure 5 and solving for several strains at fixed force levels, it was possible to calculate the strain of the material and create Figure 6. The calculations also provide a wedge motion as shown in Figure 7, a linear function with force as was assumed.

The calculations indicated that although true strain, as could be measured by a large deformation transducer, was not measured directly, a measure of it could be found. The strains attributed to the material look reasonable and the assumed wedge motion plots as a linear function of applied force.

There was only one known source of data for comparison. The stress-strain curve for Type VIII nylon measured statically was available from Carr and Singley [4] and had evidently been measured using a five inch gage length strain device. The two curves are shown on Figure 8 indicating the favorable agreement at the lower force levels.

Similar procedures of analysis were used with the curves of the two nylon webbings. The raw data curves are shown in Figures 9 and 10. The processed data with removal of wedge motion are shown in Figures 11 and 12.

The final stress-strain curves indicate that the Type VIII nylon material is the "softest" material for the range of strain rates tested. Additionally, the material is apparently nonlinear at low strain rates and low strains. However, the data are to be used only for low force level applications. It is reasonable to assume, based upon existing human test data, that we are primarily interested in predicting belt response at forces of approximately 1,000 pounds maximum. Hence, the linearity assumption may be adequate.

The Type XIII nylon stress-strain curve indicates the least viscoelastic response in that the static and dynamic curves overlap one another. This does not mean that they do, in fact, cross but rather that the analysis used and the accuracy of the data do not permit the separation of curves as should exist for linearly viscoelastic media.

Type III polyester stress-strain curves look like classical viscoelastic curves in that there is a linear slope from the origin with a gentle curvature at the higher strains. The effects of increased strain rate are evident in the increasing "stiffness" with strain rate.

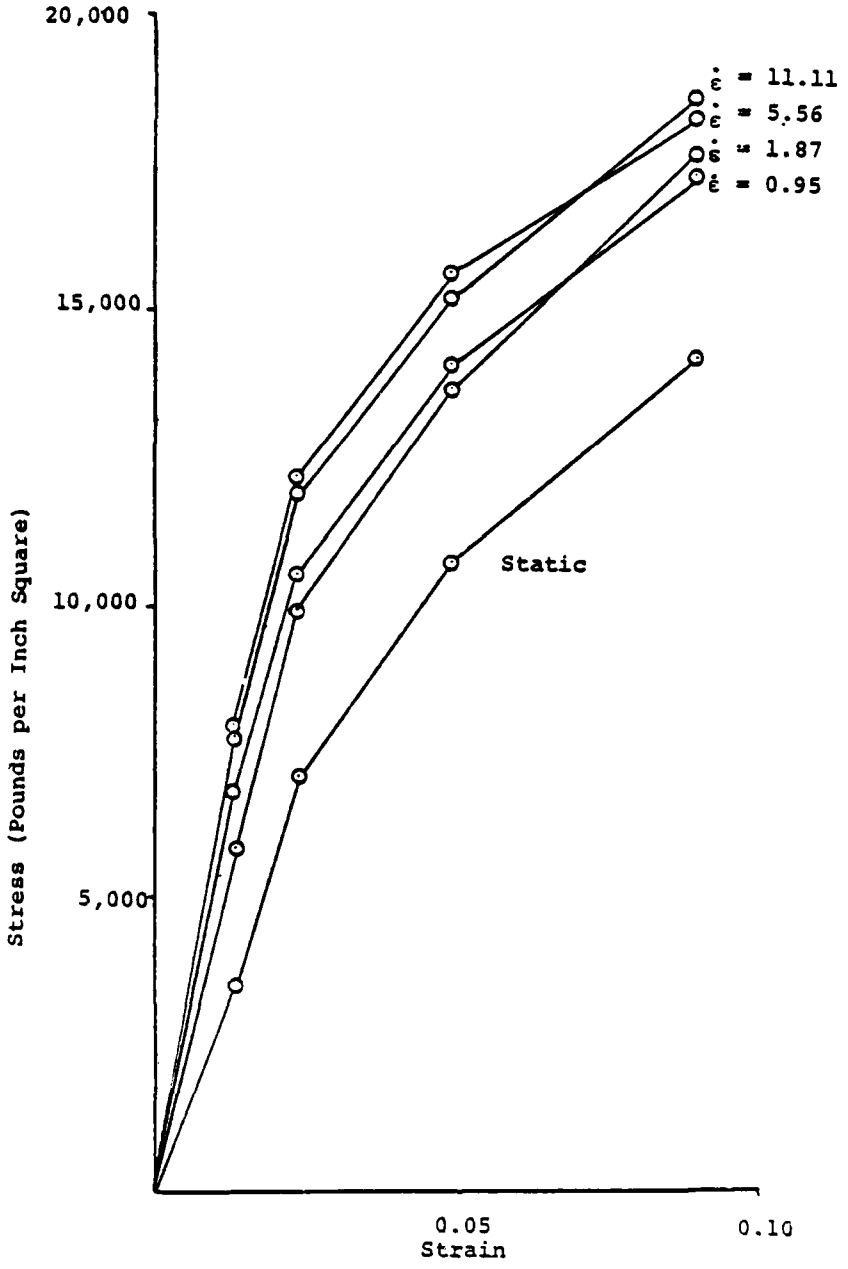

Figure 6 Final Stress-Strain Curves for Type III Polyester.

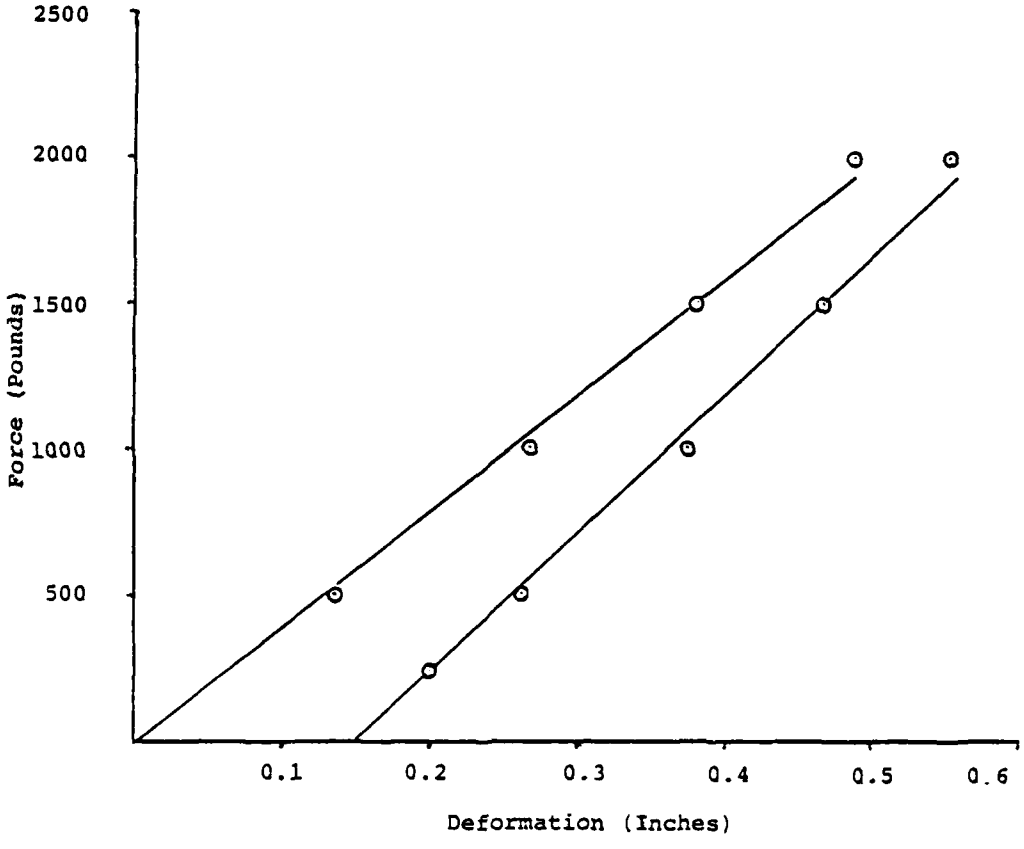

Figure 7 Deformation of Wedges versus Measured Force.

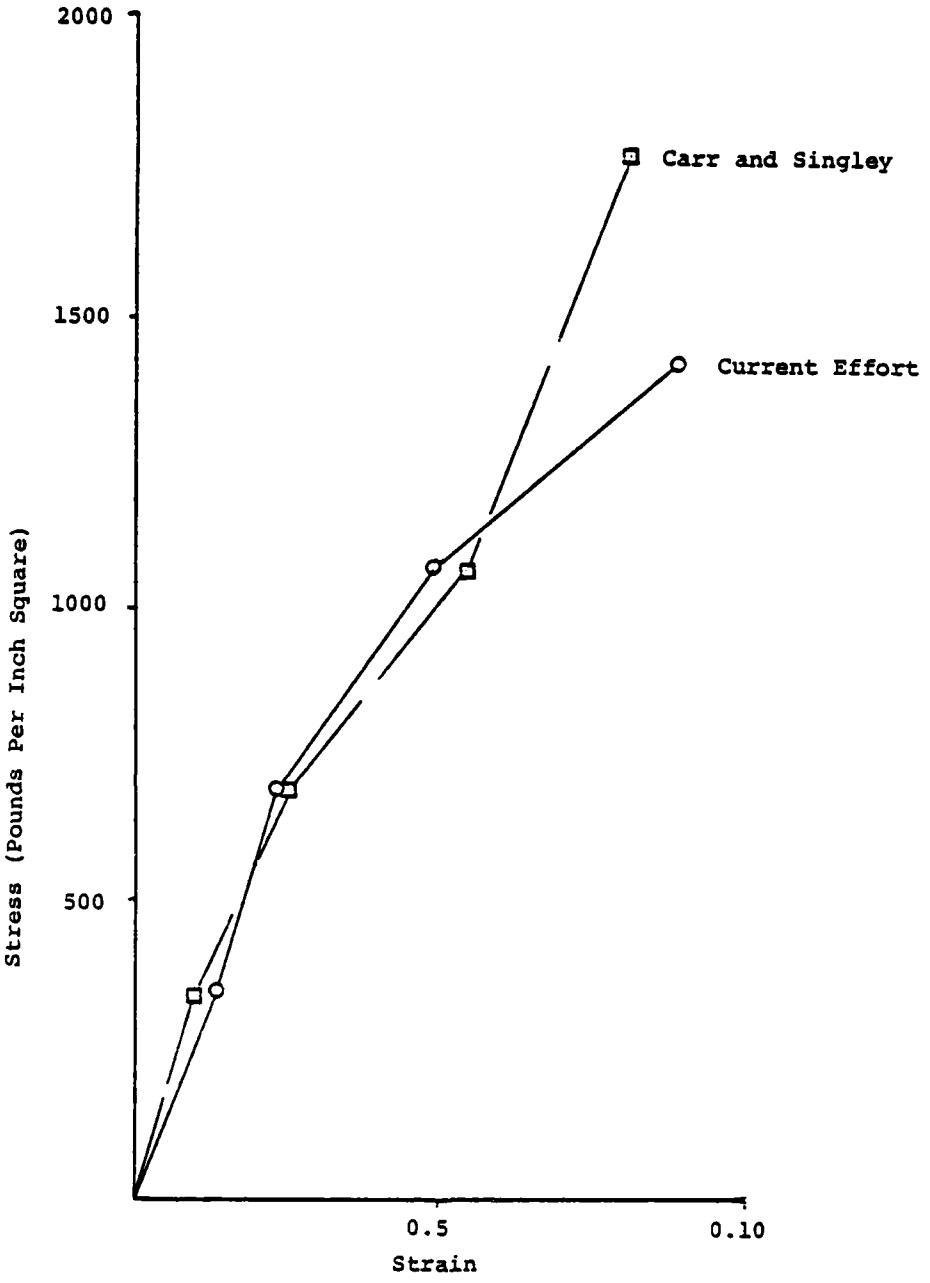

Figure 8 Calculated Stress-Strain for Type III Polyester and Referenced Work.

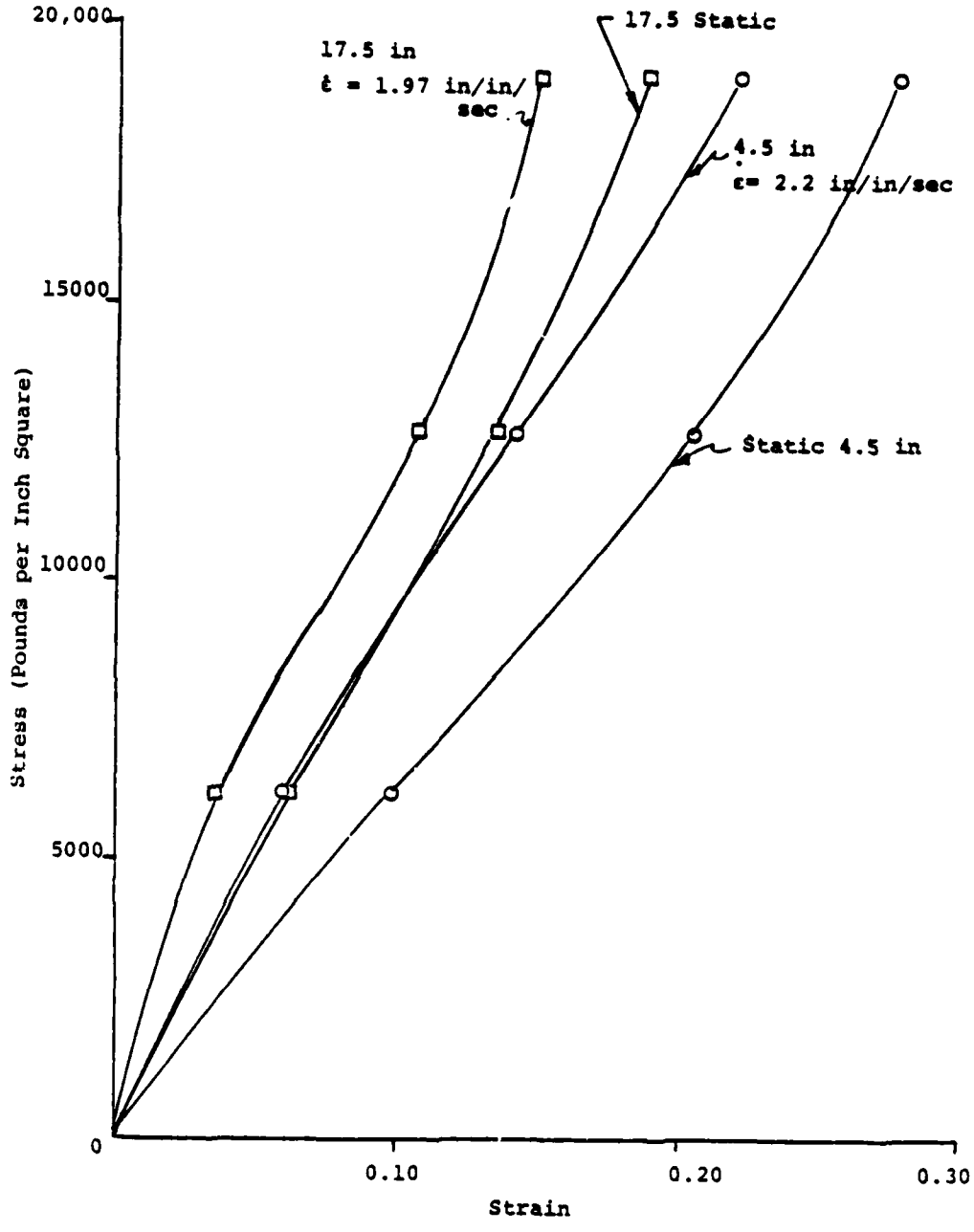

Figure 9 Initial Stress-Strain Curves for Type VIII Nylon.

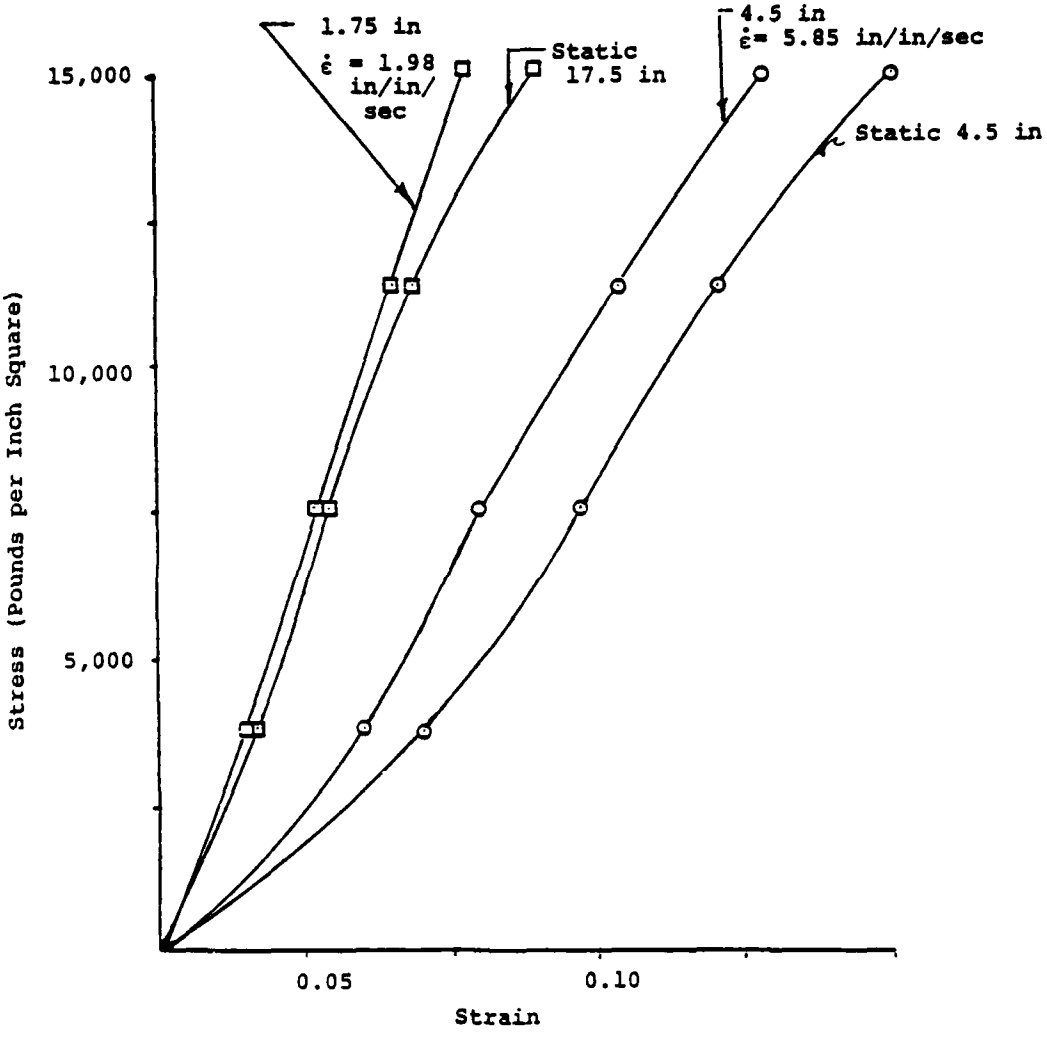

Figure 10 Initial Stress-Strain Curves for Type XIII Nylon.

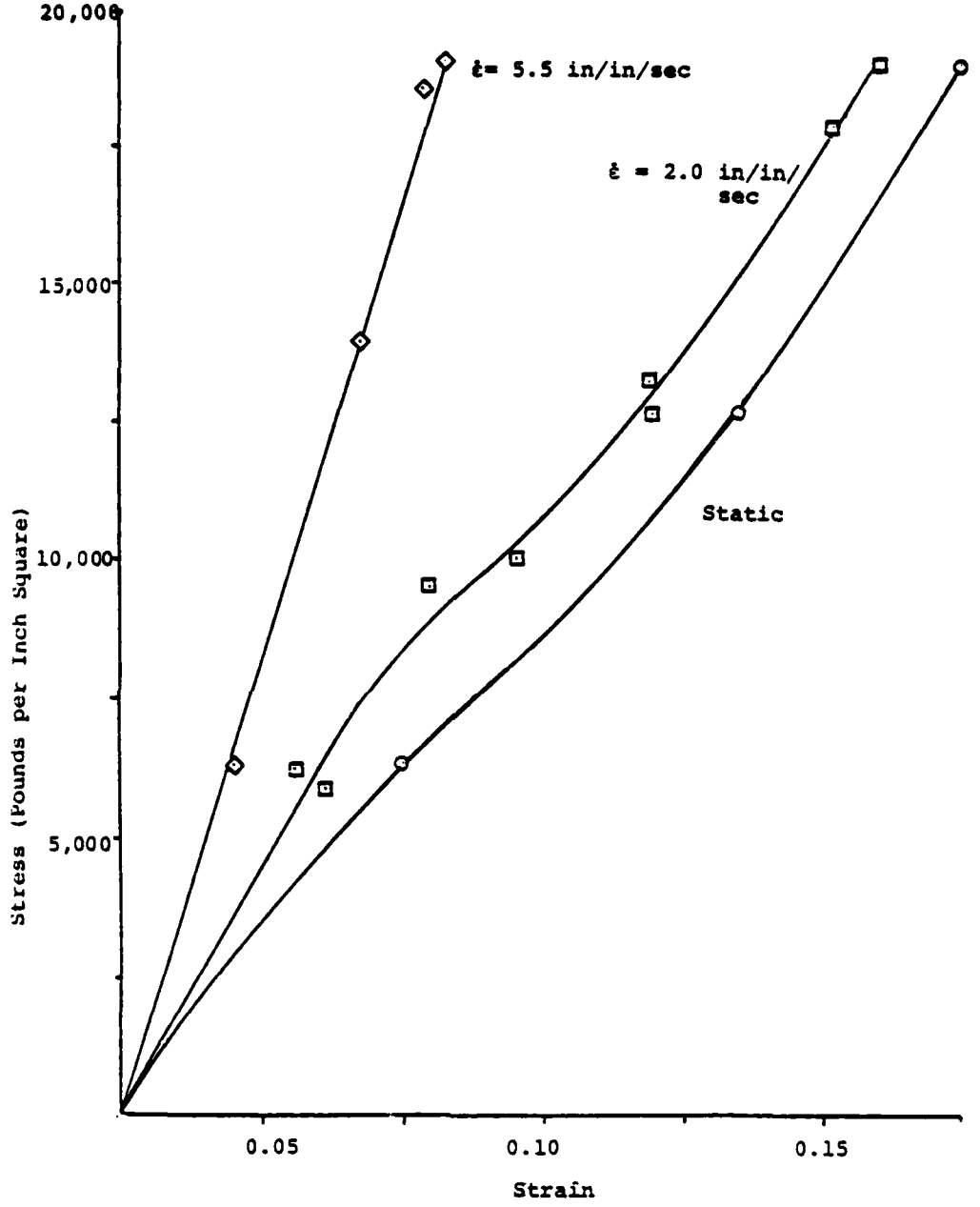

Figure 11 Final Stress-Strain Curves for Type VIII Nylon.

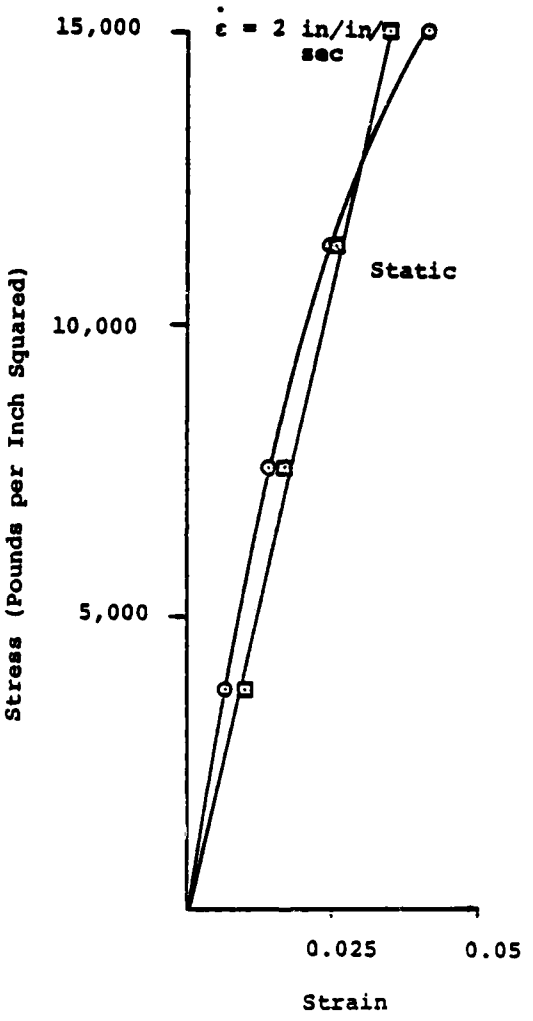

Figure 12 Calculated Stress-Strain for Type XIII Nylon.

VISCOELASTIC MODEL OF RESTRAINT MATERIALS

The objective of the research described in this section was to find a relatively simple viscoelastic model to duplicate the observed stress-strain behavior of three types of restraint harness webbings over a range of strain rates from zero to 10 in/in/sec. From the discussion of previous paragraphs the four-element fluid model is represented as:

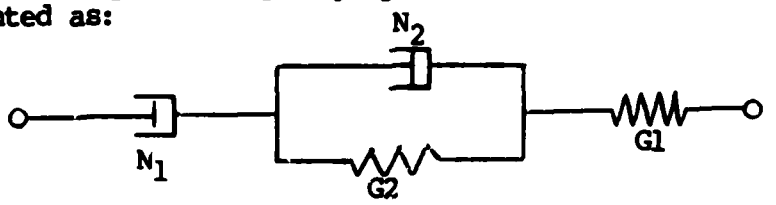

Figures 6, 11 and 12 show experimental $\sigma - \varepsilon$ curves to be duplicated for tests run at constant strain rates of 0.002 ε/sec., 2.0 ε/sec., and 5.5 ε/sec.

Stress-Strain Equation for the Four-Element Fluid

If $\varepsilon = Kt$ (constant strain rate), the differential equation governing the relationship between stress and strain for the four element fluid can be integrated to give stress as a function of time:

$$\sigma(t) = K\{N1 + C_3[C_1 e^{\gamma_1 t} + C_2 e^{\gamma_2 t}], \text{where} \quad (1)$$

$$\gamma_{1,2} = \{-\frac{P_1}{P_2} \pm [(\frac{P_1}{P_2})^2 - (\frac{4}{P_2})]^{\frac{1}{2}}\}/2 \quad (2)$$

$$C_1 = (q_1 - \gamma_1 q_2)/\gamma_1 \quad (3)$$

$$C_2 = (q_1 - \gamma_2 q_2)/\gamma_2 \quad (4)$$

$$C_3 = 1/P_2 - (\gamma_1 - \gamma_2)] \quad (5)$$

$$P_1 = \frac{N1}{G2} + \frac{N1}{G1} + \frac{N2}{G2} \quad (6)$$

$$P_2 = \frac{N1\ N2}{G1\ G2} \quad (7)$$

$$q_1 = N_1 \quad (8)$$

$$q_2 = \frac{N1\ N2}{G2} \quad (9)$$

Equation (1) is poorly conditioned for digital evaluation, since, for the webbings of Figures 6, 11 and 12, C_1 and C_2 are always of opposite sign and of magnitudes up to 10^{15}. However, the equation is

very useful for estimating values for the spring and dashpot parameters which will reproduce any particular stress-strain curve.

Some Interpretations of the Behavior of the Four Element Fluid

We note from Equation (2) that γ_1 and γ_2 will always be negative, and that the magnitude of γ_2 must always be equal to or greater than that of γ_1.

Considering the type of model assumed, it can be shown that:

(1) G1 determines the slope of the stress-strain curve at t = 0, and that slope is the same for all strain rates.

(2) N1 causes the slope of the stress-strain curve to approach zero after a period of time determined by the value of N1.

(3) G2 produces a different, and smaller, slope of the stress-strain curve over a period of time determined by the value of N2.

(4) The slope of the stress-strain curve decreases monotonically with increasing time.

(5) Equation (1) shows that when γ_1 and γ_2 have significantly different values, the term $C_2.e^{\gamma_2 t}$ will have a predominate effect on changing the slope of the stress-strain curve for small values of time, while $C_1.e^{\gamma_2 t}$ will predominate for larger values of time.

As an example of the application of these, consider figure 13. The initial slope is 1200 ksi at E = 0.005. Therefore, $e^{\gamma_2 t}$ must produce the change from 1200 to 400 within this strain, while the $e^{\gamma_1 t}$ must be adjusted to produce the rest of the curve for K = 0.002. However, the curves for K = 5.5 and 2.0 have a slope of 400 at stresses of 11 ksi and 8 ksi, respectively. If the $e^{\gamma_1 t}$ is to produce the measured curve at the low strain rate, it will have no effect on the curves at the high strain rates. Thus, we can conclude that it will not be possible to reproduce all stresses above 8 ksi.

For Figure 11, the curve for K = 0.002 has a greater initial slope than those for K = 2.0 and 5.5. Thus, it will not be possible to reproduce the curve for K = 0.002 if good correspondence is desired for the other two curves.

For Figure 12, the curves for K = 2.0 and 0.002 show an increase in slope at stresses above 10 ksi, which makes it impossible for the model being used to reproduce those curves at stresses higher than 10 ksi. In addition, those curves exhibit drastically different slopes at small strains, which makes it impossible to use the $e^{\gamma_2 t}$ term to reproduce both curves even at low strains.

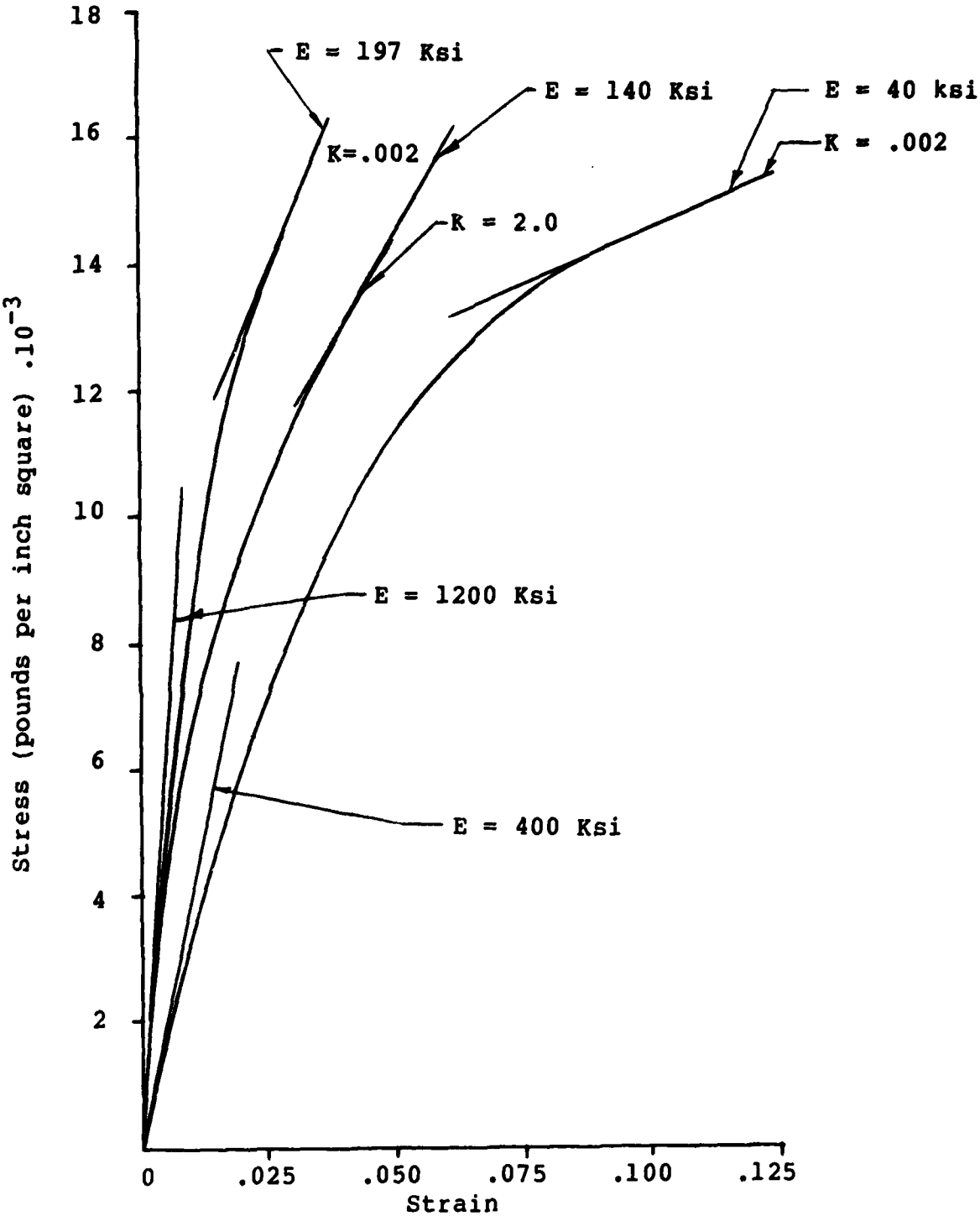

Figure 13 Use of Stress-Strain Slopes to Refine Material Properties of Polyester Type III

DETERMINATION OF APPROXIMATE VALUES FOR THE SPRING AND DASHPOT PARAMETERS

For the sake of illustration, consider the webbing of Figure 13. Figure 13 shows the initial slopes desired at each of the strain rates. The initial slope is to be 1200 ksi. Therefore, G1 = 1.2E06. The slope for K = 2.0 is to be 400 ksi at a stress of 8 ksi, and the slope for K = 0.002 is to be 400 ksi at a strain of 0.005. Also, for K = 0.002, $e^{(\gamma_2 t)}$ should be very small at the strain 0.005 since it is intended to use the e_1^t term to reproduce the rest of the curve. Assume that $e^{(\gamma_2 t)} = 10^{-6}$ at $\varepsilon = 0.005$ will be satisfactory. Since $\varepsilon = Kt$, the time required to produce a strain of 0.005 will be

$$t = \frac{0.005}{0.002} = 2.5 \text{ sec.}$$

Solving for the required value of γ_2:

$$\gamma_2 t = \ln 10^{-6}, \text{ or } \gamma_2 = -4.6.$$

Checking the first condition, slope = 400 ksi at $\sigma = 8$ ksi for K = 2.0, the time required is $\varepsilon/2.0$. The curve for K = 2.0 shows a strain of 0.014 at 8 ksi. Then

$$t = \frac{0.014}{2} = 0.007, \text{ and}$$

$$e^{(\gamma_2 t)} = 0.968.$$

Thus, some sort of compromise must be made since $e^{(\gamma_2 t)}$ is too large to produce the desired slope. Note that $e^{(\gamma_2 t)}$ must go to zero for a small value of t to give the initial slope of 400 ksi when K = 0.002, and that the final slope of the curve for K = 2.0 should be 140 ksi. Since $e^{(\gamma_1 t)}$ must produce the required change in slope of the curve for K = 0.002 over a time period of about 45 sec., γ_1 must be very small, and the term $e^{(\gamma_1 t)}$ will not have any effect on the slope of the curve for K = 2.0. This means that it will not be possible to achieve a final slope of 141 ksi for that curve. In fact, the best that can be done is to have a final slope of 400 ksi. Therefore, γ_2 is set to make $e^{(\gamma_2 t)}$ very small over the time interval for the curve of K = 2.0, which has a maximum strain of 0.048.

$$t = \frac{0.048}{2} = 0.024 \text{ sec}$$

$$\ln 10^{-6} = \gamma_2 (0.24), \text{ or } \gamma_2 = 480.$$

The procedure for determining the value of N2 for the known value of γ_2 is discussed below.

It is necessary to determine the value of spring G2 so that the slope is 400 ksi when $e^{(\gamma_2 t)} = 10^{-6}$. Assuming that t = 2.5, $e^{(\gamma_1 t)}$ is very close to unity (the N1 dashpot is essentially rigid), the model becomes

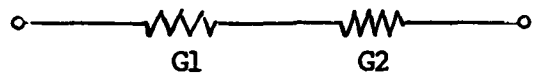

Allowing a change in stress of 1 ksi, the strain produced is

$$E = \frac{\sigma}{G1} + \frac{\sigma}{G2}$$

But, we want $E = \sigma/\varepsilon = 400$, so that $\varepsilon = 1/400$. If γ_1 is the strain in G1, and γ_2 the strain in G_2,

$$\varepsilon_1 + \varepsilon_2 = \varepsilon$$

Since G1 is known,

$$\varepsilon_1 = \frac{1}{1200}, \text{and } \varepsilon_2 = \varepsilon - \varepsilon_1 = \frac{1}{600.}$$

Now, $G2 = \frac{\sigma}{\varepsilon_2} = 600$ ksi

In order to determine a starting value for γ_1, note that its principal effect is on the curve for K = 0.002. Assume that the slope of $e^{\gamma_1 t}$ should equal the slope of the stress-strain curve for K = 0.002 at a stress of 14.2 ksi. The dimensionless slope at 14.2 ksi equals 0.4545. Thus,

$$e^{\gamma_1 t} = 0.4545.$$

since e^u is its own derivative. At the point concerned, $\varepsilon =$ 0.091, and $t = \frac{0.091}{0.002} = 45.5$. Thus

$$\gamma_1 = \frac{\ln 0.4545...}{45.5} = -0.173.$$

Calculation of N1 and N2

Equations 2 for γ_1 and γ_2 contain the spring and dashpot parameters in the p_1 amd p_2 terms. Since there are two equations and two unknowns, it is possible in theory to solve for the values of N1 and N2.

$$P_2 \gamma_1^2 + P_1 \gamma_1 + 1 = 0$$

$$P_2 \gamma_2^2 + P_1 \gamma_2 + 1 = 0$$

Substituting Equations (6) and (7), produces

$$\frac{N_1 N_2}{G_1 G_2} \gamma_1^2 + \frac{N_1 N_2 + N_1 G_2 + (N_2 G_1)}{G_1 G_2} \gamma_1 + 1 = 0$$

$$N_1 N_2 \gamma_2^2 + \frac{N_1 G_1 + N_1 G_2 + (N_2 G_1)}{G_1 G_2} \gamma_2 + 1 = 0$$

Solving simultaneously gives

$$[(\gamma_1^2 \gamma_2 - \gamma_1 \gamma_2^2)\ (G1+G2)]\ (N1)^2 + [(\gamma_1 - \gamma_2^2)\ (G1\ G2)]\ (N1) + [(\gamma_1 - \gamma_2)\ (G1)^2\ G2] = 0 \qquad (10)$$

$$N2 = \frac{-\gamma_1 [N1\ G1 + N1\ G2)] - (G1\ G2)}{(\gamma_1^2\ N1) + (\gamma_1 - G1)} \qquad (11)$$

For the values above: G1 = 1.2E06, G2 = 6E05, $\gamma_1 = -0.173$, and $\gamma_2 = -480$. Placed in Equations (10) and (11), we get

N1 = 2.31047E06 and N2 = 3.75513E03

where the extraneous root for N1 has been omitted.

Placing these values and the values for G1 and G2 into Equations (2), (6), and (7) gives

$$\gamma_1 = -0.173096$$

$$\gamma_2 = -479.69$$

which reproduces the desired values within the limits of round-off error.

Note that Equations (2), (6), and (7) appear to indicate that considerable interaction exists between N1 and N2 in determining the values of γ_1 and γ_2; i.e., changing N1 will change γ_2 and vice versa. However, Figure 13 indicates that there should be no interaction, and testing indicates that there is negligible interaction.

Figure 14 shows the curves produced for the values of G and N determined in this section. Since γ_1 primarily affects the curve for K = 0.002, the graph shows that N1 should be increased. Similarly, the value of N2 should be decreased in order to increase the curvature of the plots for K = 5.5 and 2.0. Consequently, it is apparent that it is difficult to predict the model coefficients accurately using manual techniques without an iteration of values.

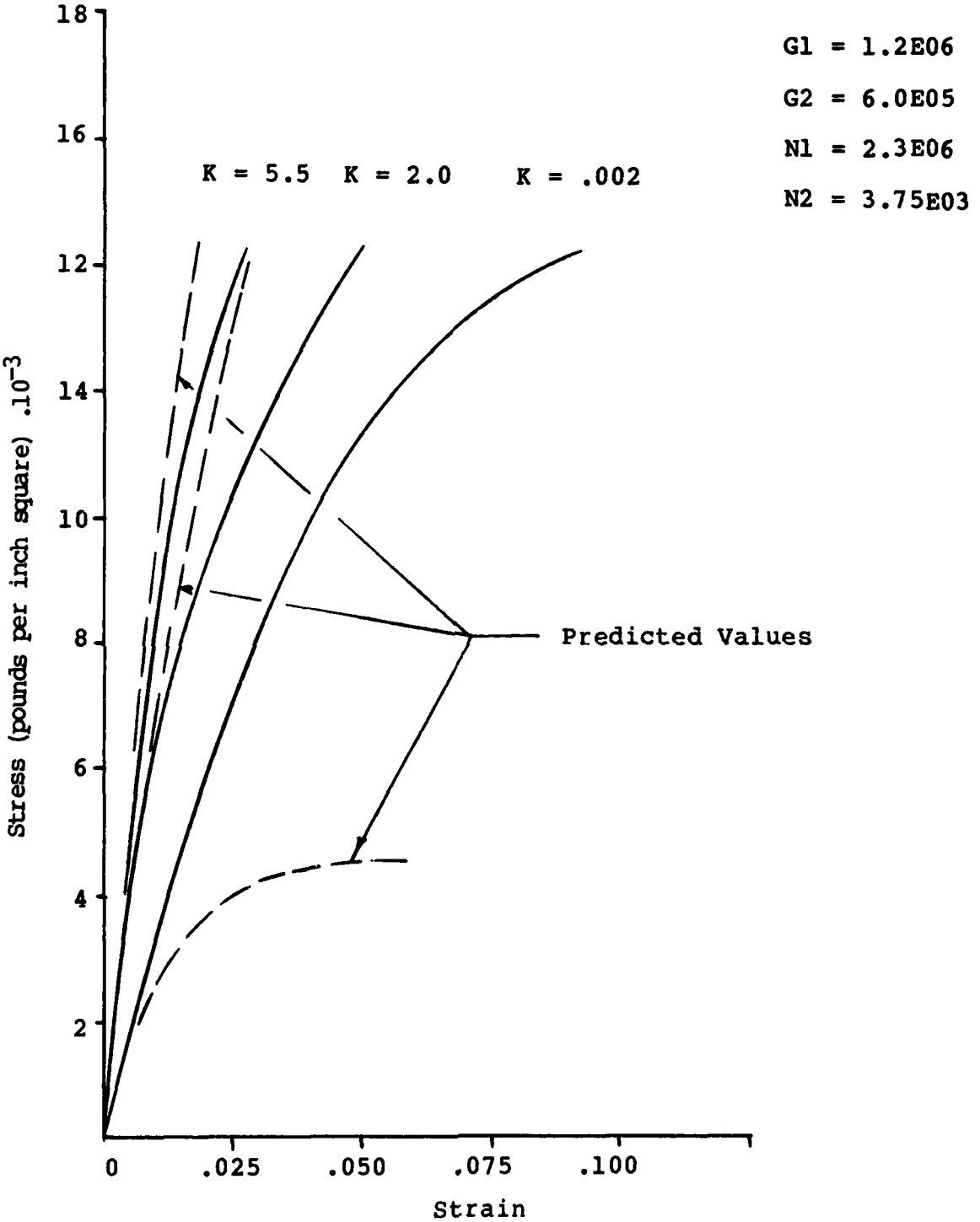

Figure 14 Predicted Stress-Strain Curves Using Slopes Approximation Technique for Polyester Type III.

Calculation of Stress-Strain Curves

In addition to the fact that Equation (1) is ill-conditioned for digital evaluation, it is also not suitable for the ultimate goal of evaluating the performance of a restraint harness. This is so because Equation (1) is limited to constant strain rates, and the restraint harness is subjected to strain rates which vary from zero to 10/in/in/sec. Therefore, it was necessary to program a digital integration of the equation governing the relation between stress and strain. The equation has the form

$$p_2\ddot{\sigma} + p_1\dot{\sigma} + \sigma = q_1\dot{\varepsilon} + q_2\ddot{\varepsilon} \qquad (12)$$

An integrator of ordinary differential equations called MIMIC was used. The algorithm employed by MIMIC is a variable step-size fourth order Runga-Kutta method.

Since the curves of Figures 5 through 13 were developed at constant strain rates, it becomes necessary to supply MIMIC with the strain rate at each interval of time. Figure 15 shows the desired function of strain versus time.

However, the integrator cannot operate with the desired function, since $\ddot{\varepsilon} = \infty$ at $t = 0$. Thus, it becomes necessary to introduce a finite, but possibly large, acceleration for a short period of time near $t = 0$. One criterion is that the strain-time function used in MIMIC should approximate the desired function sufficiently well. Part of this criterion is satisfied by making the extension (dashed line in Figure 16) of the straight line portion of the E-t curve pass through the origin. Further discussion of the precise meaning of "sufficiently well" appears below.

Since the restraint webbings may not all have the same length, the relation $\delta = L\varepsilon$ was used where δ is the deformation and L is the length of the webbing, in the following discussion.

Taking the first and second time derivatives of the curve in Figure 16 gives velocities and accelerations of the form shown in Figure 17.

The graph of $\ddot{\delta}$ in Figure 17 indicates that an expression of the form

$$\ddot{\delta} = A - A \cos(wt') \qquad (13)$$

where $t' = t + t_1$ would give the desired result. The equation is valid over the range $0 \leq t' \leq 2t_1$.

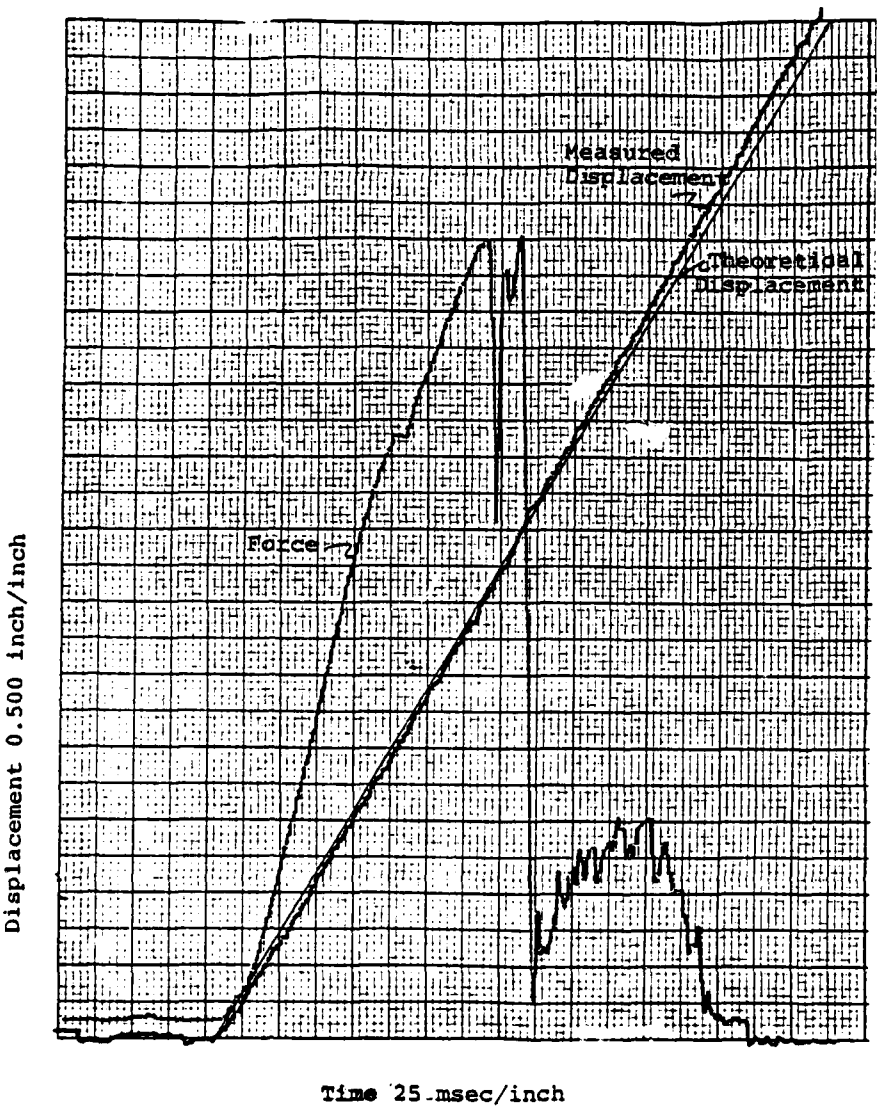

Figure 15 Constant Strain Rate Function, Theoretical and Measured.

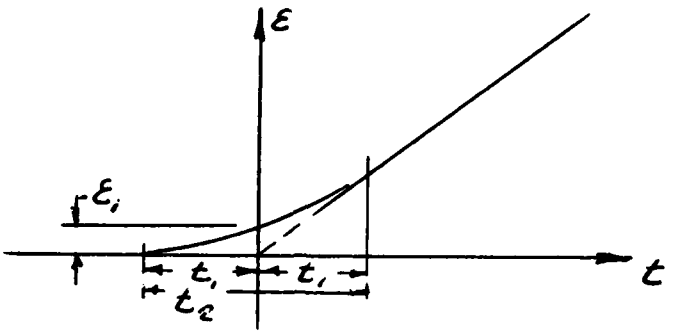

Figure 16
Strain Verses Time Representation

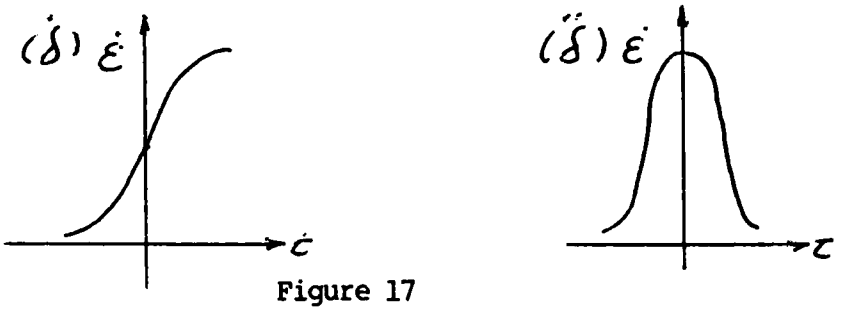

Figure 17

Strain Velocity and Acceleration for Assumed Strain Representation

Integrating,

$$\dot{\delta} = At' - \frac{A \sin (wt')}{w} + C_o \qquad (14)$$

where $C_o = 0$, since the $t' = 0$, $\dot{\delta} = 0$.

Integrating again,

$$\delta = \frac{A(t')^2}{2} + \frac{A \cos (wt')}{w^2} + C_1 \qquad (15)$$

where $C_1 = -\frac{A}{w^2}$, since at $t' = 0$, $\delta = 0$.

Applying the condition

$$\ddot{\delta} = 0, \text{ when } t' = 2t_1, \text{ gives } wt_1 = \pi. \qquad (16)$$

when $t' \geq t_1$, $\dot{\varepsilon} = K$. Since $\delta = L\varepsilon$, or $\dot{\delta} = KL$. But $\dot{\delta}$ is the slope, m, of the δ-t graph, so that

$$\dot{\delta} = m = KL \qquad (17)$$

Applying the condition that Equation (14) and (17) must give the same value of $\dot{\delta}$ for $t' = 2t$, gives

$$\dot{\delta} = m = 2At_1 \qquad (18)$$

At $t' = t_1$, Equation (15) gives

$$A = \frac{\delta_1}{0.297(t_1)^2} \qquad (19)$$

Eliminating A between Equations (18) and (19) gives

$$t_1 = \frac{\delta_1}{0.1487m} \qquad (20)$$

Equations (17) through (20) contain five unknown values (m, L, A, δ_1, and t_1) and these are sufficient to define the curves for δ, $\dot{\delta}$, and $\ddot{\delta}$. The length, L, of the restraint webbing is not considered to be an unknown, since it can be measured for any particular webbing to be analyzed. For the work described here, the length was arbitrarily chosen to be 20 inches. Since there are five unknowns and four equations, one unknown may be chosen so as to define the deformation-time function sufficiently well. It was decided to choose

$$\delta_1 = 0.01\delta_{max} \qquad (21)$$

where δ_{max} is the deformation to rupture, obtained from the experimental stress-strain curves. As a check on the validity of this choice, two tests were run for the same webbing, one with the value in Equation (21) and the other with $\delta_1 = 0.001\delta_{max}$. There was no significatn difference between the stress-strain curves produced, which indicates that equation 21 gives a small enough value of δ_1 so that the desired strain-time curve is reproduced sufficiently well.

Computer Results

In MIMIC the user must choose an integration step size (dt), as well as a total time (t_{max}). The value of t_{max} can be calculated from the experimental stress-strain curves. The choice of dt was determined by the characteristics of the output function of MIMIC. The user can elect to print and/or plot the values of stress and strain, but only those values computed at the end of each interval, dt. In addition, if a plot is requested, the output is limited to 100 pairs of stress and strain. Because of this last condition, dt was chosen to be $0.01t_{max}$ so as to produce the maximum possible number of points on the plot. It should be remembered that MIMIC reduces the value of the chosen dt to the extent necessary to bring the local relative error below $5x10^{-6}$. The user's choice of dt merely determines the number of output values.

The program was run on a CDC 660 computer, calculating 15 stress-strain curves for each run. Time consumed varied over a range of 10 to 100 CPU seconds, depending on the number of integration intervals needed to achieve the required accuracy. As might be expected, some values of the spring and dashpot parameters cause the time of integration to become unbounded. In this case, the algorithm terminates the integration when CPU time exceeds 300 seconds.

Figure 18 shows the final results for the webbing of Figure 6. In the experiments, the webbing was tested to rupture. In service, the stresses do not exceed eight ksi. Therefore, when it was found that the model could not accurately represent the experiment results to rupture, emphasis was placed on obtaining the best possible fit up to the service maximum stress of eight ksi.

Figure 19 shows the results for the webbing of Figure 11. Here, the service maximum stress is 14 ksi. It is not possible for the model to reflect the experimental results of the curve for K = 0.002 having a greater initial slope than the curves for K = 2.0 and 5.5 (which were identical). The parameters were adjusted so that the curve for K = 0.002 would show the correct strain at the stress of 14 ksi.

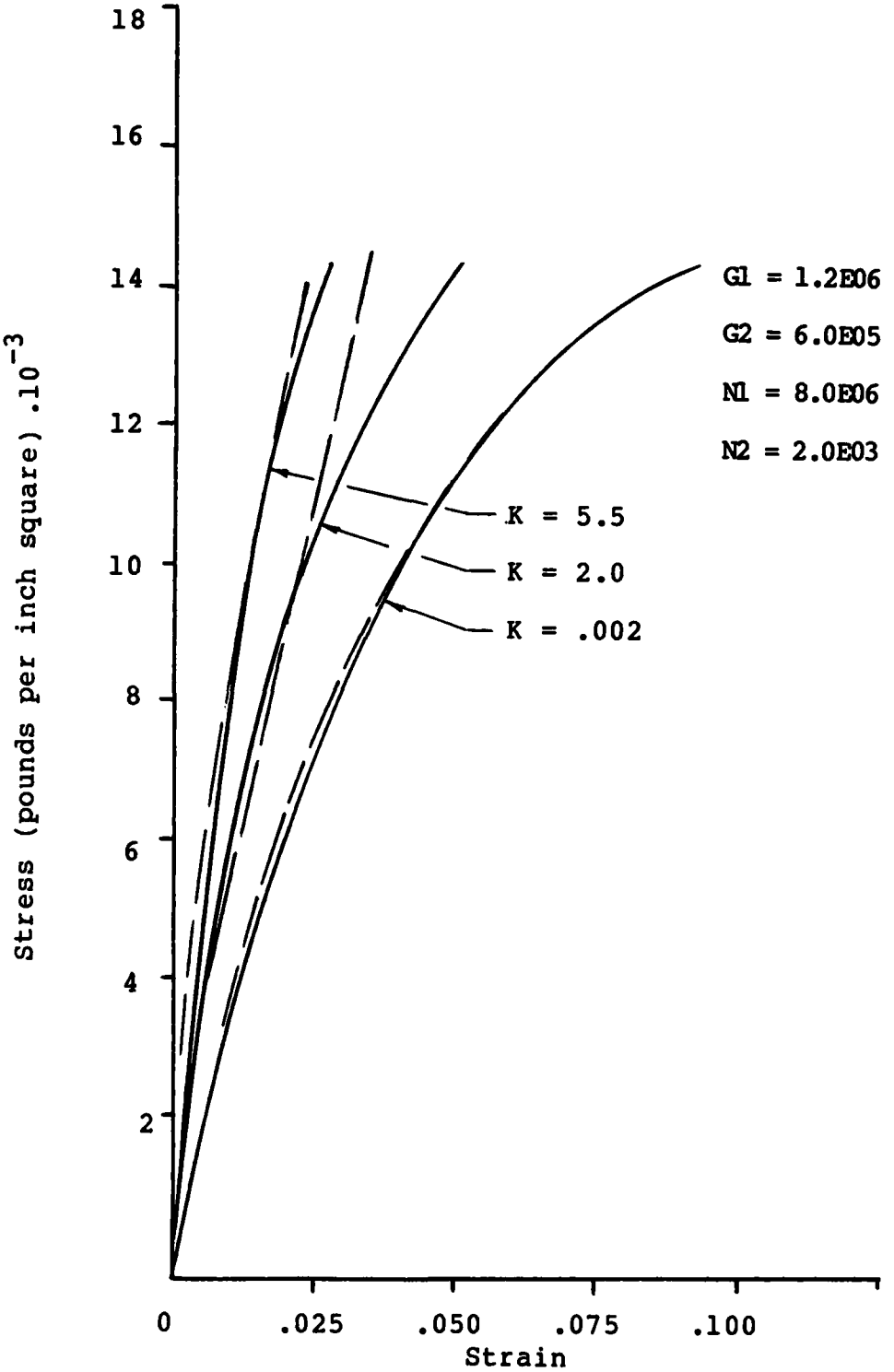

Figure 18 Predicted Stress-Strain Curves Using Computer Model for Polyester Type III.

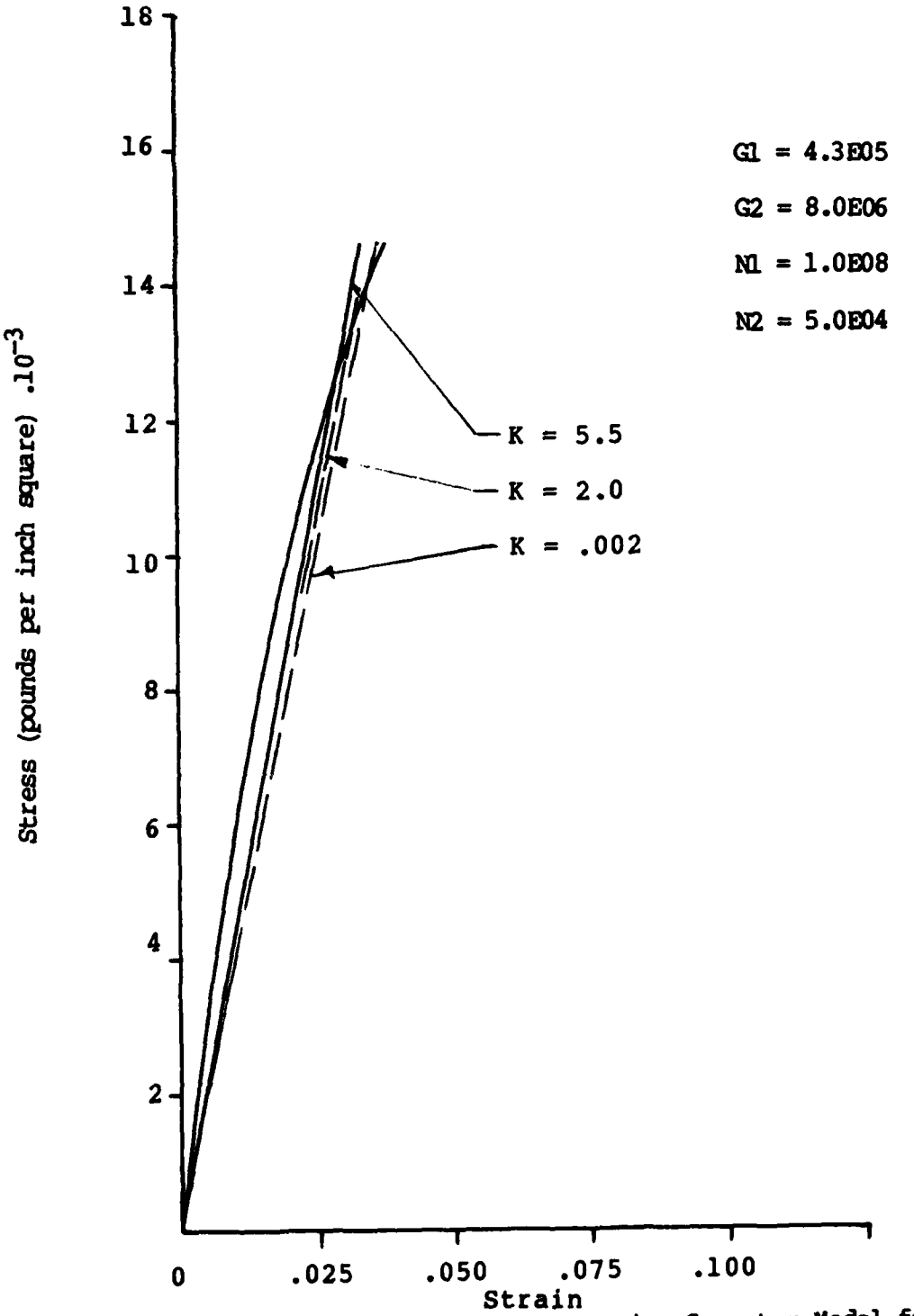

Figure 19 Predicted Stress-Strain Curves Using Computer Model for Polyester Type XIII.

For the material of Figure 12, which also has a service maximum stress of 14 ksi, there is a different initial slope for each of the three strain rates. Since the model cannot reproduce all three curves, two sets of parameters were determined, one set which would match for K = 5.5 and 0.002, and the other to match for K = 2.0 and 0.002. Figure 20 shows the results for K = 5.5 and 0.002. Since the model cannot reproduce the increase in slope for K = 0.002 above a stress of 10 ksi, it was decided to produce the best straight line fit by making $e^{(1,t)}$ very close to unity up to the maximum stress. The parameter N2 was adjusted to produce an essentially straight line for K = 5.5 without producing too much deviation from the experimental curve for K = 0.002. Note that the curve for K = 2.0 is forced by the choice of parameters to be almost identical to that for K = 5.5.

Figure 21 shows the results for K = 2.0 and 0.002. As it is not possible for the model to reproduce these curves, a best possible straight line fit was found for the time after $e^{(1,t)}$ becomes essentially zero. Note that the curves for K = 5.5 and 2.0 are considerably different.

SUMMARY OF RESTRAINT MATERIALS STUDY

Three types of standard restraint materials were tested to determine their material properties over the range of strain rates expected in a retraction environment. Special test fixtures were necessary for testing with a test machine having adequate force and strain rate capability. Strain was evaluated by subtracting extraneous wedge motion from the crosshead data. This was possible because the tests were conducted at strain rates duplicated over a spectrum of coupon lengths.

The stress-strain curves can be modeled by a four-element linearly viscoelastic fluid but only for a limited strain. For reasonable limits on strain, and hence force also, the materials have been modeled and coefficients found which will duplicate the response of the belt to selected constant strain rates. Assuming there are no discontinuous characteristics to the material, or other unknown phenomena which could occur during arbitrary strain-time waveforms, the models will predict webbing response to arbitrary strain-time waveforms at strain rates of "static" to 10/in/in/second.

A procedure was discussed to permit calculation of the model coefficients for constant strain rate inputs. The nature of the equations and the approximations required with the data, permit finding a first approximation to the coefficients desired. For a range of application, in terms of forces developed, the data can well be duplicated. Whether or not such duplication is required is discussed in a later section.

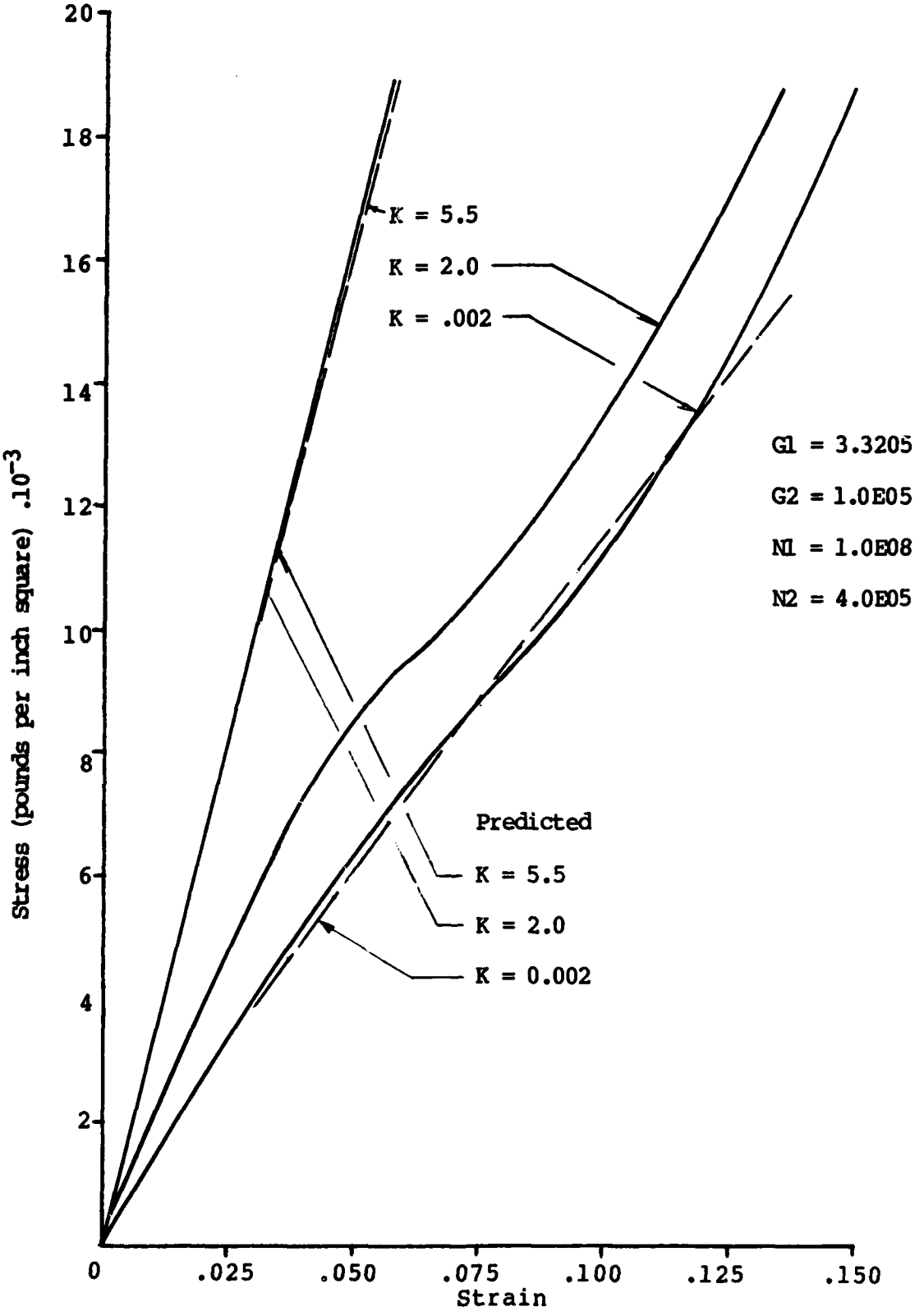

Figure 20 Predicted Stress-Strain Curves Using Computer Model for Nylon Type VIII N2 Value of 4.10^5.

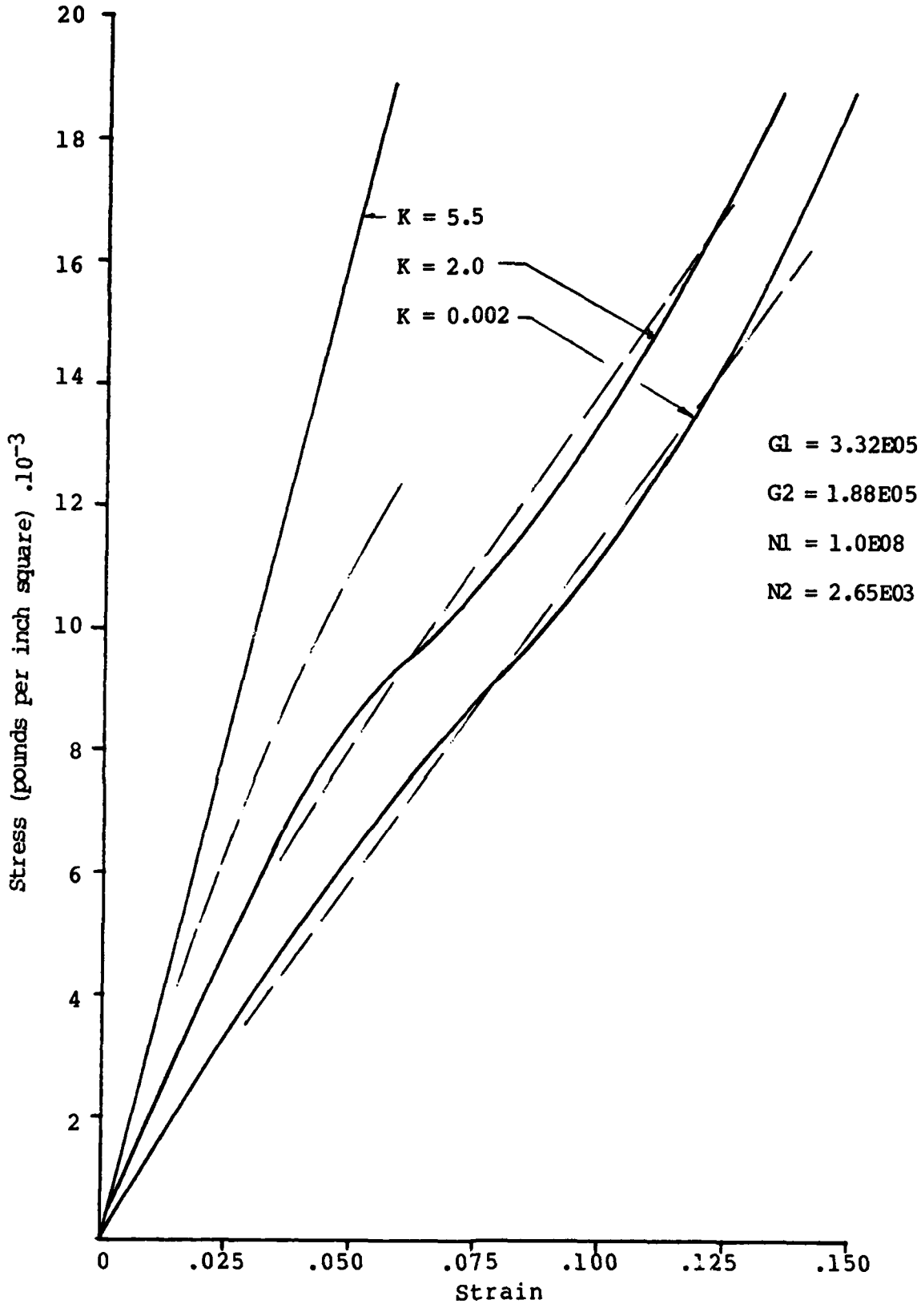

Figure 21 Predicted Stress-Strain Curves Using Computer Model for Nylon Type VIII N2 Value of $2.65.10^3$.

The procedure developed to calculate model coefficients was a manual procedure specifically for constant strain rate testing. As was pointed out, even constant strain rate devices generate transients and only approximate constant rates. Consequently, a MIMIC routine which can accept any quantitatively described strain, or strain rate, is recommended for establishing coefficients more efficiently and accurately.

SECTION 3

RESTRAINT SYSTEM MECHANICS AND HUMAN INERTIAL RESPONSE

INTRODUCTION

The restraint system consists of several components. These are: the restraint retraction and tensioning device, the straps between retraction device and harness, and the torso harness. The inertial reel, or retraction device, is a physical entity that can be taken out of the system and tested separately to determine its characteristics. Similarly, the restraint straps can be tested separately. However, it is difficult to separate harness and torso effects. The harness does have straps of known materials which can be tested. The configuration is known or can be observed and quantitatively described. But the calculation of its response on a deformable body is very difficult to analyze. While the response may be found with an exotic finite element routine, examination of the "real world" harness with its cross-weaving, buckles and adjustments, makes it questionable whether or not an "exact" analysis would be possible.

One method of circumventing complexities is to "test" around them. Since the harness with all of its complexities responds in conjunction with torso elasticity, one way to separate or eliminate the interaction is to eliminate torso elasticity. If the human torso is replaced by a rigid torso of little elasticity but with known inertial response, then testing of any harness configuration motion yields a measure of how it responds without the interaction of a crushable chest or a viscous hip joint. This was the approach used and described in this section. A rigid torso was constructed as a test device to permit tests under controlled conditions which could utilize a standard harness subjected to retraction environments of the Body Position and Retraction Device (BPRD) available at the Air Force Aerospace Medical Research laboratory. By comparing test results for a given harness fitted to the rigid torso with those when fitted to humans, the effects of harness elasticity and configuration change might be separable from those due to human inertial response.

DEVELOPMENT OF RIGID TORSO TEST DEVICE

Design Criteria

The torso developed would match the dimensions of the 95 percentile man. The torso would be free to pivot at the hips and capable of locking at that joint. The head and arms used would be rigid, clumped weights typical of the 95th percentile man and the shape of the torso duplicate as nearly as possible a typical human shape in the areas contacted by the restraining harness and retracting

belts. The compressibility of the chest would have to be an order of magnitude greater than that of the human. A test value for the stiffness of the human chest of 200 pounds per inch was believed typical [5]. The mass moment of inertia of the upper torso was to be matched, and the mass and location of the center of gravity of the upper torso were to be duplicated. The torso would be capable of sitting upright or leaning forward to the limits of the restraint system (approximately 36 degrees from vertical).

Figure 22 illustrates the coordinate system used in the analysis of the rigid torso. Tests to be performed were only concerned with the inertia about the y axis and the location of the center of gravity in the z direction; however, the dummy was to be symmetrical about the z axis. The weight and dimensions of all body segments of the rigid dummy were to be those of the 95th percentile man.

Table 3 contains typical dimensions of the 95th percentile man, location of the center of gravity, and the value of the moment of inertia. Table 4 indicates the weight of various body segments of interest [6].

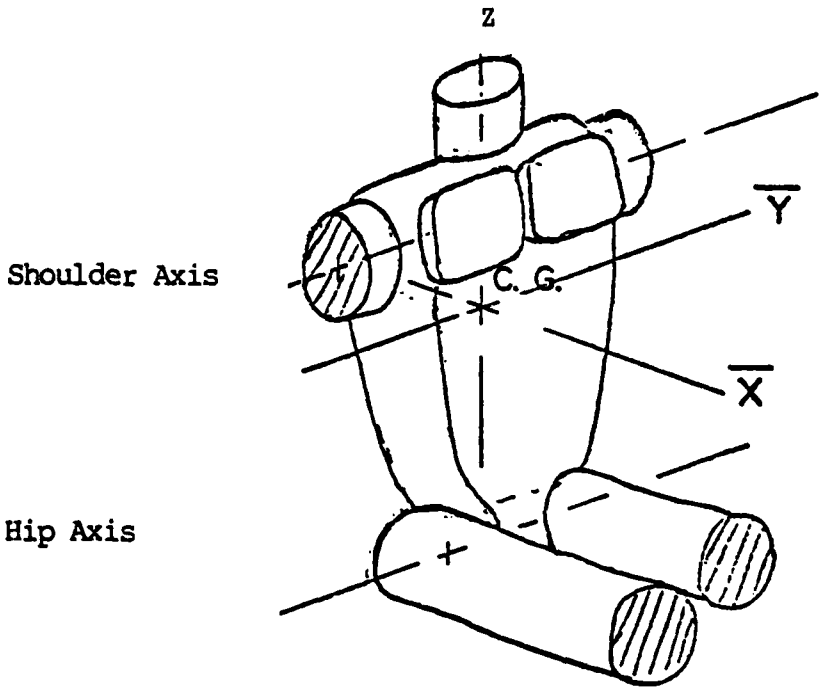

Figure 22. Coordinate System of Rigid Torso

TABLE 3. TYPICAL DIMENSIONS OF THE 95th PERCENTILE MAN

Torso Moment of inertia about y axis	1.125 slug ft.^{2}
Location of C.G. of upper torso - 13 inches above hip pivot axis - 56% of distance from hip to shoulder pivot.	
Length of upper torso hip pivot to shoulder pivot	- 23.24 inches
Chest circumference	- 43.2 inches
Waist circumference	- 37.5 inches
Upper leg circumference	- 25.3 inches
Upper leg diameter (mean)	- 8.05 inches
Neck circumference	- 16.2 inches
Neck diameter (mean)	- 5.16 inches

TABLE 4. WEIGHT OF BODY SEGMENTS FOR 95th PERCENTILE MAN

Segment	Weight Range
Total body weight	198 lb.
Upper torso	91.2 - 99.2 lb.
Upper and lower leg and foot (each)	30.8 - 33.6 lb.
Head	13.3 - 15.6 lb.
Upper and lower arm (each)	9.6 - 13.4 lb.

CONCEPTS EXPLORED

The initial concept considered was the development of the rigid torso constructed of sheets or slabs of material or box structures. Several configurations were designed and analyzed. During this phase, dimensional data were obtained and familiarity was gained with the relative proportions of the 95th percentile man as well as an appreciation for the lack of information on some body proportions especially in the neck and shoulder area. The major difficulties foreseen in the fabrication of a slab torso involved the large number of parts required which would make the fabrication cost high plus the difficulty of predicting the final mass, center of gravity, or the moment of inertia. The parts required to obtain an adequate shape would have included plates for the back, chest, shoulders, seat, hips, and upper legs, and possibly the waist area. So many variables, masses and locations, were introduced that analysis became impractical.

The second concept considered involved a basic aluminum box structure which could be used to support the arms, neck and legs with appropriate masses and centers of gravity. The box would be built up to body contour using lightweight sculptured styrofoam which could be covered by epoxy resin impregnated fiberglass cloth or tape. Questions of the final rigidity and the overall complexity and overdesign of this approach, however, led to the study of other concepts. Another approach taken was to seek a fiberglass or molded plastic store mannequin of appropriate size which could be purchased and modified by the addition of movable legs and appropriate weights.

Time was spent trying to locate a source of mannequins. Mannequin sizes were usually limited to approximately an average or small man, and most importantly, the body proportions were generally not realistic. In addition, body dimensions and stiffness data were not available which made the selection of a "useful" mannequin very uncertain.

The manufacturer of a standard test dummy was contacted with the objective of purchasing a rigid test dummy or useful dummy parts. However, prices and deliveries of these were discovered to be unreasonable for the requirement of this application.

Finally, an Alderson dummy of the 95th percentile size was obtained from AFAMRL. The test dummy would provide a rigid substructure and mounts for arms, legs, and head weights and a rigid foundation. The basic structure of the dummy would have proportions approximating a smaller man, perhaps in the 40th or 50th percentile which could be used without additions or modifications. For limb attachment it would require additional structure for a longer rigid chest and shoulders.

FINAL DESIGN

The difficulties of modifications to the Alderson dummy were overcome by adding to the dummy's steel torso substructure a rigid low mass aluminum shell backed up by 3/4-inch plywood panels. The aluminum shell, although of simple construction, provided lifelike shape and dimensions to the shoulder and neck, back, chest, and waist areas. A pair of steel tubular upper legs was added to the assembly which had appropriate mass, upper leg diameters, and hip pivot locations. These parts adequately defined the hip and seat contours. Weights within the steel Alderson upper torso structure were shifted and weights were added to increase the mass and to adjust the position of the center of gravity.

Clumped steel weights were added to the upper torso to simulate arm masses. The original head was retained. As in the original Alderson design, the torsional resistance of the hip pivots could be adjusted or locked to prevent motion.

The Alderson dummy deviated in one respect from the required dimensions shown in Table 3 in that the length from hip to arm pivots was only 20.31 inches, approximately 3 inches too short. The tolerance on the required distance is +5.3 percent (+1.23 inches). The center of gravity of the modified dummy was placed above the hip pivotat the same relative location as required in the data of Table 3.

DETAILED SPECIFICATIONS

Table 5 gives the dimensions and measured physical constants of the rigid torso which was developed. Symbols used for the measured and calculated quantities are also illustrated.

DETERMINATION OF PHYSICAL CONSTANTS OF RIGID TORSO

The rigid torso was mounted to swing in the configuration of a physical pendulum in order to measure its mass moment of inertia. A pair of steel knife edges were attached to the torso at the location of the shoulder pivots. A steel framework was fabricated so that the torso could be swung with the knife edges in contact with flat steel surfaces. These pivots provided minimal resistance to rotation such that 3 minutes time elapses before the amplitude of the swing of the torso is reduced from 1.9 degrees to 1.3 degrees (3/4-inch to 1/2-inch swing at lower extreme of pendulum). The moment of inertia of a physical pendulum is given by the equation:

$$I = (T/2\pi)^2 Mgd$$

The moment of inertia of the pendulum about an axis through the pendulum center of gravity $\bar{I}$

TABLE 5. SPECIFICATIONS OF RIGID TORSO.

Item	Symbol	Value	Units	Tolerance
Body size		95th	percentile	
Upper torso weight	W_T	99.719	pounds	$\pm$ 0.0063 lb.
Total leg weight (2)		81.797	"	
Total arm weight (2)		26.094	"	"
Head weight		12.938	"	"
Chest circumference		42-1/4	inches	$\pm$ 1/16
Chest width		14-5/16	"	"
Chest depth		9-13/16	"	"
Waist		42-1/4	"	"
Upper leg diameter		9-7/8	"	"
Upper arm diameter		4	"	"
Neck diameter		5-1/4	"	"
Arm to hip pivot length	ℓ	20.31	"	$\pm$ 0.01 in.
Location of center of gravity (above hip axis)	h	12.097	"	"
Mass Moment of inertia of torso about its center of gravity	I_{OT}	1.066	slug ft^2	$\pm$ 0.0. slug ft^2
Stiffness of Chest area	S	6000	pound/inch	1%
Weight of knife edges	W_K	3.342	pounds	0.1%

$$\bar{I} = I - md^2 = \frac{WdT^2}{4\pi^2} - \frac{Wd^2}{g}$$

where W = total weight

T = period

d = distance from pivot axis to center of gravity

g = gravitational constant.

The error in this equation as a result of the small angle approximation is zero (to four decimal places) for angles less than 2 degrees.

The calculation of the torso moment of inertia thus requires measurement of the weights of the pendulum, the distance from the pivot point to the center of gravity, and measurement of the period (time) of oscillation. Corrections must be made for the local value of the acceleration of gravity and for the effects of the mass and inertia of the knife edges used in the pendulum experiment. The results of measurements and calculations of the physical parameters of the torso as well as a discussion of the techniques and instruments used in the measurement and an error analysis follow.

STIFFNESS

The stiffness of the chest area of the modified rigid torso was measured by supporting the back area on a 6 x 9 inch steel plate and statically loading the chest with a 5-11/16 inch diameter piston. Three load versus deflection curves were obtained as the torso was loaded consecutively from 0 to 700, 1400, and 2000 pounds. The load deflection curves are presented in Figure 23. The curves all indicate a stiffness in compression of approximately 6000 lb/in. for loads from 0 to 200 lb and a stiffness of 13,000 lb/in. from 200 to 2000 lb. The lower of these values is a factor of 30 greater than would result from similar tests on a human torso.

WEIGHT

The weight of each of the components of the rigid torso was measured on a model 2081 Toledo scales with a range of 200 lb. The scales had been calibrated to an accuracy of +0.06 percent of reading with a resolution of approximately 1/2-ounce (0.031 pound). The weights of various components are given in Table 5.

ACCELERATION OF GRAVITY

The value for the acceleration of gravity at sea level and 45

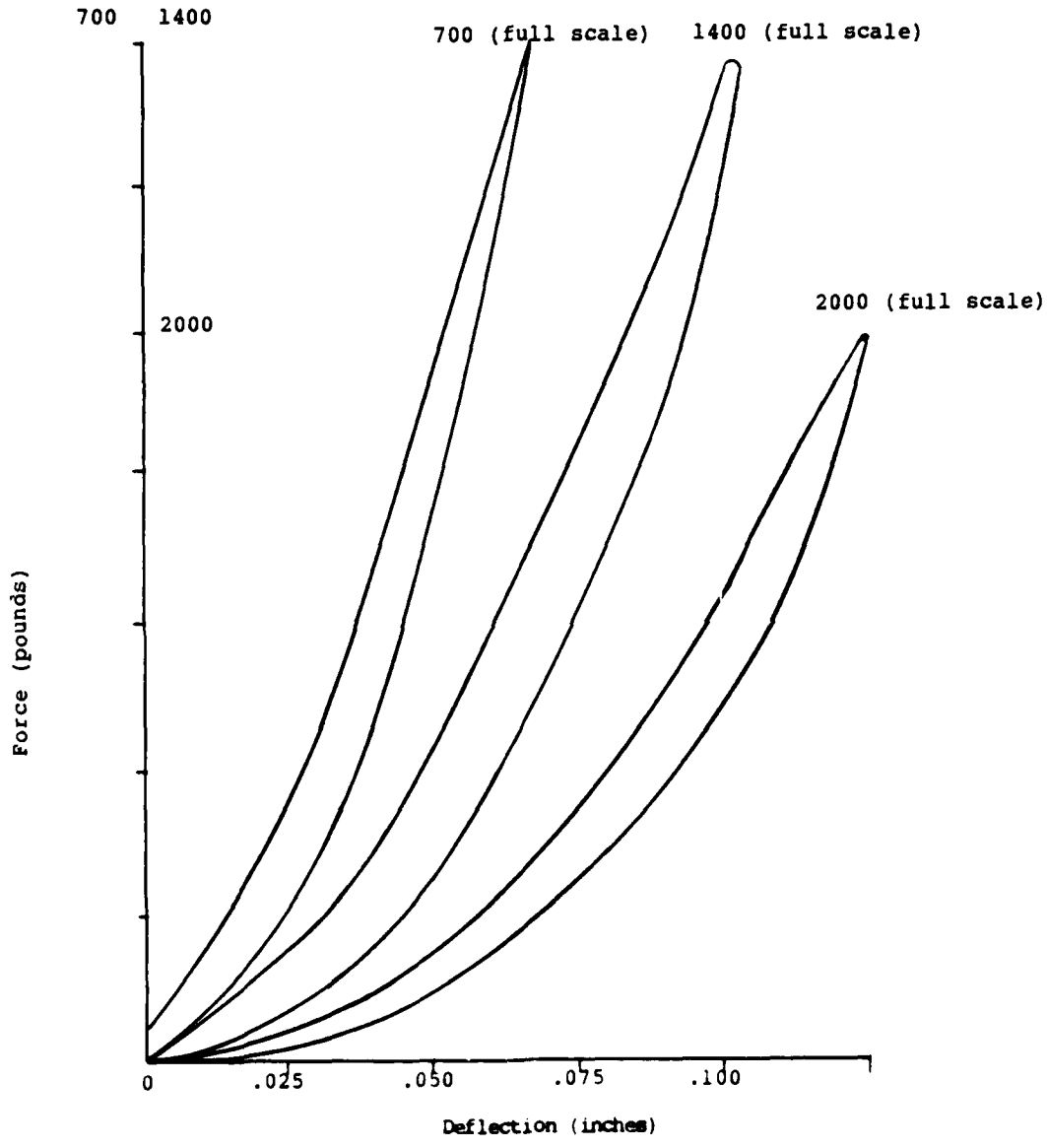

Figure 23 Load versus Deflection of Rigid Torso Chest.

degrees latitude is 32.1740 ft/sec$_2$. This value was corrected to correspond to the location of our experiment which was 39 degrees 5 minutes latitude and approximately 780 foot elevation. From the U.S. Coast and Geodetic Survey tables the value for 39 degrees 5 minutes latitude is 32.1554 ft/sec$_2$. The correction for elevation is -0.003 ft/sec$_2$ per 1000 feet. The value of g corrected to 780 feet equals 32.153 ft/sec$_2$. The correction is thus 0.06 percent.

TIMING THE PERIOD OF OSCILLATION

The period of oscillation of the pendulum was measured using a Computer Measurements Company model 915 digital time interval counter with a resolution of 1 microsecond. A noncontacting switch was constructed so that the counter was started at a point near the center of the pendulum swing and the count terminated as the pendulum returned to that position on the next swing.

The noncontact switch consisted of a fast photoelectric detector approximately 1 mm by 1 mm which was continuously illuminated by a helium neon laser beam. A small brass flag was attached to the lower edge of the swinging torso opposite to the knife edge pivot. The flag was approximately 0.5 inch long by 0.1 inch wide and 0.010 inch thick. A simple counting logic circuit was constructed which counted two light interruptions after initiating the counter, before changing voltage output level to stop the count, thus allowing the timing of a full period. The counter was started and stopped by the flag cutting the light beam from the same direction.

The pendulum's period was measured at two angles of swing corresponding to 0.2 inch and 0.75 inch movement of the flag (0.51 degrees and 1.91 degrees swing, to minimize small angle approximation error). Eleven time measurements at each angle were made at approximately 3 second intervals. Table 6 shows the results of these measurements. The period measurement for determination of the location of the center of gravity (next section) was made using the same equipment and the results are shown in the same table.

TABLE 6. PERIOD OF OSCILLATION OF PHYSICAL PENDULUM

Angle (degrees)	0.51	1.91	1.27
Average time for 10 periods (sec) (T_A)	1.206421	1.207631	
Median Value of Readings (sec)	1.206421	1.207642	1.323131
Period of Pendulum about Hip Axis (sec) (T_B)			1.323151

CENTER OF GRAVITY (c.g.)

The shape of the upper torso and lack of convenient and well-defined measuring points defeated all attempts to accurately locate the center of gravity of the upper torso by balancing it over a knife edge or other pivots. Only one useful measurement could be made on the torso that being the distance between the arm and hip pivot locations (Figure 24). It was also possible to swing the torso as a pendulum from each of these locations and to time the period precisely. The moments of inertia about these two axes were measured and equated in order to determine the C.G. location. The equations are developed below.

The moment of inertia about the centroidal axis for a physical pendulum swinging about the arm axis is:

$$\bar{I} = I - \frac{Wd^2}{g}$$

The moment of inertia about the centroidal axis for a physical pendulum swinging about the hip axis B is:

$$I_A = I_B - \frac{W}{g}(\ell - d)^2$$

where I_A = inertia about A axis

I_B = inertia about B axis

W = combined weight of torso and knife edge

g = gravitational constant.

Equating the above equations and introducing the expression for I for a physical pendulum we obtain:

$$\frac{T_A^2 d}{4\pi^2} - \frac{d^2}{g} = \frac{T_B^2}{4\pi^2}(\ell - d) - \frac{(\ell - d)^2}{g}$$

where T_A and T_B are the periods of oscillation of configurations A and B.

T_A = 1.207 (from Timing the Period of Oscillation Section)

T_B = 1.323 (from Timing the Period of Oscillation Section)

g = 32.153 ft/sec^2 (from Acceleration of Gravity Section)

ℓ = 1.776 feet.

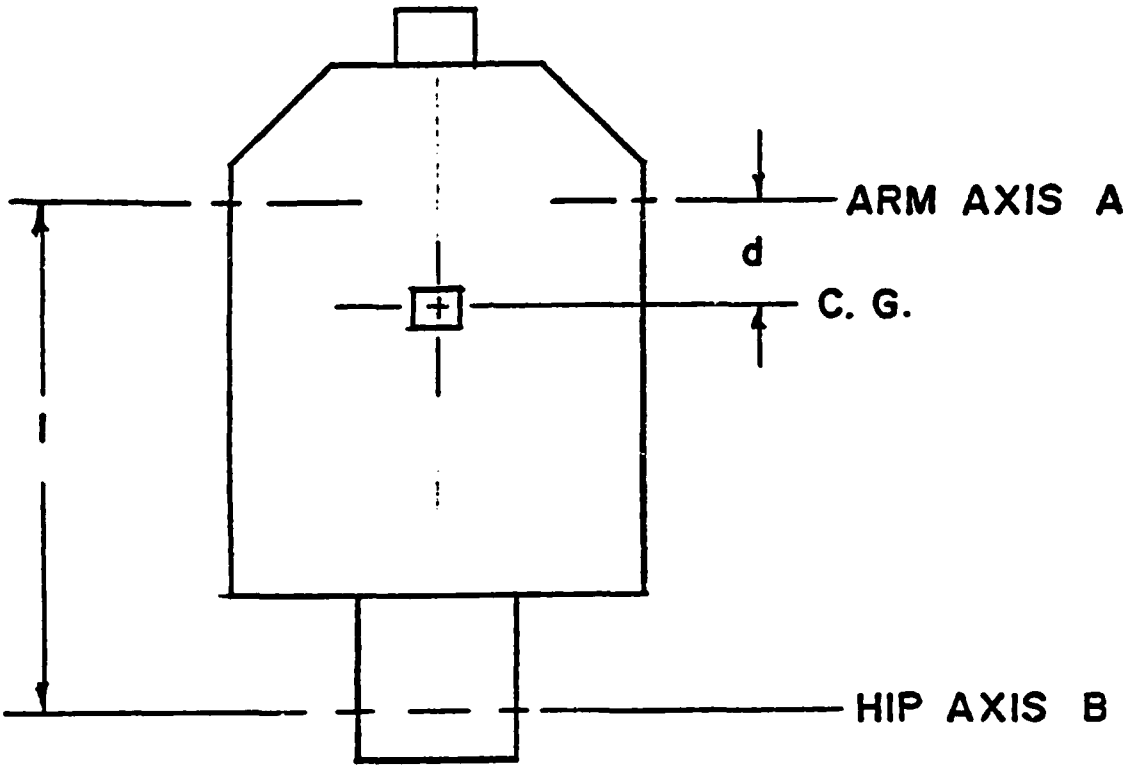

Figure 24 Location of Center of Gravity of Physical Pendulum.

The length l was measured using a vernier caliper on each side of the torso to the nearest 0.001 inch. The two values obtained were 32.323 and 31.303 inches. The average value of 31.313 inches (1.776 ft) was used for the calculation of d. The value for d obtained from performing this analysis was 0.6622 feet or 7.9469 inches.

CALCULATION OF THE MASS MOMENT OF INERTIA I. OF THE PHYSICAL PENDULUM ABOUT THE SYSTEM CENTER OF GRAVITY

The equation required is:

$$I = \frac{T_A^2}{4\pi^2} Wd - \frac{Wd^2}{g}$$

where T = period of oscillation

W = weight of torso and knife edges ($W_K + W_T$)

d = length from axis of rotation (arm) to system center of gravity.

T_A = 1.207 sec (from Table 4)

W_T = 99.719 lb (from Table 3)

W_K = 3.342 (from Table 3)

g = 32.153 ft/sec^2 (from Acceleration of Gravity Section)

d = 0.662 ft (from Center of Gravity Section).

By performing the above calculation the value of I is found to be:

1.113 slug feet^2.

CORRECTION IN C. G. POSITION WITH KNIFE EDGE PIVOTS REMOVED

The knife edges which were added to the upper torso at the location of the upper arm axis were also used in determination of the location of the center of gravity. They raised the center of gravity about the C. G. of the torso mass. The location of the C. G. of the torso was determined analytically by taking moments about the measured C. G. location. The weight of the knife edges and the torso were measured independently. (See Figure 25.)

$$W_K d = W_T X$$

$$X = \frac{W_K d}{W_T} = 0.2662" = 0.022'$$

The location of the center of gravity of the torso above the hip axis (h) was therefore:

$$l - d - x = h = 12.097 \text{ inches}$$
$$= 1.008 \text{ feet.}$$

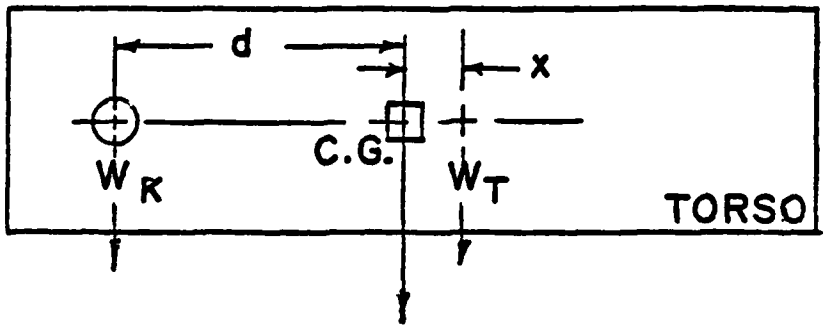

Figure 25. Shift of Center of Gravity with Knife Edges Removed.

W_K = weight of knife edges
= 3.342 lb. (Table 3)

W_T = weight of torso
= 99.719 lb. (Table 3)

C.G. = measured center of gravity

d = calculated location of C.G.
= 7.947 inches = 0.662 feet (paragraph 6.5)

x = shift in C.G. location after removal of knife edge mass.

This position is approximately 0.6 of the distance from the hip pivot to the arm pivot.

CALCULATION OF KNIFE EDGE MASS INERTIA

A sketch of the steel knife edges used to swing the torso as a pendulum is shown in Figure 26. The centerline of the knife edge is the axis of rotation of the physical pendulum. The moment of inertia of the two knife edges is calculated in two parts. First, for the right circular cylinder (I_C) and then for the 60 degree segment of the cylinder (I_S). The equation for the right circular cylinder is:

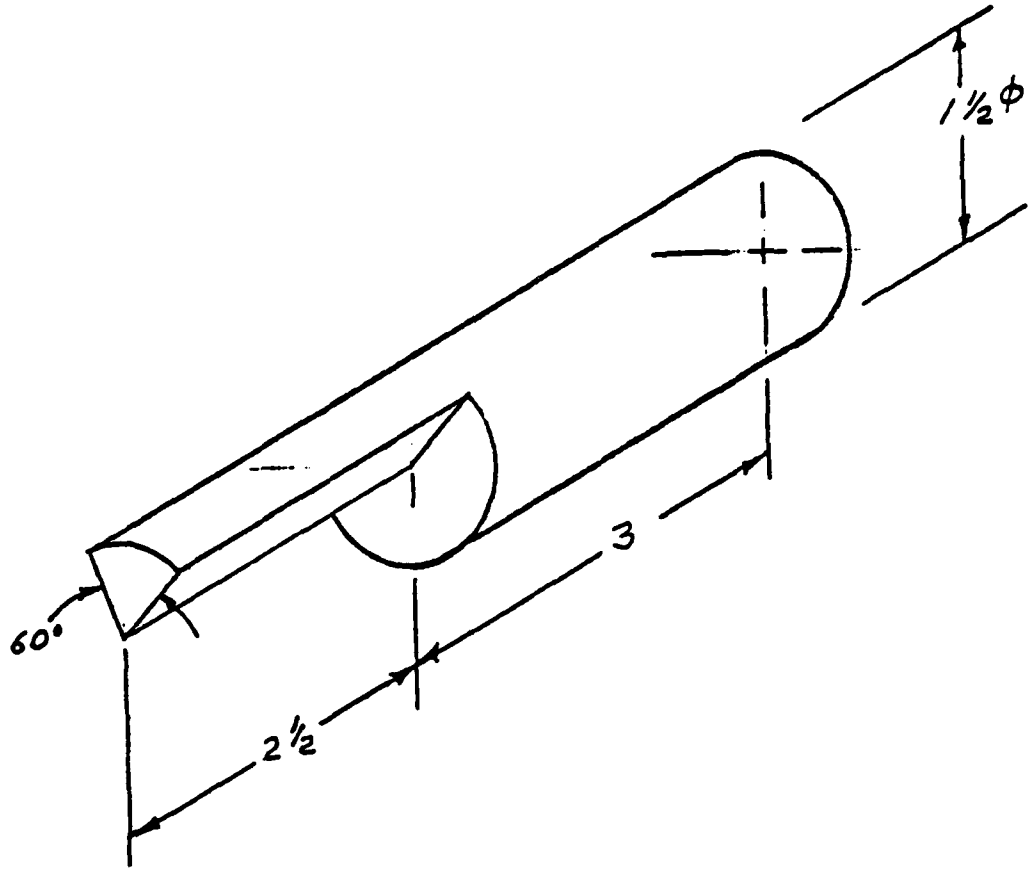

Figure 26 Knife Edge Pivots.

$$I_C = \frac{1}{2} m r^2$$
$$= \frac{\pi r^4 \ell \rho}{2}$$

where r = 3/4 inches = 0.063 feet

ℓ = 3 inches = 0.25 feet

ρ = mass density = 15.206 slug feet^3.

I_C for two knife edges is thus 1.822 x 10^{-4} slug feet^2.

From the 60 degree segment of the cylinder the equation for inertia is:

$$I_S = \frac{\pi t r^4 \rho}{12}$$

where t = 2-1/2 inches.

I_S for two knife edges is 0.253 x 10^{-4} slug feet^2.

The total moment of inertia for both knife edges I_{OK} is 0.000207 slug feet^2. This value is negligible compared to the value I obtained for the system and can thus be ignored in the correction.

DETERMINATION OF MOMENT OF INERTIA OF TORSO

The moment of inertia of the torso along I_{OT} about its center of gravity may be determined from the measured moment of inertia of the system by removing the effects caused by the knife edge supports.

The moment of inertia of the physical pendulum I (see Figure 27) equal:

$$I = I_{OK} + I_{OT} + \frac{W d^2}{g} + \frac{W x^2}{g}$$

where I_{OK} = moment of inertia of knife edges about axis of rotation

= 0.0002 slug feet^2 (from Calculation of Knife Edge Mass Inertia Section)

I_{OT} = moment of inertia of torso about torso C. G.

d = distance from axis of rotation (arm) to the system center of gravity

x = 0.662 feet (from Center of Gravity Section)

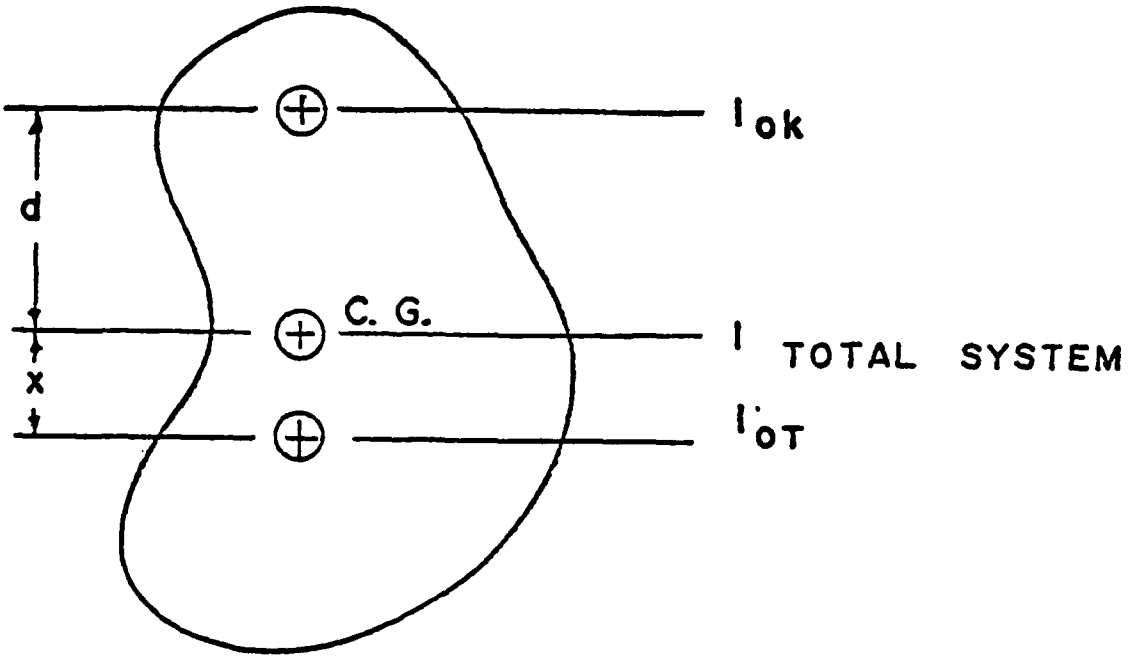

Figure 27 Moment of Inertia of Torso.

x = distance from center of gravity of torso to system center of gravity

= 0.022 feet (from Correction in C. G. Position with Knife Edge Pivots Removed)

I = 1.113 slug feet^2 (from Calculation of the Mass Moment of inertia I, of the Physical Pendulum About the System Center of Gravity

W_T = weight of torso

= 99.719 lb (from Table 3)

W_K = weight of knife edges

= 3.342 lb (from Table 3)

g = 32.153 ft/sec^2 (from Acceleration of Gravity Section).

The torso moment of inertia I_{OT} therefore equals:

$$I_{OT} = I - I_{OK} - \frac{W_K d^2}{g} - \frac{W_T x^2}{g}$$

The moment of inertia I_{OK} for the knife edges is small and is neglected, so that:

$$I_{OT} = I - \frac{W_K d^2}{g} - \frac{W_T x^2}{g}$$

The value of the moment of inertia of the torso is found to be 1.066 slug feet^2.

ERROR ANALYSIS

The effects of measurement errors in each of the measured parameters involved in the calculation of the moment of inertia of the physical pendulum were determined by assuming an error of +0.1 percent in the value of the moment of inertia and calculating the variation in each of the measured parameters which would cause that error. Nominal values for each parameter were used in the calculations and all were held constant except the parameter being investigated. This analysis gives some idea of the measurement accuracy required for each parameter. Table 7 shows the results of this analysis. By comparing the magnitude of the parameters with the established measurement accuracy the timing and measurement of weight and length are apparently within the values required for a 0.1 percent change in mass moment of inertia.

TABLE 7. RESULTS OF ERROR ANALYSIS.

	Moment of Inertia I	Weight W_T	Weight W_K	Time of Period T_A	Acceleration of Gravity g	Location of Center of Gravity d	Location of Center of Gravity ℓ
	slug ft^2	lb	lb	sec	ft/sec^2	inches	inches
Nominal Value	1.066	99.719	3.342	1.207000	32.153	7.9464	21.3120
Variation in Parameter to Cause 0.1% Error in I							
Positive Error of 0.1% in I	1.067	0.0927	-0.270	0.000240	0.022	-0.020	-0.024
Negative Error of 0.1% in I	1.065	-0.0927	0.270	-0.000240	-0.022	0.020	0.024
	% Error in Parameter	0.09	8.1	0.002	0.07	0.25	0.11

TESTING OF THE RIGID TORSO TEST DEVICE

The rigid torso was tested in the Body Positioning and Restraint Device (BPRD). The parameters controlled are retraction length and hydraulic pressure for a given subject and restraint configuration. The retraction length is measured directly at a piston rod that retracts. The torso retraction was therefore thought to be identical to piston stroke. The hydraulic pressure device delivered to the actuator is the variable causing a change in the test environment. The stroke lengths have been varied from a maximum of 18 inches, and pressures have been varied from 200 to 900 psi with human subjects.

The tests conducted were to measure the response in such a manner that the results could be used to separate harness effects from human response effects. Therefore, the rigid torso was tested in environments where data were available from human subject tests. Data were available for humans tested at 600 to 900 psi hydraulic pressure and 12 and 14 inches stroke lengths using an integrated parachute harness, PCU-15/P. The harness was attached through simulated parachute risers to a wire cable which in turn was attached to the retraction piston. The parachute harness fittings were standard USAF Koch fittings and the parachute risers were standard 1-3/4-inch wide nylon webbing.

The human subjects were placed in the BPRD, seated snugly by adjustment of seat belt and riser straps, and the retraction length was established by releasing the piston the required distance. The subject then leaned forward with enough effort to place a 20 pound preload on the retraction cable.

The tests conducted with humans were instrumented for cable force, retraction motion, chest accelerations, head accelerations, seat pan force and seat back force. High speed photographic data were also recorded. Similar measurements were required for the rigid torso except for the head accelerations which would not exist.

The test environments selected for the rigid torso were stroke lengths of 4.5, 9.0, 12.0, and 14.0 inches, with 600 and 900 psi actuator pressure. The larger stroke lengths and actuator pressure were selected to duplicate the human test environments and the lesser values were selected since it seemed reasonable to test at stroke lengths of more "operational" value rather than an extreme required by a specification. The eight tests were to be conducted using the rigid torso with PCU-15/P harness and with a fixed cable attachment at the back of the neck. By using the rigid torso alone the test device would be calibrated in that a retraction acceleration acting against a freely pivoted rigid body would generate a torso acceleration proportional to the applied cable force. Torque should equal mass moment of inertia times angular acceleration. Even though the torso had been calibrated in finding the mass moment of inertia, verification from measured data collected on the test device was desireable. The tests conducted later with the harness would then provide a measure of the effects of the harness on the torso even though the torso is rigid.

The rigid torso, referred to as the "tin man" was installed in the BPRD and instrumented by the same individuals who conducted the previous human test series. Chest accelerometers were installed in the same manner, the position established in the same manner, and the same harness fittings and cable were used. A special fitting was constructed to provide a pinned attachment at the back of the neck for the tests conducted without the harness.

Data were collected and outputs provided in the forms shown in Figures 28 and 29. The cable force shown is actually twice the parachute riser force desired since the measuring force cell measures cable forces over a pulley. The actuating cable goes vertically over the pulley and vertically down to another to retract the subject. Hence, the cable force and forces in the cell differ by a factor of two.

Eight tests were conducted for four stroke lengths and two hydraulic pressures. The rigid torso during installation behaved statically as though pinned at the hip joint. A strip of masking tape was used to hold the vertical position since the torso fell with the slightest disturbance. During the testing maximum stroke lengths desired had to be reduced to alleviate any interference of lap belt and torso at the hip joint.

DEVELOPMENT OF A RIGID TORSO MODEL

The first step in the development of a restrained human model is that of generating a model for a rigid torso. Since "tin man" had been developed and could be tested under controlled conditions, the test results should verify the calculated response of a rigid body to a known input. Harness effects and torso effects could then be incorporated as additional test data were available.

A restrained and seated man can be idealized as two masses connected at a pivot point as shown below.

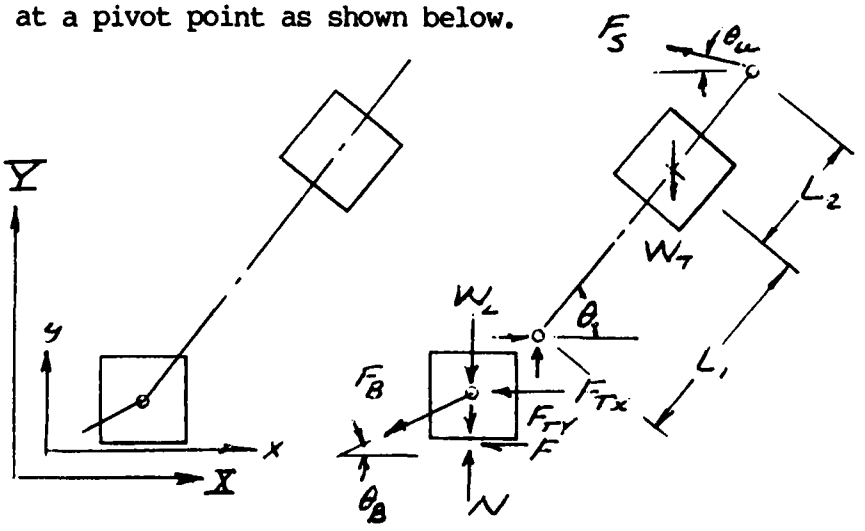

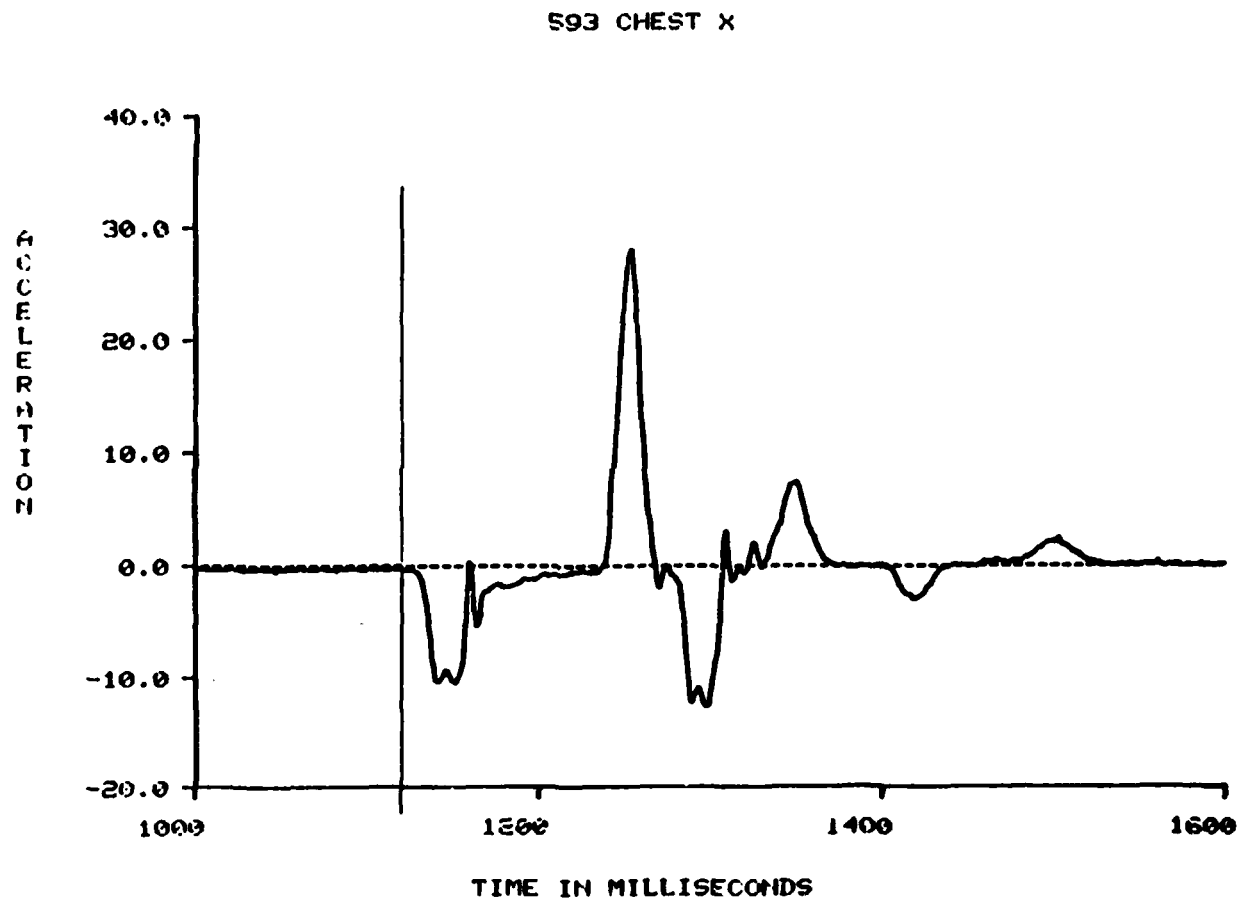

Figure 28. Typical Output Data for Rigid Torso Tests, Input Acceleration versus Time.

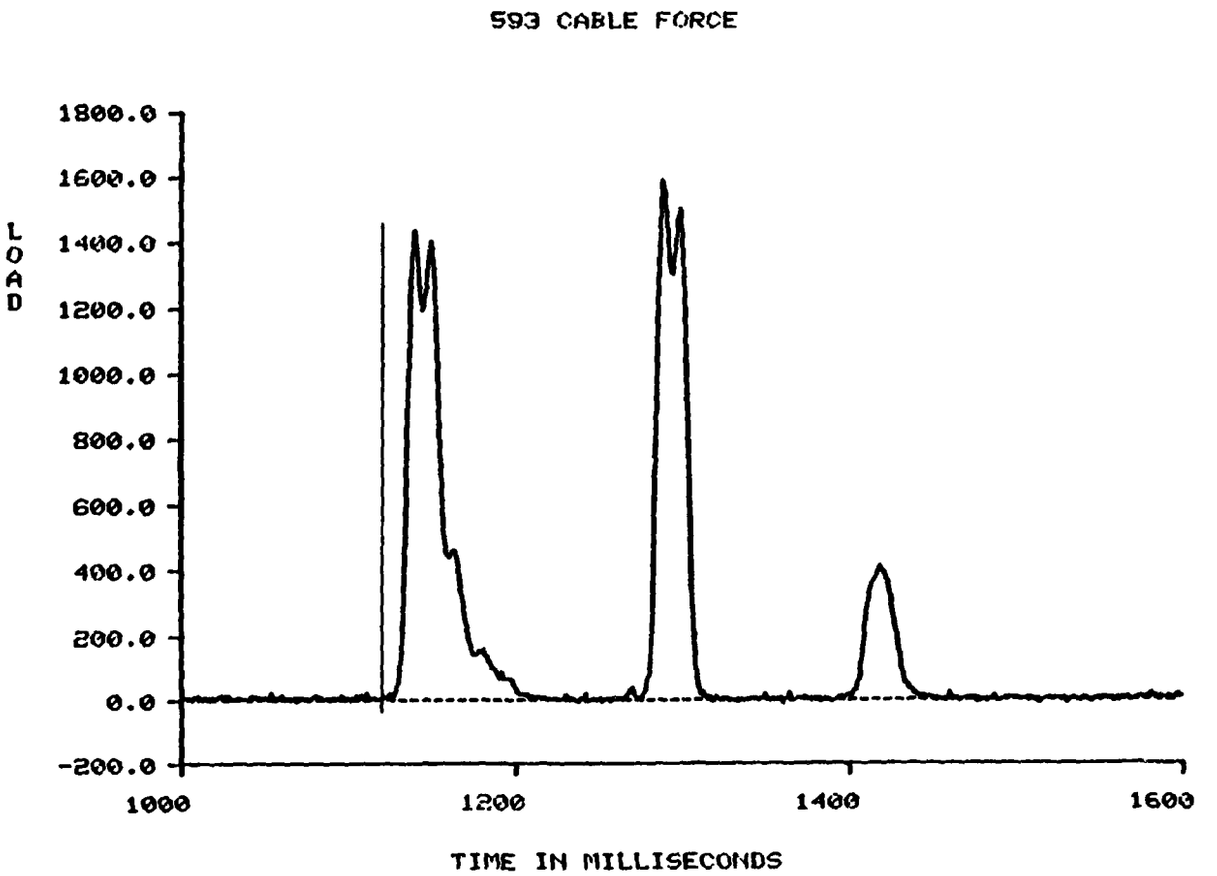

Figure 29. Typical Output Data for Rigid Torso Tests, Cable Force versus Time.

The upper mass represents the torso and upper extremities, the lower mass the lower extremities. Both masses are connected at a frictionless attachment point and are restrained by belts at a "shoulder point" and "hip joint". The system is contained within an inertial reference system X-Y and a local reference system which is the same whether representing the aircraft or a test bed. Inputs to the man come through the acceleration of the belt attachment points X_0 and X_1.

The equations of motion for the bodies are found in a classical Newtonian approach.

For the lower body: $\Sigma F_x = ma_x$

$$-F_B \cos\theta_B - F - F_{TX} = m_L \ddot{X}_L$$

where F_B is the force of the lower belt

F is the friction developed at the seat pan

F_{tx} is the force generated by the torso element at the hip joint

θ_B is the angle that the seat belt makes with the horizontal axis.

The forces are assumed to be positive to the right or upward. Consequently, the equations reflect friction acting against positive motion. Hence the friction, F, must be specified as:

$$F_B = F_B \text{ for } F_B > 0$$

$$F_B = 0 \text{ for } F_B < 0,$$

which states that if the deformation between lower body and seat attempts to generate a compressive force, the force is automatically set to zero.

$$\Sigma F_Y = ma_Y$$

$$-F_B \cos\theta_B - W_L - F_{TY} + N = m_L \ddot{Y}_L = 0$$

where W_1 is the weight of the lower torso

N is the normal force of the seat pan on the lower body

F_{ty} is the vertical component of the force generated by the torso mass.

The normal force is either compressive or zero. Hence, $N = 0$ for $N < 0$. The angular equation is not applicable since the assumed motion is that of a "particle" not a body.

For the upper body: $\sum F_x = ma_x$

$$-F_S \cos\theta_u + F_{TX} = M_T \ddot{X}_T$$

where $_u$ is the angle the upper shoulder belt makes with the horizontal.

$$F_y = ma_y$$

$$F_S \sin\theta_u - W_T + F_{TY} = M_T \ddot{Y}_T$$

where the subscript T implies the torso.

$$\sum M = I_T \ddot{\theta}_T$$

$$F_S L_2 \sin(\theta_u + \theta_T) + F_{TX} L_1 \sin\theta_T - F_{TY} L_1 \cos\theta_T = I_T \ddot{\theta}_T$$

where L_2 is the distance from torso center of gravity to the shoulder attachment point, and

L_1 is the distance from torso center of gravity to the hip pivot joint.

The system can be solved by specifying the motion in terms of two selected degrees of freedom which are then programmed. The two selected were X_L and θ_T which implies that the lower torso never leaves the seat pan. That is, Y_L must be zero and the lower particle slides along the seat pan surface.

The basic equation for X_L motion is:

$$M_L \ddot{X}_L = -F_{TX} - F - F_B \cos\theta_B$$

and the terms are:

$$F_{TX} = M_T \ddot{X}_T + F_S \cos\theta_u$$

$$F = \mu N = \mu (F_B \sin\theta_B + W_L + F_{TY})$$

$$F_{TY} = M_T \ddot{Y}_T + W_T - F_S \sin\theta_u$$

Therefore,

$$M_L \ddot{X}_L = -M_T \ddot{X}_T - \mu M \ddot{Y}_T - \mu (W_L + W_T)$$
$$-F_S \cos\theta_u + \mu F_S \sin\theta_u - \mu F_S \sin\theta_B$$
$$-F_B \cos\theta_B$$

The kinetic relations that exist between the translational accelerations are:

$$\ddot{X}_y = \ddot{X}_L - L_1 \sin\theta_t \ddot{\theta}_t - L_1 \cos\theta_t \dot{\theta}_t^2$$

$$\ddot{Y}_t = \ddot{Y}_L + L_1 \cos\theta_t \ddot{\theta}_t - L_1 \sin\theta_t \dot{\theta}_t^2.$$

Therefore:

$$M_L \ddot{X}_L = M_t L_1 \sin\theta_t (\ddot{\theta}_t + \mu\dot{\theta}_t^2) + M_t L_1 \cos\theta_t (\dot{\theta}_t^2 - \mu\ddot{\theta}_t) - \mu(W_L + W_t) - F_s (\cos\theta_u - \mu\sin\theta_u) - F_B (\cos\theta_B + \mu\sin\theta_B).$$

This establishes the equations for translational acceleration of the lower body in terms of the torso angular response.

The torso angular acceleration is:

$$I_t \ddot{\theta}_t = F_s L_2 \sin(\theta_u + \theta_t) + F_{tx} L_1 \sin\theta_t - F_{ty} L_1 \cos\theta_t$$

which generates the equation:

$$\ddot{\theta}_t (I_t + M_t L_1^2) = F_s L_2 \sin(\theta_u + \theta_t) - W_t L_1 \cos\theta_t + M_t L_1 \sin\theta_t \ddot{X}_L + F_s L_1 (\sin\theta_u \cos\theta_t + \cos\theta_u \sin\theta_t).$$

Therefore:

$$\ddot{\theta}_t = \{F_s L_2 \sin(\theta_u + \theta_t) - W_t L_1 \cos\theta_t + F_s L_1 \sin(\theta_u + \theta_t) + M_t L_1 \sin\theta_t \ddot{X}_L\} \cdot \left[\frac{1}{(I_t + M_t L_1^2)}\right]$$

which is written

$$\ddot{\theta}_t = f(\ddot{\theta}_t, \ddot{X}_L)$$

as an implicit function in the computer routine.

The belt forces are functions of the belt elongation and rate of elongation. For one belt:

$$F_s = K_s \delta_s + C_s \dot{\delta}_s$$

where K_s is the stiffness

C_s is the damping coefficient

δ_s is the relative displacement between attachment points, and

$\dot{\delta}_s$ is the relative velocity between attachment points.

The equations discussed were programmed using MIMIC and the routine is shown in Appendix A.

ANALYSIS OF TEST DATA USING RIGID TORSO MODEL

The input accelerations measured at the BPRD piston were used as inputs to the rigid torso model. The values of mass moment of inertia, weight and center of gravity location were taken from the measured data of a previous section, and the locations of attachments points on the torso and at the point of cable retraction were from measurements made at the test location.

The computed results shown in Figure 30 show the impossibility of duplicating measured data with the analytical model. Since the characteristics of the torso were known, and since the locations of attachments and accelerometers were measured, we assumed that the model was correct and the instrumentation data were incorrect or misinterpreted. If the instrumentation data were properly calibrated and processed, then the data were misinterpreted. From simple torque equals moment of inertia times angular acceleration, it appeared that the forces were correct when compared with resulting accelerations. Therefore, the input acceleration which created the force was suspect.

The force generated by the retraction cable depends upon the elasticity of the cable, the relative deformation between actuator and cable attachment to the harness, and any deformation in the support structure between actuator and harness. As the force builds in the cable, the supporting structure deforms slightly and the cable elongates. If the displacement between actuator and harness is described in terms of cable length and possible structural deformation in the direction of harness motion, the acceleration input to the torso is not the acceleration of the piston. The force at the piston and harness may be the same but the acceleration is not.

The next step was to include an elastic element into the computer

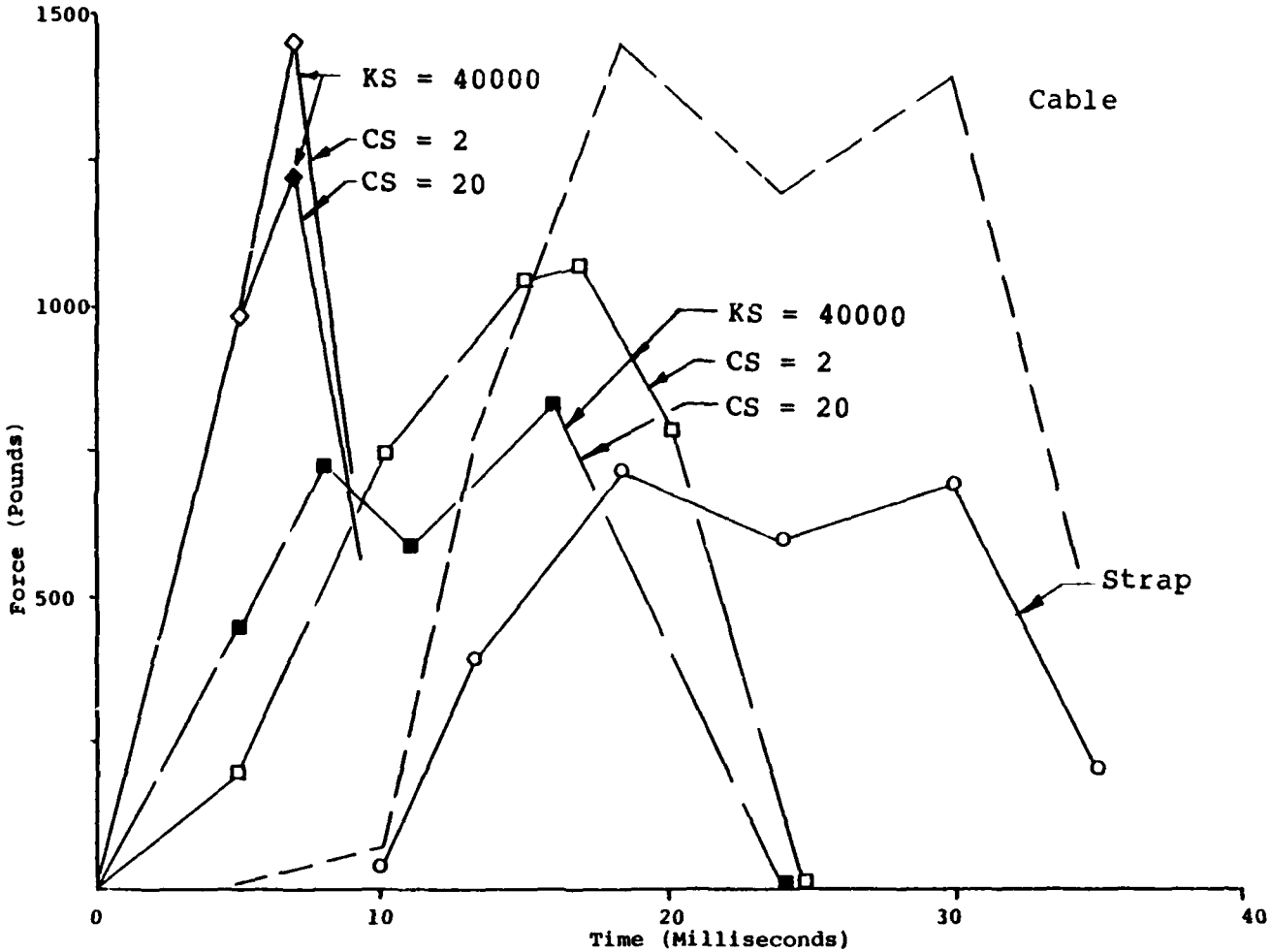

Figure 30 Computed Rigid Torso Response Compared with Measured for Initial Rigid Torso Model.

routine to reflect cable/structural elasticity. Several values of stiffness and damping were tried before a good fit in magnitude and phase was found. Figures 31 and 32 are indicative of the fits achieved. These indicate that whenever the BPRD is used to test a device or a human, the cable and structure introduce another element into the total system being considered. If the retraction is only an input which creates measured outputs correlating with themselves, chest acceleration versus head acceleration versus cable force, then there is no need to recognize the cable existence. When desirable to relate input acceleration to torso response, then the cable must be considered although the effect may be small.

The data indicate that the cable force and chest accelerations of a rigid torso can be duplicated using the BPRD actuator acceleration as input, if a cable of 900 pounds per inch stiffness and 0.2 pounds per inch per second damping coefficient are used in series with the torso.

DISCUSSION OF HUMAN HARNESSED TEST DATA

Before going into the development of a harnessed rigid torso model it is necessary to discuss the motions observed from human test data. This is necessary since it is desired to eventually have elements in the model compatible with the human, not elements unique to a harnessed rigid torso.

Data from several tests conducted by AFAMRL during a design criteria study were collected. Complete files of instrumentation data and processed outputs were available with high speed photography. The film data showed that the motion of the human torso was not in phase with the motion of the retraction cable because of several phenomena.

The test protocol stated that the subjects were seated erect with back firmly against the seat back before the retraction piston was extended to the desired length. The subject then leaned forward into the shoulder straps to create the preload. At this time the lower forward components of the harness become slack as indicated by the loops of the webbing conforming to the upper curvature of the thighs.

As the retraction begins, the Koch fittings that attach the harness to the straps travel upward over the chest without noticeable torso motion. The fittings slide up while the lower harness appears to rotate over the torso, and the lap belt is raised. This motion suggests that there is a period of time when the lower straps of the harness are seeking an equilibrium configuration. The motion is not dictated by any material property but by a configuration change. The configuration change occurs simultaneously with a compression of the bottom surface of the thighs.

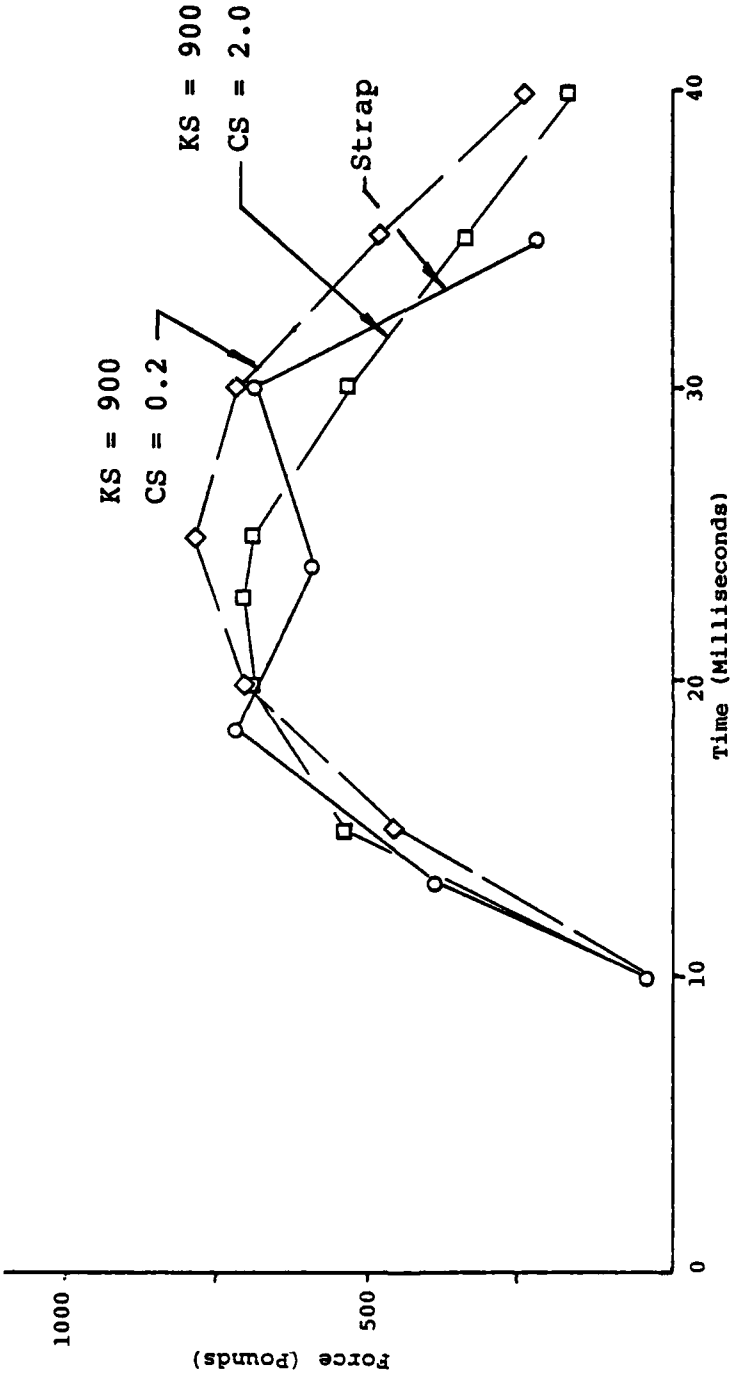

Figure 31 Computed Force versus Measured for Rigid Torso/Cable Model.

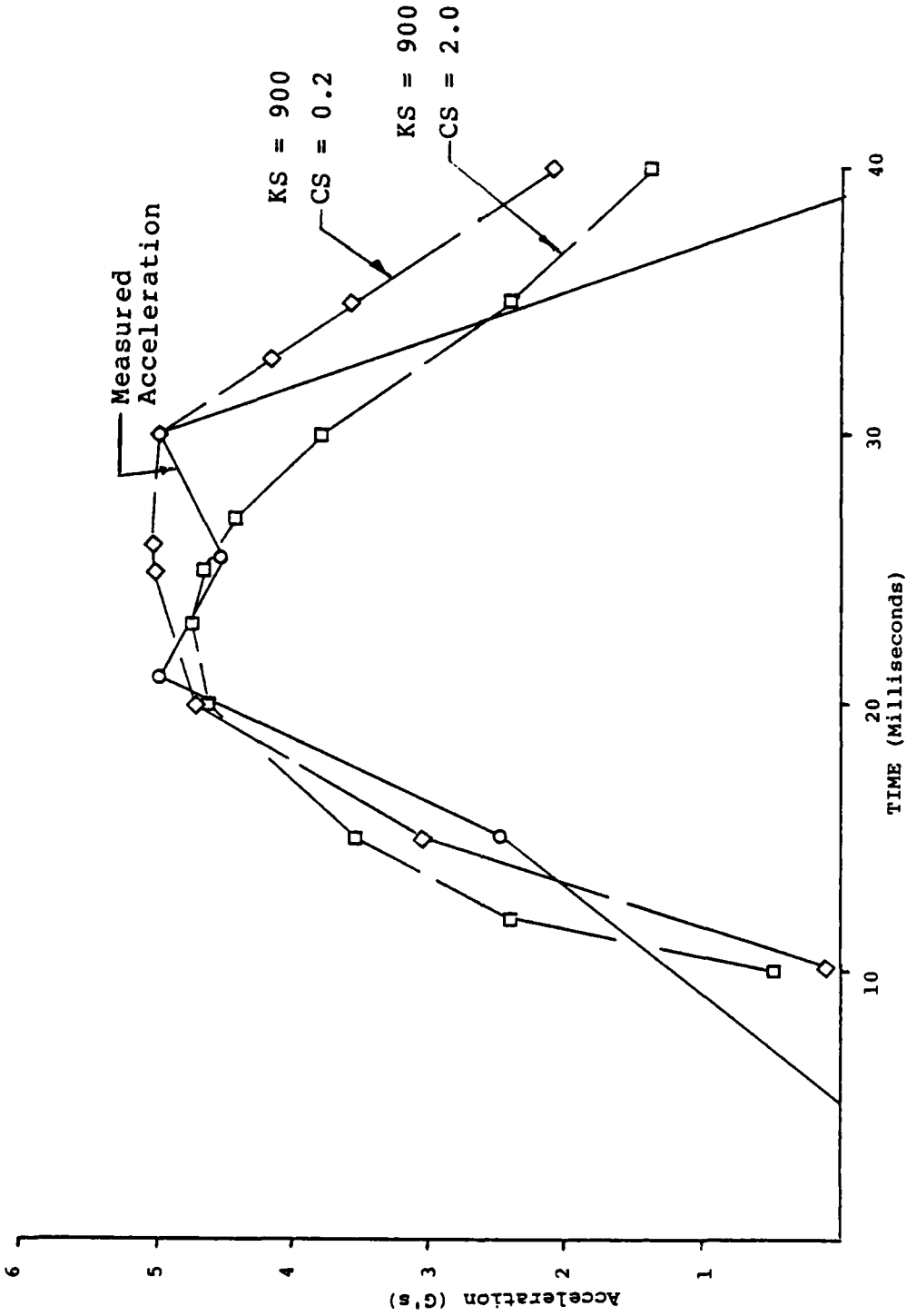

Figure 32 Computed chest Acceleration versus Measured for Rigid Torso/Cable Model.

At the end of the configuration change phase, the torso begins its backward motion and the Koch fitting remains fixed relative to the torso. At the end of the retraction, the torso moves into the seatback and the shoulders slide under the restraint straps. During this last phase the Koch fittings return approximately their original position relative to the torso.

The motion observed was quantitatively described by tracking the motion of piston and Koch fitting during retraction. The data and list of symbols are shown in Tables 8 and 9 for the tests used. The data indicate that photographically it is possible to determine the motion desired. Both piston stroke lengths observed are reasonable estimates of true actuator motion in that there is a "cushion" within the actuator which would cause the slight difference between observed stroke at "apparent" stop and preselected 12 or 14 inches of stroke.

From the analysis presented we assumed that the harness would have to be modeled by a bilinear elastic element. The configuration change phase obviously creates excessive motion with little force buildup and is followed by another phase where torso inertia, elasticity, and harness elasticity are effective. By assuming a bilinear harness for the rigid torso it is possible to isolate configuration change and harness "elasticity" before examining the interaction with the human torso.

DEVELOPMENT OF RIGID TORSO/HARNESS MODEL

The previous model development indicated the need for a representation of the cable and associated support structure in order to duplicate torso response as dictated by piston acceleration. The next requirement to be met was that of duplicating the response of a harnessed rigid torso. The cable acts through a strap and then into the harness, the harness rotates on the torso with applied force, therefore, in order to predict torso response, all components of the system must be represented in order to permit eventual evaluation of human torso characteristics.

The tests conducted using a harness and rigid torso were modeled by assuming a configuration as shown below.

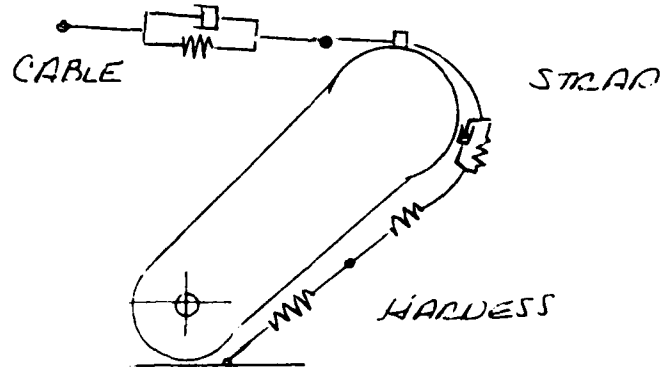

Table 8. Reduced Photographic Data Data For Human Tests With 12 Inch Piston Stroke

Test	t_1	t_2	t_3	S_{p1}	S_{p2}	S_{c1}	S_{c1}/S_{p1}	$\bar{V}_p$
456	0.028	0.110	0.112	2.90	11.43	2.45	0.845	8.66
461	0.070	0.150	0.126	3.35	11.59	2.63	0.785	6.44
462	0.062	0.130	0.114	3.87	11.45	3.45	0.891	7.35
467	0.036	0.154	0.108	3.84	11.90	2.40	0.625	6.44
468	0.054	0.126	0.108	3.41	11.42	2.16	0.633	7.56
MEAN	0.050	0.134	0.114	3.47	11.56	2.62		7.29
σ	0.018	0.018	0.007	0.40	0.20	0.49		0.92

t_1 = TIME BETWEEN FIRST OBSERVED MOTION OF PISTON AND SUBJECT.

t_2 = TIME BETWEEN FIRST OBSERVED MOTION OF PISTON AND APPARENT STOP.

t_2 = TIME BETWEEN FIRST OBSERVED MOTION OF SUBJECT AND APPARENT STOP.

S_{p1} = PISTON TRAVEL DURING t_1 (INCHES)

S_{p2} = PISTON TRAVEL DURING t_2 (INCHES)

S_{c1} = HARNESS FITTING TRAVEL DURING t_1

$\bar{V}_p$ = AVERAGE PISTON VELOCITY (FEET/SEC)

Table 9. Reduced Photographic Data Data For Human Tests With 14 Inch Piston Stroke

Test	t_1	t_2	t_3	S_{p1}	S_{p2}	S_{c1}	S_{p1}	V_p
457	0.040	0.144	0.140	3.97	13.76	2.66	0.670	7.96
458	0.040	0.148	0.104	4.18	13.46	3.21	0.768	7.58
459	0.040	0.132	0.128	3.41	13.48	2.49	0.730	8.51
460	0.034	0.124	0.128	3.68	13.60	1.75	0.476	9.14
464	0.038	0.124	0.130	4.42	13.60	2.73	0.618	9.14
466	0.030	0.116	0.130	3.50	13.30	2.82	0.806	9.55
MEAN	0.037	0.131	0.133	3.88	13.53	2.61		8.65
σ	0.004	0.013	0.006	0.38	0.16	0.48		0.76

The torso is retracted by a belt consisting of a cable, shoulder straps, and the torso harness. The cable "properties" have been evaluated and the strap material properties have been isolated. The harness is represented by an elastic element which may or may not be linear. The force developed in each element must be equal to the force in any other element, and the total displacement is equal to the displacement of the piston minus the motion of the torso in the direction of the cable.

As the cable retracts the harness over the torso, the lap belt over the thighs are raised in addition to torso harness rotation. Consequently, the force is acting beneath the thighs to raise them. If this force is carried as a force and moment to the hip joint, the torso then carries the force in equilibrium with the same force applied at the shoulders. This is the same as the shoulder joint. As the shoulder straps are retracted, they pass over a frictionless shoulder "roller." The pin holding the shoulder balances the roller with equal and opposite forces from the torso. Hence, the torso is drawn back by the belt force and compressed by the component along the spinal axis. With these assumptions, the torso is retracted by a system which is not influenced by curvature over the chest and depends only upon piston motion and torso response. True motion of the harness is buried within the coefficient found for the harness which will match both cable force and observe harness displacement.

One element of the restraint system is a cable represented by an elastic and viscous element. This is referred to as a two-parameter solid since for any long term applied force, the model ultimately behaves as a solid. The differential equation of motion is:

$$\sigma = q_1 \dot{\varepsilon} + q_c \varepsilon$$

where σ is the stress

$\dot{\varepsilon}$ is the strain rate

ε is the strain

q_1 is the viscous coefficient, and

q_o is the elastic coefficient.

This will be written

$$\sigma_c = q_{oc}\varepsilon_c + q_{1c}\dot{\varepsilon}_c$$

to denote the cable motion.

The restraint material was found to be represented by a four-element fluid which is described by:

$$\sigma + P_1\dot{\sigma} + P_2\ddot{\sigma} = q_1\dot{\varepsilon} + q_2\ddot{\varepsilon} .$$

For the four-element fluid as shown below, the coefficients are:

$$P_1 = \frac{q_1'''}{q_o''} + \frac{q_1'''}{q_o'}$$

$$P_2 = \frac{q_1'' q_1'''}{q_o' q_o''}$$

$$q_1 = q_1'''$$

$$q_2 = \frac{q_1'' q_1'''}{q_o''}.$$

The harness is an elastic element such that

$$\sigma = q_o \varepsilon_1$$

which will be written

$$\sigma_H = q_{oH} \varepsilon_H.$$

The equations are transformed for solution and are:

$$\sigma_c = (q_{oc} + q_{1c} S) \varepsilon_c$$

$$\sigma_{st} = \frac{(q_{1st} S + q_{1st} S^2) \varepsilon_{st}}{(1 + P_{1st} S + P_{2st} S^2)}$$

Since the force is desired for a given deformation the stresses are converted to forces,

$$\frac{F_c}{A_c} = (q_{oc} + q_{1c} S) \varepsilon_c$$

$$\frac{F_{st}}{A_{st}} = \frac{(q_{1st} S + q_{2st} S^2) \varepsilon_{st}}{(1 + p_{1st} S + P_{2st} S^2)}$$

$$\frac{F_H}{A_H} = q_{oH} \varepsilon_H.$$

Similarly, strains are converted to elongations

$$\frac{F_c}{A_c} = (q_{oc} + q_{1c}S)\frac{\delta c}{L_c}$$

$$\frac{F_{st}}{A_{st}} = \frac{(q_{1st}S + q_{2st}S^2)\delta_{st}}{(1 + {}_{1st}S + P_{2st}S^2)L_{st}}$$

$$\frac{F_A}{A_H} = q_{oH}\frac{H}{L_H}$$

Since all the deformations must total to a restraint motion X:

$$X = \delta_c + \delta_{st} + \delta_H$$

$$X = \left[\frac{F_c L_c}{A_c}\right]\cdot\left[\frac{1}{(q_{oc} + q_{1c}S)}\right] + \left[\frac{F_{st}L_{st}}{A_{st}}\right]\cdot\left[\frac{(1 + P_{1st}S + P_{2st}S^2)}{(q_{1st}S + q_{2st}S^2)}\right] + \left[\frac{F_H L_H}{A_H}\right]\cdot\left[\frac{1}{q_{oH}}\right]$$

but all forces must be equal, hence the differential equation for the system becomes

$$A_1\dot{X} + B_1\ddot{X} - C_1\dddot{X} = D_1F + E_1\dot{F} + F_1\ddot{F} + G_1\dddot{F}$$

where

$$A_1 = q_{oc}q_{1st}q_{oH}$$

$$B_1 = q_{oH}(q_{oc}q_{2st} + q_{1c}q_{1st})$$

$$C_1 = q_{oH}q_{1c}q_{2st}$$

$$D_1 = \frac{L_{st}}{A_{st}}q_{oH}q_{oc}$$

$$E_1 = q_{1st}(q_{oH}\frac{L_c}{A_c} + q_{oc}\frac{L_H}{A_H}) + q_{oH}(P_{1st}q_{oc} + q_{1c})\frac{L_{st}}{A_{st}}$$

$$F_1 = q_{oH}q_{2st}\frac{L_c}{A_c} + q_{oH}\frac{L_{st}}{A_{st}}(q_{oc}P_{2st} + q_{1c}P_{1st}) + \frac{L_H}{A_H}(q_{oc}q_{2st} + q_{1c} + q_{1st})$$

$$G_1 = q_{1c}(q_{oH}P_{2st}\frac{L_{st}}{A_{st}} + q_{2st}\frac{L_H}{A_H}).$$

The coefficient for cable and harness are also:

$$q_{1st} = \eta_1 \qquad q_{oc} = K_s\frac{L_c}{A_c}$$

$$q_{2st} = \eta_1\eta_2/G_2$$

$$P_{1st} = \eta_1/G_2 + \eta_1/G_1 + \eta_2/G_2 \qquad q_{1c} = C_s\frac{L_c}{A_c}$$

$$P_{2st} = \eta_1\eta_2/G_1G_2. \qquad q_{oH} = K_H\frac{L_H}{A_H}.$$

The equations above were programmed in MIMIC and are presented in Appendix B.

ANALYSIS OF RIGID TORSO/HARNESS DATA

The data for eight tests conducted with the rigid torso and harness were available in the same format as discussed earlier in the rigid torso/cable alone tests. However, because of the need to match harness motion as well as force and acceleration data, analysis of the photographic data was necessary. The output from the film data are tabulated in Table 10. Tests indicate that even for a rigid torso it takes approximately 0.020 seconds after observable piston motion before there is observable motion of torso. During that time the Koch fittings, and hence the harness, move about one inch. Therefore, the cable and strap had to be modeled in series with a harness of unknown stiffness which could duplicate the motion, force, and acceleration simultaneously.

Many values were selected for the two stiffness coefficients and for the displacement of the harness which would cause the bilinear stiffness to change from "soft" to "hard". After many iterations for several inputs, the values of 100 and 750 pounds per inch at a harness displacement of 0.5 inches duplicated the measured responses most favorably. The results are shown on figures 33, 34, and 35 as indicative of the agreement achieved. Using these coefficients, the

Table 10. Reduced Photographic Data for Rigid Torso Tests

Test	Δt_1	Δt_2	S_{p1}	S_{p2}	S_{c1}
Rigid Tors With Harness					
578	0.026	0.058	1.69	4.01	1.06
579	0.018	0.106	1.42	8.72	1.06
580	0.016	0.120	1.25	11.57	0.98
581	0.020	0.138	2.14	13.26	0.65
582	0.022	0.038	2.31	4.09	1.23
583	0.018	0.76	1.51	8.46	0.82
584	0.020	0.102	2.14	11.66	1.55
Rigid Torso With Cable					
586	0.010	0.054	0.71	3.74	-
587	0.008	0.096	0.62	8.72	-
588	0.008	0.114	0.53	11.57	-
589	0.016	0.136	0.89	13.17	0.37
590	0.018	0.048	1.42	3.92	0.19
591	0.010	0.078	0.71	8.72	0.37
592A	0.010	0.0096	0.71	11.57	0.19
592B	0.010	0.108	0.89	13.35	0.19

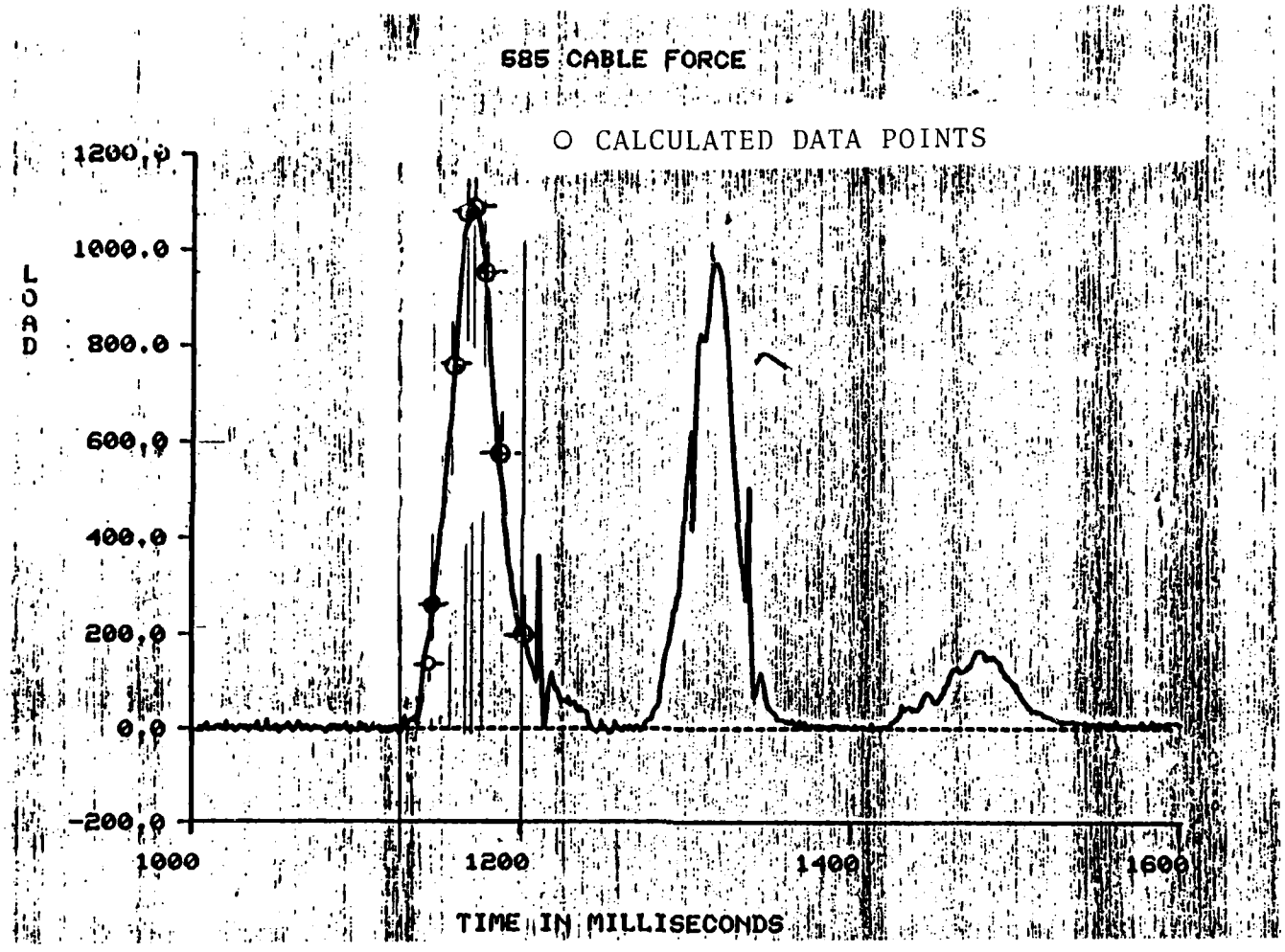

Figure 33 Predicted versus Measured Cable Force for Harnessed Tin Man Test 585.

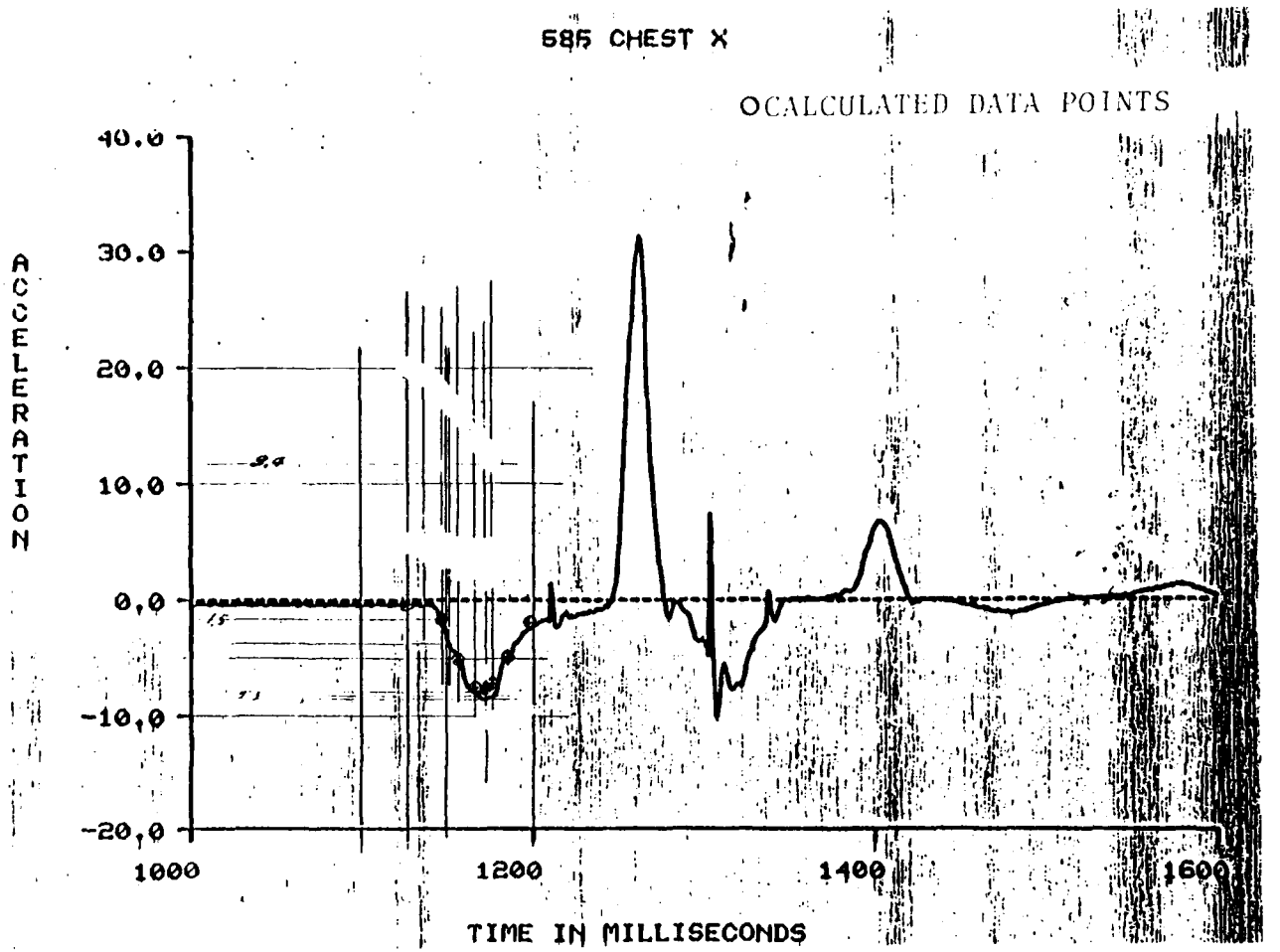

Figure 34 Predicted versus Measured Chest Acceleration in the Force and Aft (X) Direction for Harness Tin man Test 585.

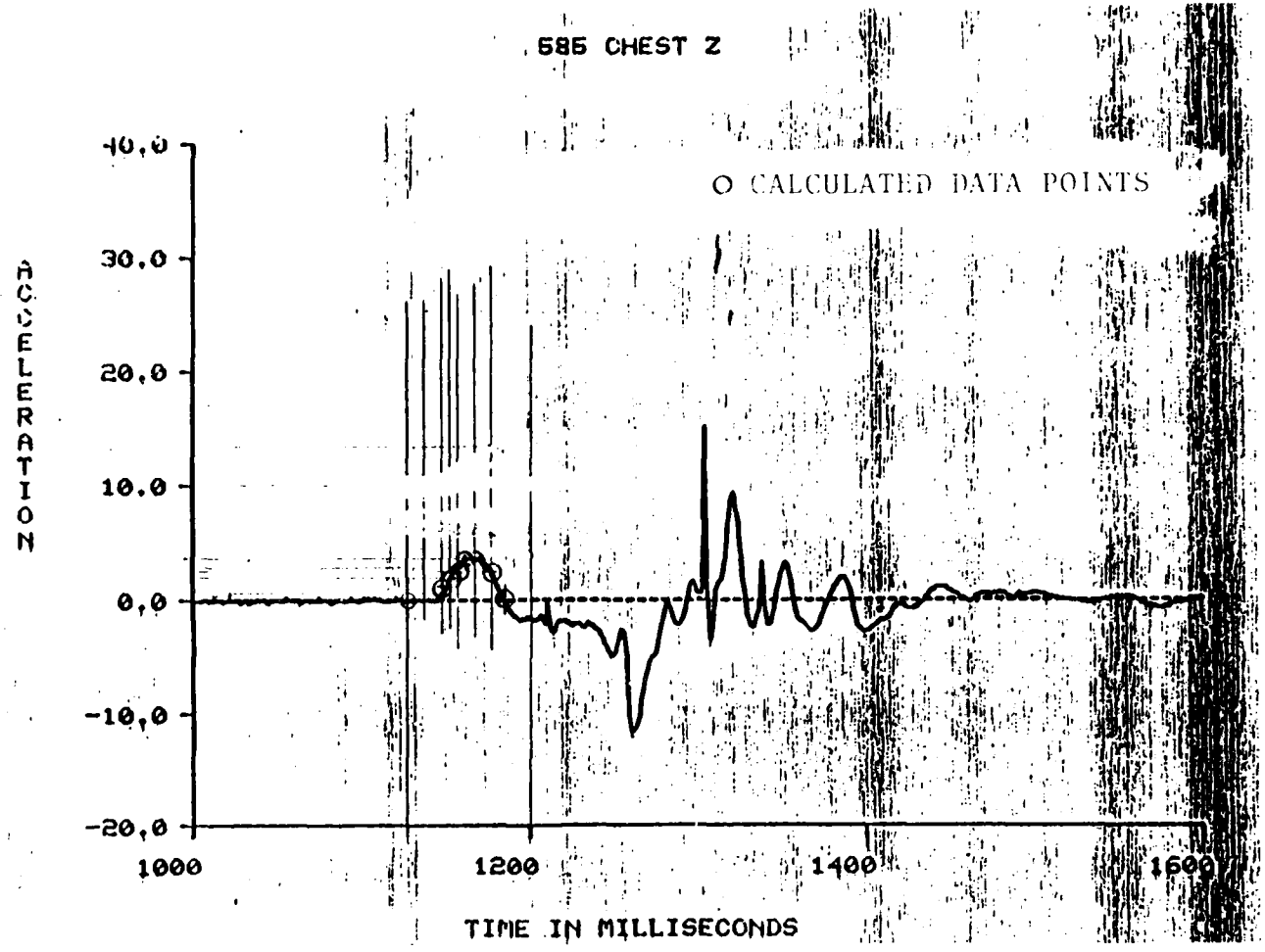

Figure 35 Predicted versus Measured Chest Acceleration in the Vertical (E) Direction for Harness Tin man Test 585.

rigid torso model analytically generates a harness motion that moves up the torso with a "soft stiffness" until 0.5 inches have been traveled. At that point the harness continues to rotate at a greater stiffness while the torso accelerates and the correct forces are generated by cable and strap.

DEVELOPMENT OF FULL TORSO/NECK/HEAD MODEL

Once the rigid torso model had been validated using the harness/strap and cable analogs, the model was revise to incorporate the head and neck system.

The head is represented by a rigid body having a center of gravity offset from an attachment point at the neck. The head is schematically shown below.

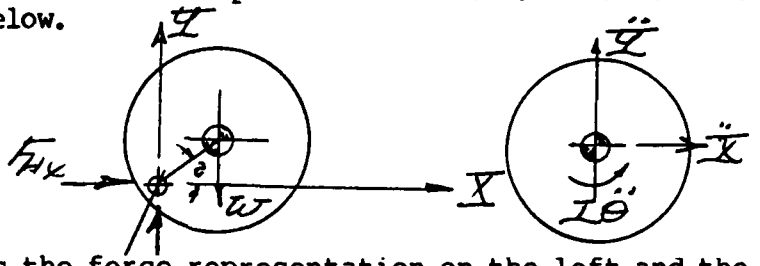

The sketch shows the force representation on the left and the inertia vectors on the right. From these, equations of motion can be found:

$$\Sigma F_x = ma_x$$

$$F_{xH} = m_H \ddot{X}_h$$

$$\Sigma F_y = ma_y$$

$$F_{yH} = m_H \ddot{Y}_H + W_H$$

where F_{Hx} is the horizontal force at the head/neck junction

F_{Hy} is the vertical force at the head/neck junction

X_H is the horizontal acceleration of the head center of gravity

Y_H is the vertical acceleration of the head center of gravity

I_O is the head mass moment of inertia about the lateral axis through the pivot point

$\ddot{\theta}_H$ is the pitching acceleration of the head

θ_H is the angle between the line connecting the head/neck attachment joint and the center of gravity, and the horizontal axis of the head

M_H is the moment at the head/neck joint generated by elastic and viscous moments, and

L_H is the length from attachment joint to the center of gravity.

The neck has a similar representation as shown below.

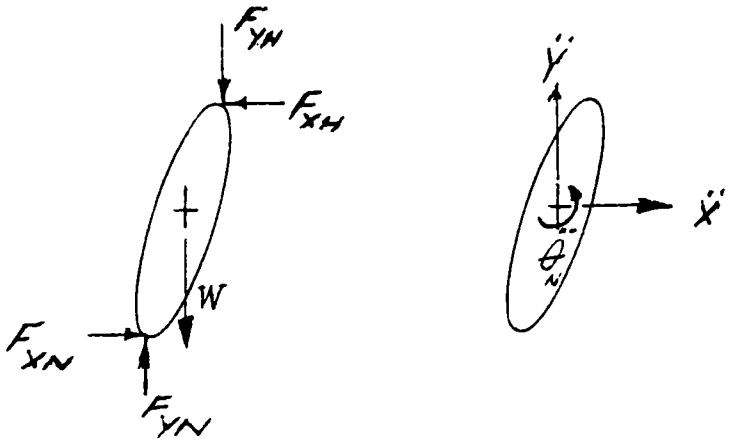

where F_{xN} is the horizontal force at the neck/shoulder joint

F_{yN} is the vertical force at the neck/shoulder joint

X_n is the neck horizontal acceleration

Y_n is the neck vertical acceleration

I_{oN} is the mass moment of inertia of the neck about the pivot point

$\ddot{\theta}_n$ is the pitching acceleration of the neck

M_N is the moment at the neck/shoulder joint due to elastic and viscous moments, and

L_N is the distance from pivot to neck center of gravity

L_H is the length of the neck between attachment joints.

The kinetic relations for centers of gravity accelerations are:

$$\ddot{X}_N = - \ell_N \sin \theta_N \ddot{\theta}_N - \ell_N \cos \theta_N \dot{\theta}_N^2 + \ddot{X}_S$$

$$\ddot{Y}_N = \ell_N \cos\theta_N \ddot{\theta}_N - \ell_N \sin \theta_N \dot{\theta}_N^2 + \ddot{Y}_S$$

$$\ddot{X}_H = -\ell_N \sin \theta_N \ddot{\theta}_N - \ell_N \cos\theta_N \dot{\theta}_N^2 - L_H \sin\theta_H \ddot{\theta}_H - L_H \cos\theta_H \dot{\theta}_H^2 + \ddot{X}_S$$

$$\ddot{Y}_H = L_H \cos \theta_N \ddot{\theta}_N - L_N \sin \theta_N \dot{\theta}_N^2 + L_H \cos\theta_H \ddot{\theta}_H - L_H \sin\theta_H \dot{\theta}_H^2 + \ddot{Y}_S$$

Where $\ddot{X}_S$ and $\ddot{Y}_S$ are the accelerations at the attachment point of neck and shoulder.

By some algebraic manipulation:

$$\ddot{\theta}_N = \{M_N - M_H - m_H L_H \ell_N (\cos(\theta_H - \theta_N) \ddot{\theta}_H + \sin (\theta_H - \theta_N) \dot{\theta}_H^2)$$

$$- (m_n q \ell_N + m_H q L_H) \cos\theta_N + (m_N L_N + m_H \ell_N)(\ddot{X}_S \sin\theta_N - \ddot{Y}_S \cos\theta_N)\}$$

$$\times \frac{1}{(I_{oN} + (m_H L_N^2 + m_N \ell_N^2)} .$$

Similarly:

$$\ddot{\theta}_H = \{M_H - m_H\{ L_H L_N \cos (\theta_H - \theta_N) \ddot{\theta}_N + \ell_H L_N \sin (\theta_H - \theta_N) \dot{\theta}_N^2$$

$$- m_H L_H q \cos\theta_H + m_H L_H \{\ddot{X}_S \sin \theta_H - \ddot{Y}_S \cos \theta_H\}\}$$

$$\times \frac{1}{(I_{oH} + m_H L_H^2)}$$

The neck moment coefficients are:

$$M_H = -(C_H(\dot{\theta}_H - \dot{\theta}_N) + K_H(\theta_H - \theta_N)) + M_{Ho}$$

$$M_N = -(C_N(\theta_N - \theta_T) + K_N(\theta_N - \theta_T)) + M_{No}.$$

The initial moment coefficients are necessary to create a static condition at the beginning of the acceleration pulse. Since the head is held at any angle by an internal moment, and yet the elastic coefficients are based upon a dynamic response, a coefficient, M_{Ho}, was used to create an initial equilibrium state. During the dynamic response, the moment is dictated by the K and C values thought to be realistic.

The initial values are:

$$M_{Ho} = W_H L_H \cos\theta_{Ho}$$

$$M_{No} = (W_N \frac{L_N}{2} + W_H L_N) \cos\theta_{No} + W_H L_H \cos\theta_{Ho}$$

The torso equations were also modified as required. By drawing the free body diagram, writing the equations of motion and then inserting the proper kinematic relations, the final equation for torso angular acceleration is

$$\ddot{\theta} = \{M_T L_1 + (M_H + M_N)(L_T)\ddot{X}_L \sin\theta + F_S L_T \sin(\theta_u + \theta)$$

$$(M_H + \frac{M_N}{2}) L_N L_T \{\sin(\theta_N - \theta)\dot{\theta}_N^2 - \cos(\theta_N - \theta)\ddot{\theta}_N\}$$

$$(M_H L_H L_T \{\sin(\theta_H - \theta)\dot{\theta}_H^2 - \cos(\theta_H - \theta)\ddot{\epsilon}_H$$

$$- ((W_N + W_H)L_T + W_T L_1)\cos\theta + C_N(\dot{\theta}_N - \theta)$$

$$+ K_N((\theta_N - \theta_o) - (\theta - \theta_o)) - W_H L_H \cos\theta_{Ho}$$

$$- W_H L_N + W_N \frac{L_N}{2}) \cos\theta_{NO} - C_T\dot{\theta} - K_T(\theta - \theta_o)$$

$$+ W_H L_1 \cos\theta_o + W_H\{L_H \cos\theta_{Ho} + L_N \cos\theta_{No} + L_T \cos\theta_o\}$$

$$+ W_N \frac{L_N}{2} \cos\theta_{No} + L_T \cos\theta_o - F_{So} L_T \sin(\theta_{uo} + \theta_o)\}$$

$$\cdot \left\{\frac{2}{I_T + M_T L_1^2 + (M_H + M_N) L_T^2}\right\}$$

Similarly, the lower element of the model has translational acceleration which is:

$$\ddot{X}_L = M_T L_1 \sin\theta(\ddot{\theta} + u\dot{\theta}^2) + M_T L_1 \cos\theta(\ddot{\theta}^2 - u\dot{\theta})$$

$$- u\,(W_T + W_L - F_S\,(\cos\theta_u - u\sin\theta_u)$$

$$- F_B\,(\cos\theta_B + u\sin\theta_B) - u\,F_{NY} - F_{NX}$$

$$+ u\,(W_N + W_H + W_T + W_L) + F_{So}\,(\cos\theta_{uo} - u\sin\theta_{uo})$$

The equations listed, as well as those required for the control of the routine, were programmed in MIMIC and are presented in Appendix C.

Significant difficulties were encountered in getting the routines to run correctly. The program uses input accelerations that create large derivatives of acceleration. These are used in conjunction with material properties also having large coefficients. These in combination with several implicit functions caused considerable effort in getting results. With many revisions and modifications, the program was run using extremely small integration steps and modified acceleration waveform inputs. Once that was accomplished, the integration requirements were eased to permit reasonable running times. The model presented uses a larger integration interval and unmodified acceleration inputs, yet has a reasonable running time, 5 minutes, and generates forces and acceleration within 6 percent of the "exact" solutions at maximum integration times.

ANALYSES USING THE FULL TORSO/HEAD/NECK MODEL

The model evolved was validated using available harnessed human test results. The tests were selected at random from many available at AFAMRL using the same harness and with subjects retracted at 12 to 14 inches of retraction at 700 to 900 psi actuator pressure. The eleven tests included subjects with weights from 133 to 186 pounds based upon the forces measured by the BPRD instrumentation system. The mean weight was 155.6 pounds with a standard deviation of 17.4 pounds. In order to permit the use of one model during model evaluation we assumed that the 50th percentile aircrewman would be typical for the set of data available.

By examining photographs of the human tests and assuming the dimensions and weight distributions of the 50th percentile man, the coefficients required for the model were selected. The primary values required are:

	WEIGHT (pounds)	MASS MOMENT OF INERTIA (pound/inches/seconds squared)
HEAD	8.5	0.151
NECK	3.5	0.032
TORSO	78.9	11.160
LOWER BODY	54.1	Not applicable
UPPER LIMBS	19.0	Not applicable
	164.0	

The torso was assumed to be 24.5 inches in length from hip pivot to neck pivot; the neck length is 5.0 inches from neck pivot to head pivot; and the head center of gravity is 2.0 inches from the head pivot point. Both torso and neck were 58° from horizontal and the head pivot to center of gravity line was 60° from the horizontal. Although originally stated as assumed values, these reflect photographic data and the examination of three reference works.

Film data were available for analysis and the motions observed during human tests were tabulated and used to plot Figure 36. The figure shows that the harness rotates on the torso over a greater distance and requires more time to reach an "equilibrium" condition. There are several approaches to be taken in modifying a harnessed rigid torso into a harnessed human model. The delay in achieving harness equilibrium can be due to thigh elasticity, chest elasticity, torso hip joint characteristics, and probably several other phenomena. However, hip joint characteristics are assumed not to create significant forces since the torso rotates very little and achieves little angular velocity. Chest elasticity could create some relative motion but it is normal to the motion needed, and hence we assumed that the motion observed was a function of thigh elasticity.

The motion of the harness was discussed previously indicating that the straps do compress the lower part of the thigh as the harness rotates. The previous paragraphs indicated that it was possible to find a harness model which for a rigid torso would duplicate measured kinetics and kinematics. Since the thigh response is in series with the harness, we assumed that another element could be added to the harness to represent thigh elasticity. The added element was necessary to change the harness model from one generating about one inch of motion to one creating about 2.5 inches of motion while building to 350 pounds of strap force. Since a "harness" had been found that duplicated rigid thigh motion, addition of a "thigh" element would retain the harness and merely add another elastic element in series. In this manner, if the harness is used with a lower thigh rigid plate, or if a harness design is changed, but lower thighs still compress, the coefficient found may still be applicable.

By trial and error, selected values of thigh stiffness were used and added to the harness element. The resulting force displacement curve found is shown in Figure 37. By using these coefficients, the

AD-A126 199 INVESTIGATION OF CREW RESTRAINT SYSTEM BIOMECHANICS(U) 2/2
DAYTON UNIV OH RESEARCH INST N S PHILLIPS ET AL.
MAY 82 AFAMRL-TR-81-103 F33615-79-C-0525

UNCLASSIFIED F/G 5/5 NL

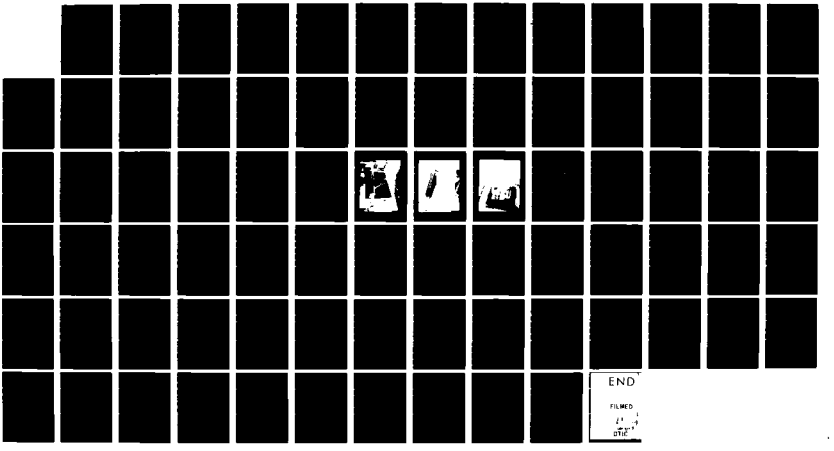

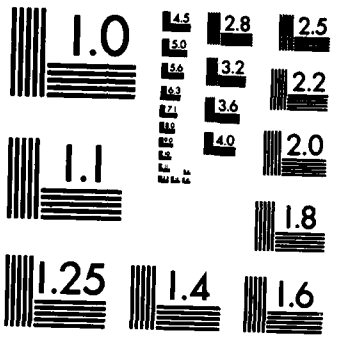

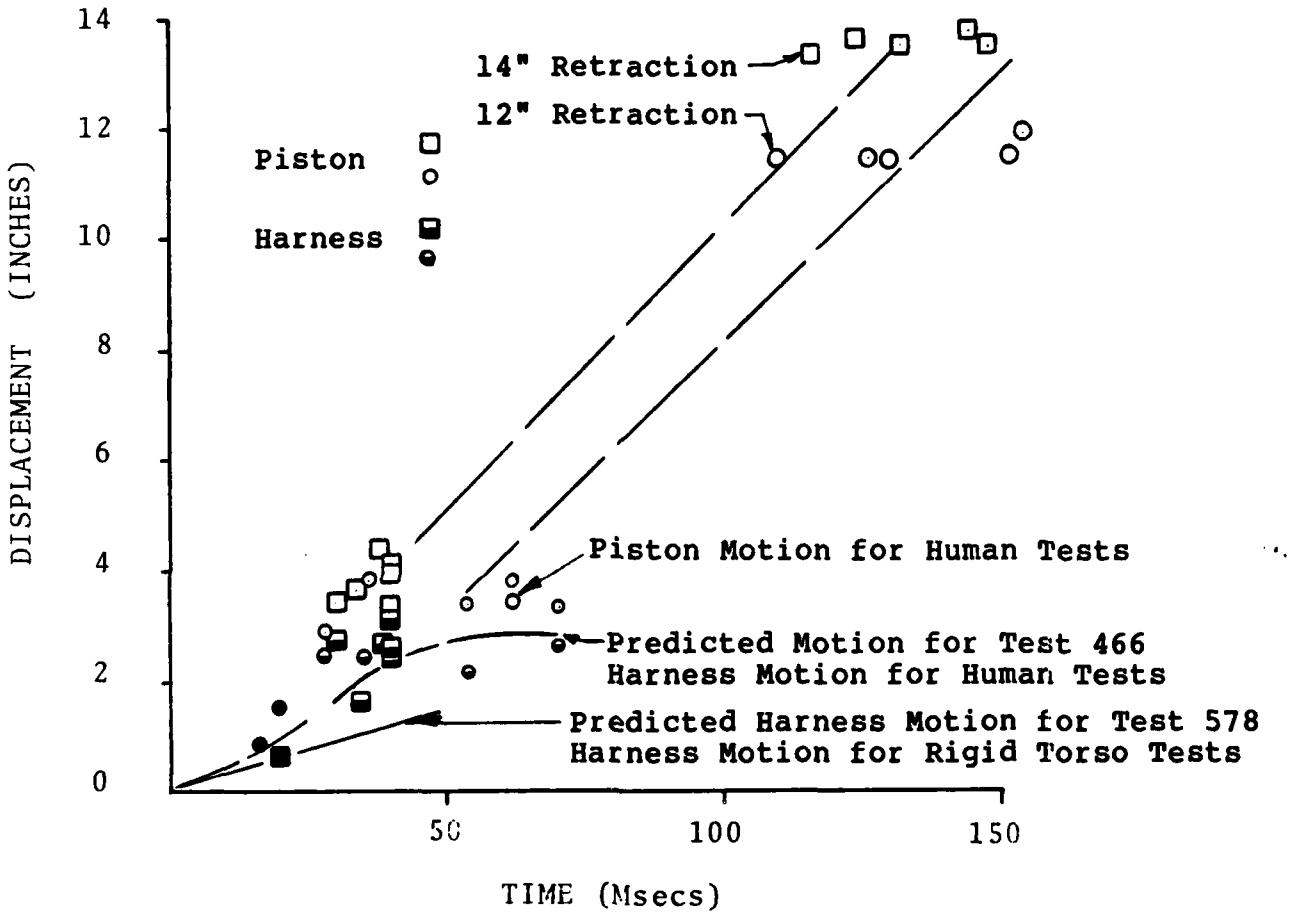

Figure 36 Motion Observed Photographically During Harnessed Tin Man and Human Tests. Time is that Elapsed Between First Motion of the Retraction Piston and First Observed Cope Fitting Motion.

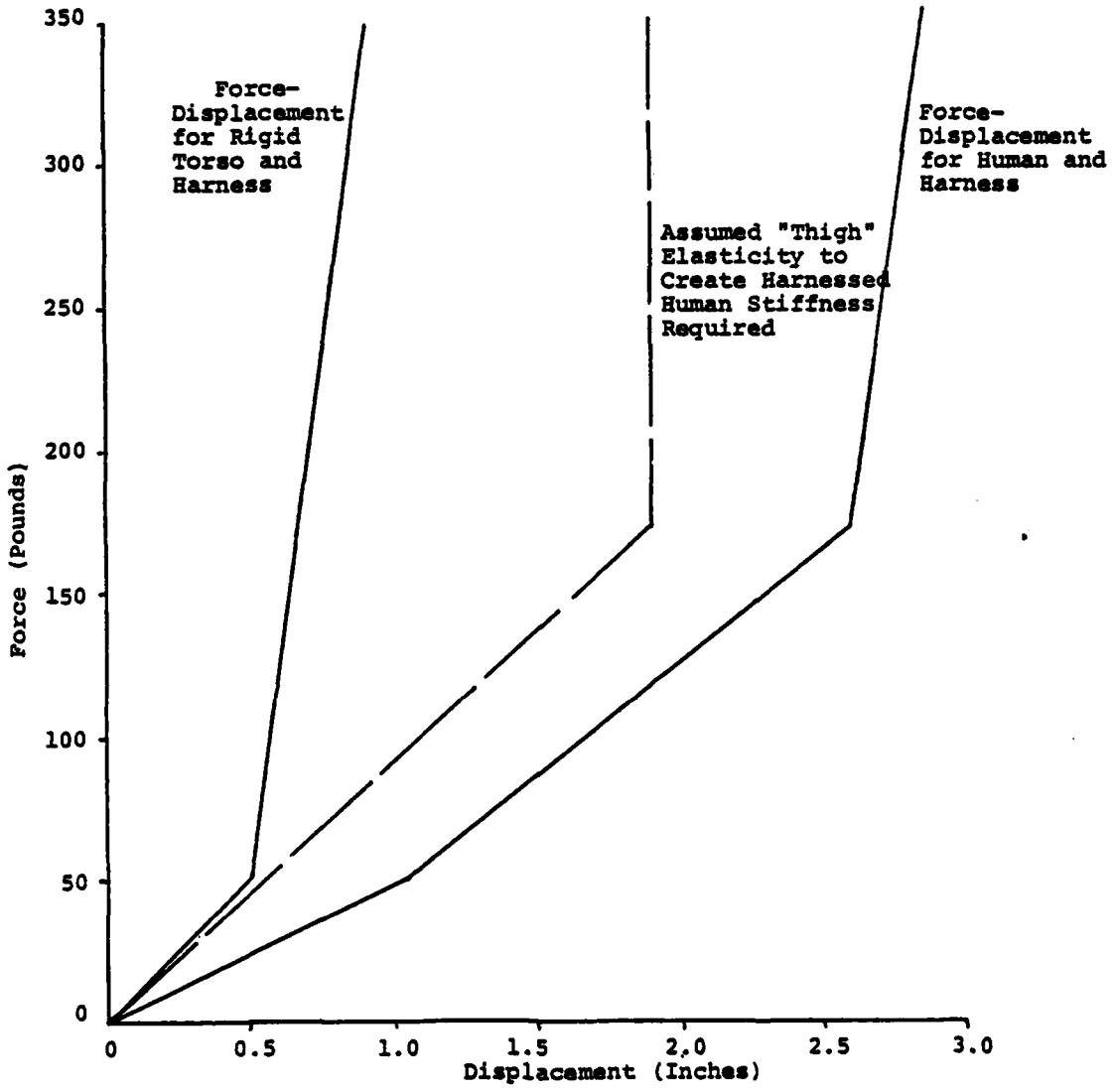

Figure 37 Force-Displacement Curves Necessary to Duplicate Harness Motion and Inertial Response Measurements.

motions calculated for the revised model matched measured data reasonably well as indicated in Figure 38.

Another aspect considered in the development of the human model was that of chest elasticity. Although values for harness stiffness can be found which can duplicate the observed harness motion and approximate measured forces and accelerations, it was desirable to examine the effect of chest compressibility to further improve the model.

As the strap pulls the harness up over the chest, the force is low in relation to the maximum forces possible. The tension passes over the surface and back into the retraction device. Schematically, the torso is represented as shown below.

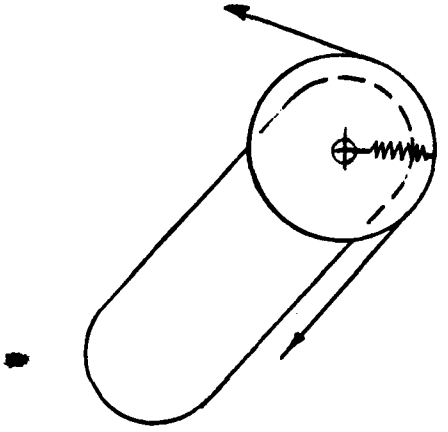

The tension is assumed to act on a roller attached at the shoulder pivot point. The roller is assumed to have compressibility which is representative of thoracic elasticity as available in the literature.

At this point, the model is only a representation with elements indicative of the phenomenon known to exist. Although there is no shoulder "roller", there are forces acting on the chest which act as though a tension member passed over a frictionless curved surface. With this approximation, it is possible to include elasticity into the roller to permit chest compressibility. Although this may not be the true mechanism of load transfer from shoulder force to torso force, existing biomechanical data can be used and gain a qualitative, or possibly quantitative, assessment of the effects of chest elasticity.

There are several references available calculating thoracic elasticity. A combination of several sources is used. From the work of Kaleps [6], the chest is represented as a two degrees of freedom system having a chest wall and impactor. For this particular application the impactor is not necessary but the surface characteristics are of interest. The values used are:

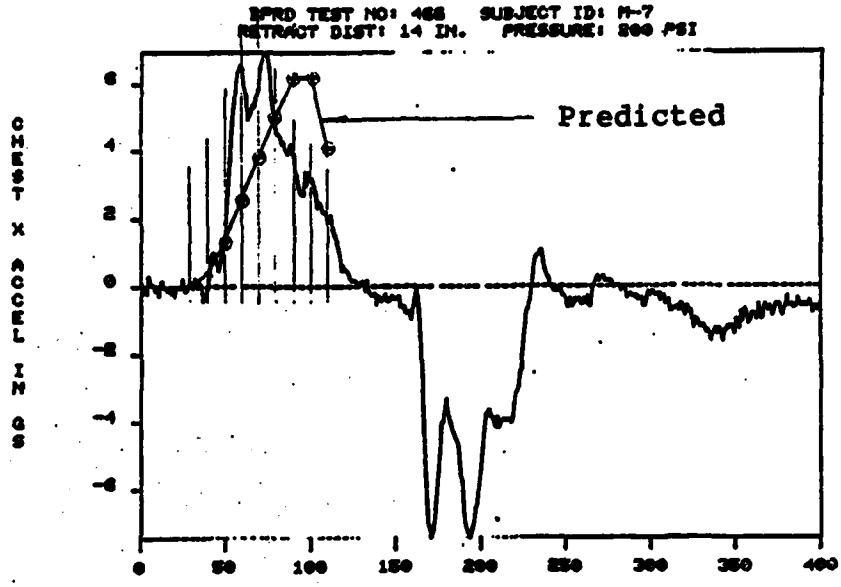

Figure 38a.

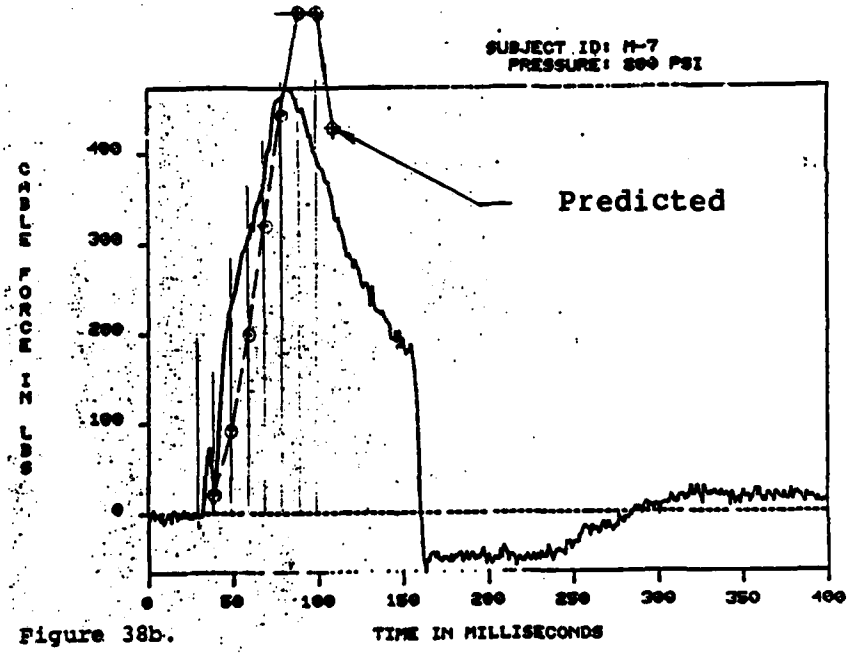

Figure 38b.

Figure 38 Predicted Cable Force and Chest Acceleration versus Measured for Human Model.

K_S = 1598 pounds/inch

C_S = 5.71 pounds/inch/second

M_{CW} = .0685 pounds/inch/second square

K_{CW} = 171 pounds/inch

C_{CW} = 0.571 pounds/inch/second

Where the subscript S refers to the surface, or skin characteristics, the subscript cw refers to the chest wall. These indicate a lightly damped chest wall attached to a torso.

Since the surface and chest wall are in series, an approximation of the stiffness between impactor, or impacting surface, would be to assume both do act in series. The single stiffness value would then be approximately 154 pounds/inch.

This number agrees fairly well with the work of Patrick [8] if comparison is made with static data. Intuitively it is seems that the stiffness is only linear over a small range and that the "spring" hardens over a small displacement. The data of Patrick indicates that forces of about 1000 pounds are developed on the chest with about 1 inch of compression. Using this relation and the initial stiffness of 150 pounds/ inch, chest elasticity is approximated by:

$$F_{CW} = 150\ x + 850\ x^2$$

A relation of this was used with the representation of the chest wall to model the effects of chest elasticity. The model idealized is simply:

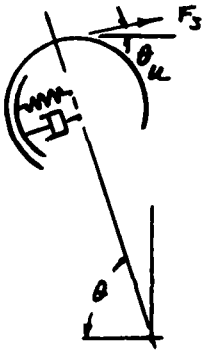

The equation of equilibrium is:

$$\ddot{X}_{CW} = (-F_S \sin(\theta + \theta_u) - (K_{CW} - K_T) - C_{CW}(\dot{X}_{CW} - \dot{X}_t))/M_{CW}$$

The equation is evolved as though the chest wall translates horizontally relative to the torso center of gravity location X_t. The strap force component acts normal to the torso. The relative motion $X_{cw} - X_t$ acts to attenuate the torso response, and the strap force is calculated as a function of the relative motion between chest wall and actuator input. Hence, the force in the strap now reflects the compressibility of the chest as it influences strap elongation and torso motion. These modifications were made to the man model, and the coefficients listed above were used as indicative of human response.

Additional computer runs were made with greater stiffness values to reflect the strain hardening effect known to occur. The initial stiffness coefficient was raised to 1000 and the secondary reduced to -300 pounds/inch. The values provide the initial 1000 pounds/inch stiffness and a force of about 1400 pounds at 2.0 inches of deflection. Hence these are indicative of "dynamic" stiffness as well as maximum possible chest loads at realistic displacements. Results are shown in Figure 39.

The initial results were disappointing. The forces and acceleration to be matched were not duplicated. This led to a re-examination of the model. Closer examination of the torso leaning forward and restrained indicates that the force on the chest is only a component of the resultant force generated by the restraints. Additionally, the chest dynamically acts as a much stiffer element. By recoding the chest wall model and increasing the chest stiffness, a series of runs was made to study the effects of chest wall location. The location established was the same location used to locate the chest accelerometers at the sternum. From the data generated we found that the chest wall must be stiffer than thoracic measurements would indicate to match forces and accelerations observed. This is not surprising since the straps pass over the bony structure of the clavicle and would realistically create a more rigid structure carrying the forces higher on the torso. Consequently, for the time of initial torso response, chest wall response contributes little to the torso response. If the retraction is started in a more vertical orientation, the effect of the chest wall may be more significant. However, if the torso attitude is vertical, little retraction is necessary.

ADDITION OF INJURY CRITERIA PARAMETER

The last addition to the human model was that of the Maximum Strain Criteria (MSC) model reference. The MSC model is a simple spring-mass-damper model driven by the acceleration of the skull. The system shown below was coded to reflect the fact that it is in a local coordinate system, and included into the completed model.

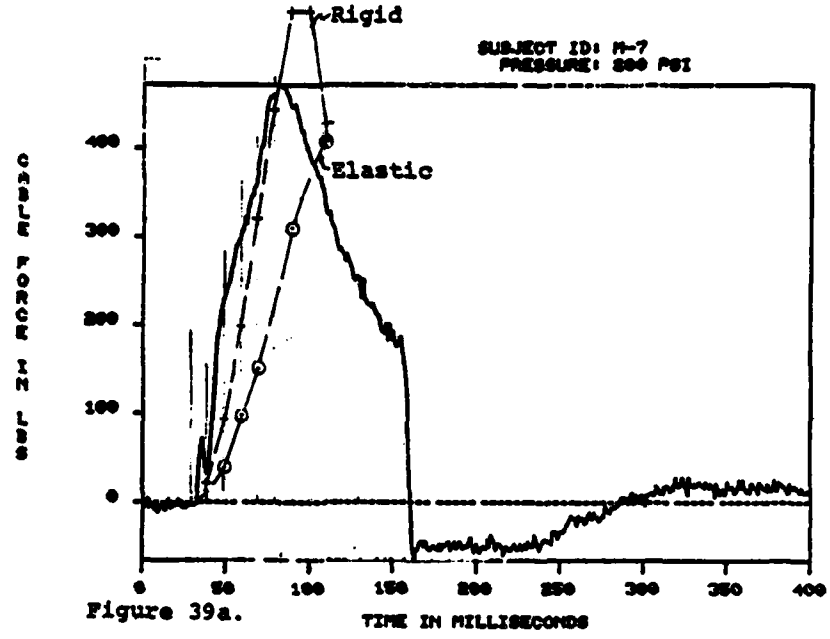

Figure 39a.

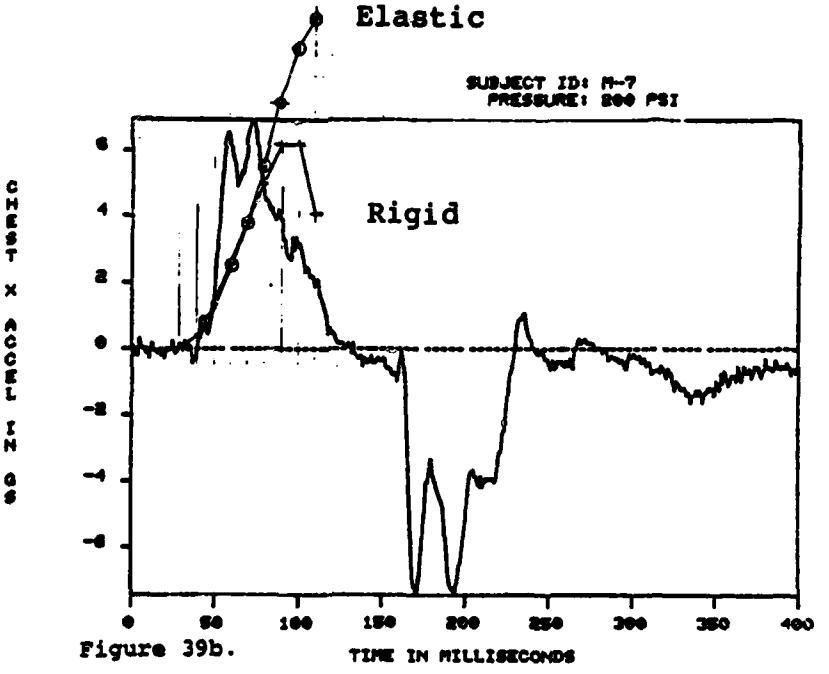

Figure 39b.

Figure 39 Predicted Cable Force and Chest Acceleration versus Measured for Rigid Chest and 1000 pound/inch Chest.

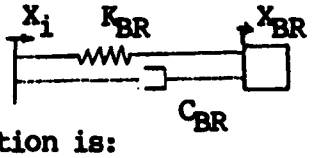

The equation of motion is:

$$M_{BR}\ddot{X}_{BR} = -K_{BR}(X_{BR} - X_I) - - C_{BR}(\dot{X}_{BR} - \dot{X}_I)$$

where X_b and X_r are brain and input displacements in a coordinate system attached to the skull. The output is the difference between the two divided by a reference length L_r. Hence,

$$\mathcal{E} = \frac{X_B - X_I}{L_r}$$

which is the strain to be compared with "tolerable" strain for the species and direction selected.

SUMMARY OF MODEL DEVELOPMENT AND ANALYSES

The original intent of the effort conducted in this segment was to generate an analytical model which could be used to predict the response of a restrained human. The model was intended to avoid the requirement for hundreds of inputs, or extensive preliminary calculation to determine the values required as inputs. We hoped that in establishing elements necessary to match experimental data, the number of elements would be those both necessary and sufficient.

The model evolved reflects torso, head and neck characteristics, restraint material and configuration, harness effect, and chest elasticity. The model also reflects the test hardware involved in data collected using the BPRD although this can be easily eliminated. Outputs available are restraint force, head and chest accelerations both translational and rotational, head and neck joint forces, seat pan force, torso forces, and strain as defined by the MSC model. Harness motion is computed as indicative of Koch fitting motion.

Each element discussed was "isolated" by means of either separate testing and analysis, as for the restraint webbing, or by examining data collected using "calibration" hardware, such as the "tin-man". Cross checks of photographic data with electronic instrumentation results led to the isolation, or inference, of the last components examined. In all cases, where possible, existing measured data from authoritative sources were used to define the human model values.

The end result of the effort is an analytical model which requires 52 inputs. These are necessary to locate all elements in space to and define inertial characteristics and material properties of the human and restraint. The program generates a like number of outputs available for comparison with preferred criteria.

RETRACTION SIMULATION STUDIES USING FINALIZED MODEL

The finalized model was exercised to compute human responses to selected inputs. The first simulation was simply the response of the human to the BPRD input previously used. The response in terms of head acceleration and strain is shown in Figure 40. The response at this input acceleration level is clearly noninjurious. The strain, 0.0005, is well below the established 0.0032 limit and the head longitudinal acceleration of 10g is not considered excessive. Additionally, the strap forces, joint forces, and angular motions are below tolerance levels. Several other runs were made at input levels three and six time greater than the measured input. Some of the results are shown in Figure 40.

The response at three times the test input created a tolerable strain value. However, examination of the data indicated that the lower body element is raised off of the seat pan. This invalidates the computer output after that point in that human test data used for model development never indicated separation of body and seat pan. Analytically it is assumed that the lower body slides forward and backward but never lifts. The dead weight and seat belt forces are insufficient to compensate for the large inertial force of the torso.

The results also indicate that other injury criteria may have been exceeded even though the strains were tolerable. The other tolerance values used were from Phillip's "Analysis and Measurement of Helmet and Aircrewman Response Resulting from Birdstrike." [9]. The tabulated numbers from the report are thought to be "reasonable" values indicative of non-concussive head and neck response. Using values of neck axial force, neck shear force, and head longitudinal acceleration of 440 pounds, 250 pounds and 40 g respectively, both the 3 and 6 amplification factors are injurious before the peak strain is reached. Hence, the injury, or concussion, would occur prior to limiting strain being reached. In addition, the limiting neck forces and head acceleration are reached at approximately the same time. This is similar to the results found in the referenced report in that several human injury parameter limits are reached at or near the same time. Although these are "injurious," the angular accelerations and velocities of the head are not, which implies support for the subinjurious strain.

Since the results were confounded by seat separation, a more realistic seat belt force coefficient was used to ikmprove the analog. Data from several references with models used to duplicate belted lower torso response were surveyed to choose the belt coefficient which had not been required before. A value of 1000 pounds/inch was used to examine lower belt stiffness effect. The results are shown on Figure 40. From this it is concluded that even significantly greater stiffness does not significantly change the response. The seat belt angle is too low and relative displacement too small, at peak strain

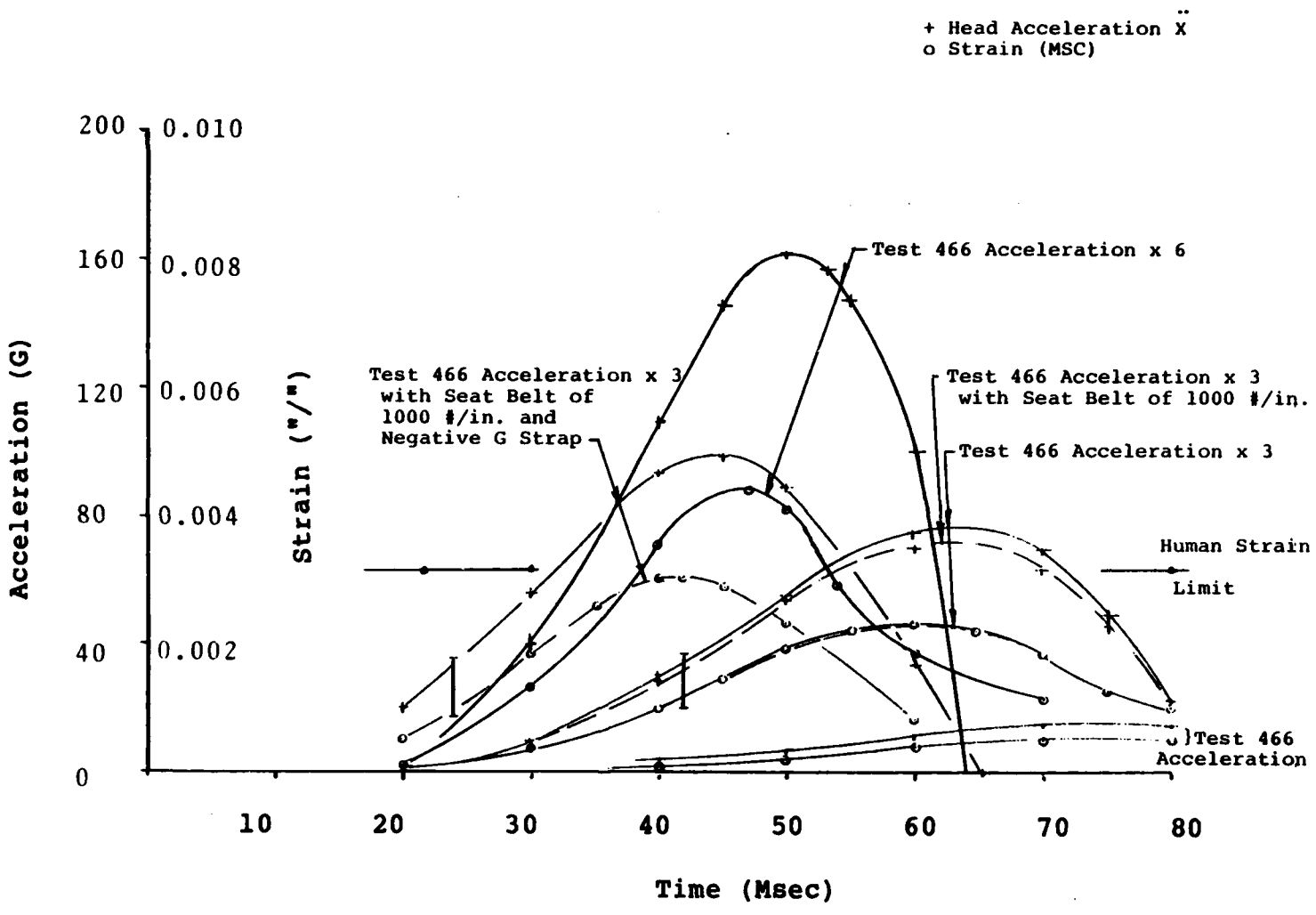

Figure 40 Predicted Human Response Due to Retraction Acceleration of Test 466 and its Variation.

and head acceleration, to alter the response. Although the force in the belt changes appreciably after the peak strain, the force is still not enough to keep the torso on the seat pan. Consequently, if the torso is to be held on the seat pan a force is required in the direction of the seat pan. If a crotch strap were used, the harness and strap would not be permitted to rotate as much. This was examined by replacing the harness/thigh elasticity by a stiffness of 1000 pound/inch. It was not necessary to alter the program. Th stiffnesses of harness configuration change and thigh elasticity we replaced by the magniture 1000 pound/inch. This is representative a belt with this stiffness that is attached from the Koch fitting the seat pan.

The addition of the crotch strap changes the response as seen Figure 40. The peak response occurs sooner and is greater. The nec forces and head fore and aft acceleration limits are again exceeded just prior to reaching limit strain. In order to find an optimum response, the acceleration input was modified and a value found where limiting injury parameters are reached at approximately the same time.

The analyses indicate that it is possible to establish a harness configuration which has acceptable response interms of neck forces and head acceleration. It also indicates that at limiting values, the time required for the torso to get "up to speed" is less than the original configuration. This demonstrates that it is possible to improve the system if the configuration can be changed by reducing the slack due to the harness prior to retraction. This also suggests the use of a crotch strap, or better yet, a strap using another reel so that as the restraint straps are withdrawn from the inertia reel, the crotch strap is reeled onto another.

As a final step, the material properties of the restraint strap were changed. Although the analytical straps are only 12 inches in length, the effects of the change are shown in Figure 41. The results indicate that although the effects of material properties were not large at the testing levels used for humans, they are more significant at higher levels. This is because the "slack" is taken out of the system and hence the lower frequency elements no longer dominate. With a harness having greater stiffness, 1000 pounds/inch, the harness and straps are of the same relative stiffness. This suggests that at the high testing levels desired, the material properties of the strap will have to be considered.

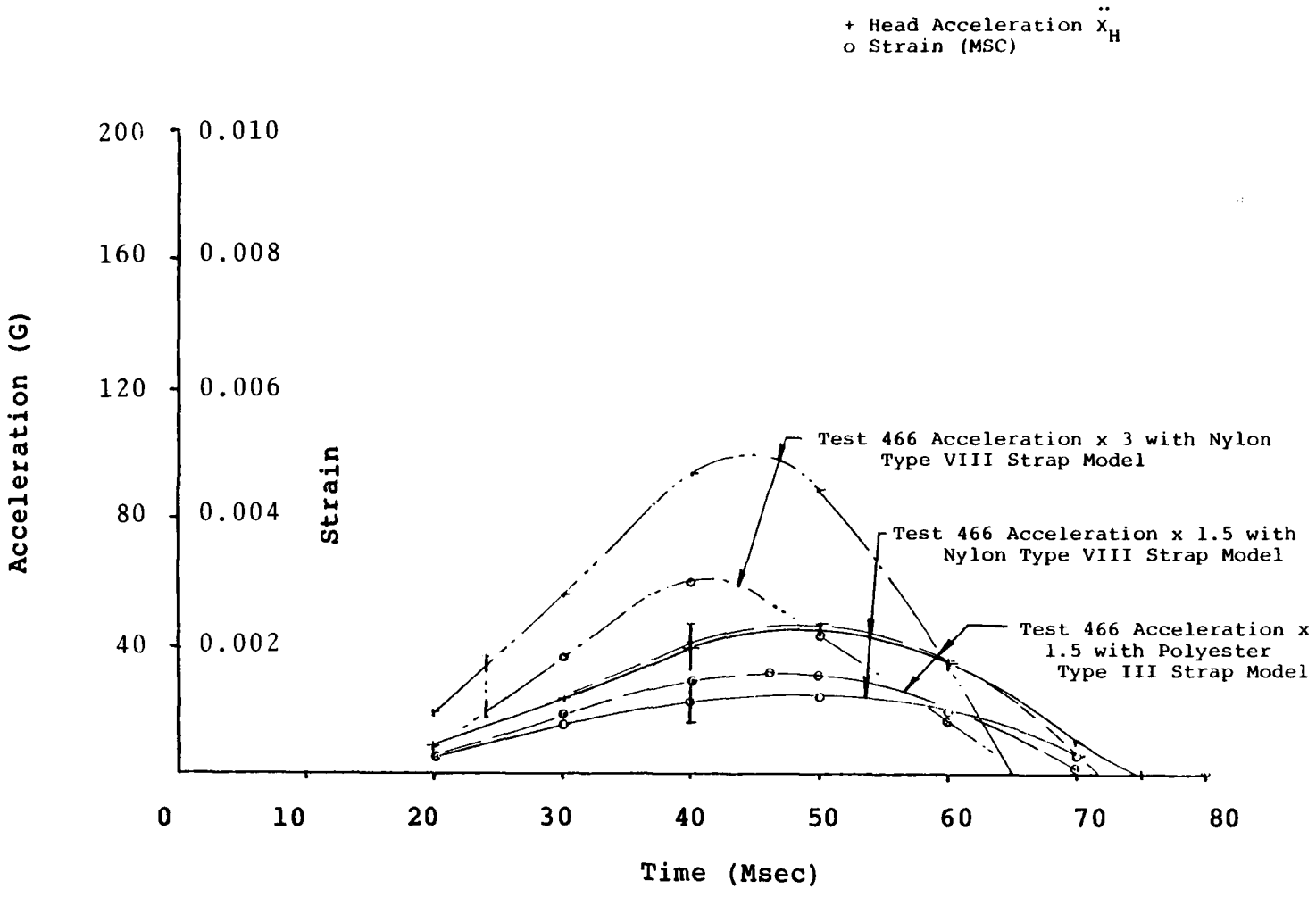

Figure 41 Predicted Human Response Due to Retraction with Variations Due to Model Strap Variations.

SECTION 4

RESTRAINT HAULBACK AND TENSIONING DEVICE PERFORMANCE

INTRODUCTION

The final element of the restraint system to be analyzed was the restraint retraction device, the pyrotechnically activated inertia reel. A model of the device which could simulate mechanical performance was required. Tests were to be conducted which would permit evaluation of the device under various input conditions compatible with the aircraft maneuvering environment.

At the beginning of the research we realized that data would be required from an equipment manufacturer. Although it is possible to analytically create a pyrotechnic reel, the model would probably not reflect those aspects dictated by hardware requirements. Consequently, a manufacturer was selected to assist in defining the characteristics of an operational unit as well as providing laboratory test data. The manufacturer selected was Pacific Scientific, KIN-TECH Division, because of their extensive experience in the design, manufacture, and testing of pyrotechnically activated retraction devices. Throughout the effort, coordination was maintained with Pacific Scientific to discuss model developments and test requirements.

INITIAL EFFORTS AND TEST PROTOCOL

Several reports available from AFAMRL were reviewed to establish an initial appreciation for inertia reel performance. These were:

(1) Pacific Scientific Test Report 700 dated 9 July 1965
(2) Pacific Scientific Test Report 882 dated 27 January 1965
(3) Pacific Scientific Test Report 708 dated 7 August 1968
(4) "Determination of Performance Parameters for a Powered Haulback Inertia Locking Shoulder Harness Take-Up Reel," NADC-AC-6810, dated October 1968.

The objectives of the studies were to evaluate human response for a given device, to compare mechanical analog response with human response, to examine cartridge performance, and to study the effects of long-term strap forces transmitted through a specific harness.

Examination of the reports indicated that although performance data were available to indicate acceptance or rejection, little data were available to quantitatively describe reel performance except as reflected in accileration of a simulated torso mass, strap forces, and gas pressures. In each report, strap material descriptions were unavailable. Although data were collected to indicate strap force,

head or chest acceleration, and chamber pressure if applicable, the data did not provide a description of the reel as a separate entity. Tests specifically designed to study the reel would be required.

From the data available operation of the reel was infered. The pyrotechnic is discharged and creates a high pressure, high temperature gas. The gas acts upon a piston which must have a lead screw to change translational motion into rotational in order to rotate a shaft. Webbing is attached to the shaft and is wound into the device as the force develops within the strap. The strap force acts upon the restrained body to create the observed motion.

The source of all motion is the pyrotechnic charge. Discussions with Pacific Scientific personnel revealed that the testing of a cartridge, as compared with testing using a nitrogen gas bottle, would create significantly higher costs per test. Consequently, we decided to test using high pressure nitrogen gas prior to "refining" the model with the pyrotechnic charge. We also realized that operationally the reel would work against several torso sizes and weights at various distances from the reel. In addition, the forces developed were functions of the material properties of the strap. These considerations led to the development of a test plan submitted to Pacific Scientific.

The tests were to be conducted using an operational reel and both nitrogen gas and a pyrotechnic charge. The tests desired were as follows.

(1) A series of tests using nitrogen gas and Kevlar straps with two retarding forces, two stroke lengths, and two pressures.

(2) A series of tests using nitrogen gas, Kevlar straps and two masses with the same stroke lengths and pressures previously specified.

(3) A series of tests identical with those above in (1) above, but using two different materials for straps.

(4) A series of tests identical with those of (2) above using two different materials for straps.

(5) A series of tests to replicate selected configurations of the above series, but using a pyrotechnic device.

The tests outlined were to start with the fewest number of variables and progress to more realistic configurations. The first series with Kevlar attempted to minimize strap effect, eliminate pyrotechnic variations and inertial response of the payload by collecting retarding force, strap force, chamber pressure, and strap travel with an "inextensible" strap. Without an inertial mass, and with negligible strap extension, the forces and motions measured would

be more easily related to piston travel, lead screw pitch, and chamber pressure. With each new test series, one additional variable would be introduced for incorporation within the model.

Based upon the literature reviewed, retarding forces of 75 and 100 pounds, stroke lengths of 9 and 18 inches, pressures of 1000 and 4000 psi, and dead weights of 75 and 125 pounds were proposed. Measurements were required to present strap force, strap travel, mass acceleration, retarding force, and strap motion.

After many months of discussion with Pacific Scientific the proposed test plan was revised and modified to reflect costs and scheduling limitations limitations. The data which were finally collected are discussed in a later section.

FIRST REEL MODEL

The inertia reel that was modelled consisted of a plunger which translates down a shaft, and a drum which rotates the plunger by roller surfaces which act on the drum and force it to rotate aft with the lead angle of the roller-drum interface. The motion of the plunger is dictated by the pressure that acts on it, and the pressure is developed by the rapid temperature increase in the air trapped between plunger and pyrotechnic support surface. The system assumed is shown below.

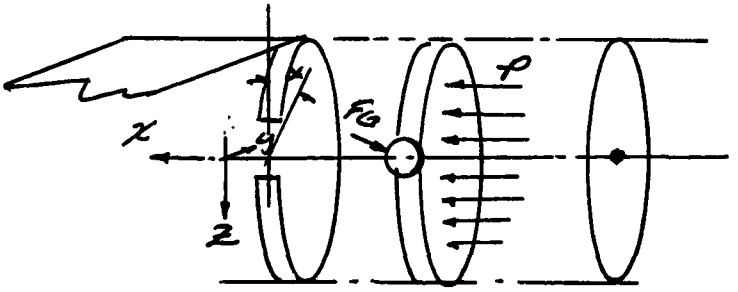

The plunger translates in the X direction due to the pressure applied and its motion is described by:

(1) $\Sigma F_x = MA_x$

$$PA_x - F_G \cos\alpha - F_F = M_p \ddot{X}$$

(2) $\Sigma F_y = 0$

(3) $\Sigma F_z = MA_z$

$$F_G \sin\alpha - F_N + W_p = 0$$

(4) $\Sigma M_x = I\alpha_x$

$$-F_G \sin\alpha\, r_p + M_{RX} = 0$$

(5) $\Sigma M_y = 0$

(6) $\Sigma M_z = 0$

$$-F_G \cos\alpha\, r_p + M_{RZ} = 0$$

The primary equations of motion are:

$$pA - F_G \cos\alpha - F_F = m_p\ddot{X} \qquad F_G \sin\alpha - F_N + W_p = 0$$

Since $F_F = u\, F_N$

$$pA - F_G \cos\alpha - u\,\{F_G \sin\alpha + W_p\} = M_p\ddot{X}$$

Considering the magnitude of the forces involved, the weight of the plunger might be ignored, likewise the frictional force. However, the frictional force should be included until proven unnecessary.

The drum rotates as dictated by the guide force and belt force.

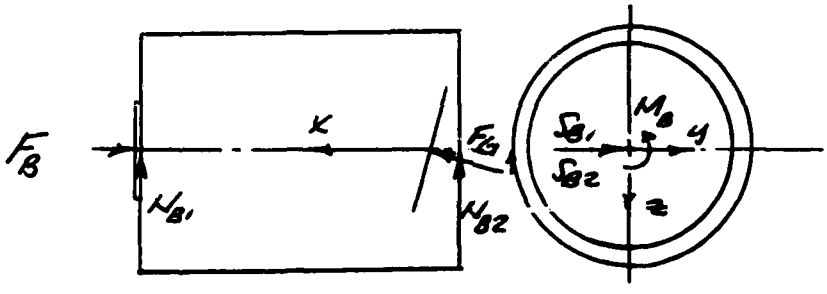

(1) $\Sigma F = ma_x$

$$F_G \cos\alpha - F_B = 0$$

(2) $\Sigma F_y = ma_y$

$$S_{B1} + S_{B2} - F_W = 0$$

(3) $\Sigma F_z = ma_z$

$$N_{B_1} + N_{B_2} - W_D = 0$$

(4) $\Sigma M_x = I_x X_x$

$$F_G \sin\alpha\, r_D - F_W r_D - M_B = I_x\alpha_x$$

(5) $\Sigma M_Y = I\alpha_Y$

(6) $\Sigma M_Z = I\alpha_Z$

$$S_{B1}\frac{X_t}{2} - S_{B2}\frac{X_t}{2} + F_G \text{ Cos } \alpha r_D = 0.$$

The primary equations are:

$$F_G \text{ Sin}\alpha r_D - F_\omega r_D - M_B = I_D\alpha$$

$$F_G \text{ Cos } \alpha - F_B = 0.$$

The resisting couple at the bearing is a function of the applied axial force, therefore,

$$M_B = \mu_B r_B F_B,$$

$$F_G\text{Sin}\alpha r_D - F_\omega r_p - \mu_B r_B F_G \text{ Cos } \alpha = I_D\alpha_x$$

Since we do not know whether or not the couple due to friction is significant it is retained initially.

Both dependent parameters are related by the lead angle.

$$X = (r_d \tan\alpha)(\theta)$$

Therefore:

$$\ddot{X} = r_o \tan\alpha \ddot{\theta}_x$$

Since the force in the guide is not necessary and ties both equations together, it is eliminated.

$$pA - \frac{I_D\ddot{\theta}_x\{\text{Cos } \alpha + \mu \text{ Sin}\alpha\}}{(\text{Sin}\alpha r_G - {}_B\text{Cos}\alpha r_B)} - \frac{F_w r_o\{\text{Cos}\alpha + \mu\text{Sin}\alpha\}}{(\text{Sin}\alpha r_G - \mu_B\text{Cos } \alpha r_B)} - \mu W_p = M_p\ddot{X}$$

Since most of the terms are fixed for a particular configuration, the equation is written

$$pA = N_1 I_D\ddot{\theta}_X - N_1 F_\omega r_D - \mu W_p = m_p\ddot{X}_p \quad \text{or}$$

$$pA - N_1 I_D \frac{\ddot{X}}{r_o \tan\alpha} - N_1 F_\omega r_o - \mu W_p = m_p\ddot{X}_p$$

$$pA - N_2 I_o \ddot{X} - N_1 F_\omega r_d - \mu W_p = m_p \ddot{X}_p$$

$$pA - N_1 F_\omega r_o - \mu W_p = (m_p + N_2 I_o) \ddot{X}_1$$

or,

$$pA - N_1 I_p \ddot{\theta}_x - N_1 F_u r_p - \mu W_p = m_p r_o \tan \alpha \ddot{\theta}_x$$

$$pA - N_1 F r_o - \mu W_p = (m_p r_o \tan \alpha + N_1 I_o) \ddot{\theta}_x$$

rewriting:

$$pA - N_1 F_\omega r_o - \mu W_p = N_2 \ddot{\theta}_x.$$

As the belt winds around the drum the belt travels a distance X . An inertial mass is attached which travels a distance X_I.

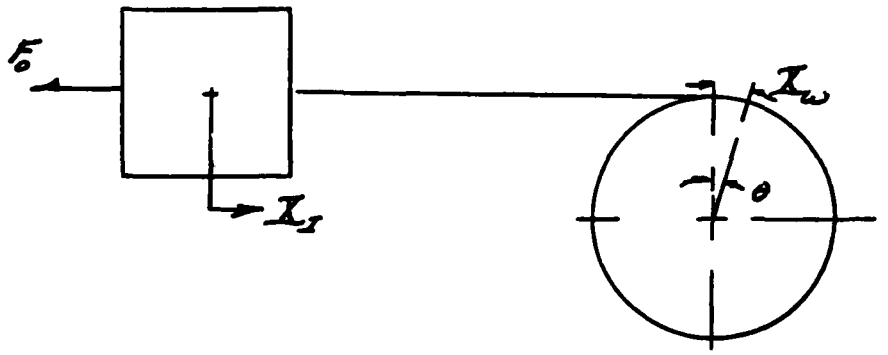

Across the webbing, if we assume a four-element fluid, the equation of motion is:

$$\sigma + p_1 \dot{\sigma} + p_2 \ddot{\sigma} = q_1 \varepsilon + q_2 \ddot{\varepsilon}$$

Since we are concerned with forces and lengths

$$\frac{F_\omega}{A_\omega} + p_1 \frac{\dot{F}_\omega}{p_\omega} + p_2 \frac{\ddot{F}_\omega}{A_\omega} = \frac{q_1}{L_\omega} (\dot{X}_\omega - \dot{X}_I) + \frac{q_2}{L_\omega} (\ddot{X}_\omega - \ddot{X}_I)$$

For the inertial mass:

$$-F_o + F_\omega = M_I \ddot{X}_I .$$

The displacement of the webbing at drum attachment is X and is related to the angular displacement of the drum simply by

$$X_\omega = r_p \theta$$

which can be substituted when necessary.

The pressure acting on the plunger is created by the pyrotechnic in a unknown manner. However, the pressure should obey a law similar to

$$\frac{P_o V_o}{T_o} = \frac{p_1 V_1}{T_1} .$$

Hence, it is assumed that temperature is the independent variable, that is T = T(t), and is prescribed as the input, then

$$p(t) = \frac{P_o V_o}{T_o} , \frac{T(t)}{V(t)}$$

if the temperature were to increase without motion of the plunger, pressure would increase linearly with the temperature. However, the volume will change. The volume is

$$V(t) = V_o + A_p X_p$$

which relates the volume back to the plunger displacement. This is written

$$p = \frac{P_o V_o}{T_o} \quad \frac{T}{V_o A_p X_p} .$$

The equation of motion for the plunger is:

$$\frac{P_o V_o}{T_o} \quad \frac{T}{(V_o + A X_p)} \cdot A_p - N_1 F_\omega r_d - \mu W_p = (m_p + N_2 I_d) \ddot{X}_p$$

Therefore,

$$\ddot{X}_p = \frac{\dfrac{P_o V_o T(t)}{T_o (V_o + A x_p)} \cdot A - N_1 F r_o - W_p}{(m_p + N_2 I_b)} .$$

To calculate the forces in the webbing,

$$\ddot{F}_\omega = \frac{A_\omega}{P_2 L_\omega} q_1(\dot{x}_\omega - \dot{x}_I) + q_2(\ddot{X}_\omega - \ddot{X}_I) - \dot{F}_\omega \frac{p_1}{p_2} - \frac{F_\omega}{p_2}$$

and

$$X_\omega = \frac{X_p}{\tan \alpha}$$

and

$$\ddot{X}_I = \frac{F_\omega - F_o}{M_I} .$$

These are the equations required for computer solution. The constants required are:

p_o	the initial chamber pressure
V_o	the initial chamber volume
T_o	the initial chamber temperature
A_{pl}	the area of plunger acted upon by the pressure
a_1	the lead angle of the drive mechanism
r_d	the radius of the drum
r_B	the radius of the bearing
μ_B	the coefficient of friction of the roller
d	the coefficient of friction of the bearing
W_p	the weight of the plunger
I_o	the mass moment of inertia of the drum
A	the area of the webbing
L	the length of the webbing
p_1, p_2, q_1, q_2	the viscoelastic coefficients of the webbing

F_d the initial preload of the system

W_I the weight of the inertial mass

L_R the length of strap retracted.

The model will solve for retraction time and forces evolved as functions of strap length, material properties, and retraction length. Starting with a temperature versus time input, the model will calculate plunger, drum, webbing, and inertial mass motion until the mass has traveled the input strap length. At that time, the resisting force is increased and strap retention force would be computed.

The equations need to be adjusted somewhat in that, at time zero, the reel does not windup due to ambient pressure. Hence, the pressure must reflect the difference over ambient. Secondly, the retarding force on the inertia mass acts on the mass without introducing a force in the belt. Therefore, the belt force starts at zero and builds up to the initial retarding force before the inertial mass can move. This is controlled in the integration coding.

INITIAL COMPUTER ANALYSES

The equations discussed were programmed in MIMIC and assumed values for the parameters were generated. At this time the data available from Pacific Scientific were limited to one figure of measured pressure, strap force, and dead weight acceleration. Therefore, all dimensions were based upon the estimated size of an inertia reel. The values used were:

Ambient Pressure	PO = 14.7 pounds per square inch
Initial Volume	VO = 6 cubic inches
Ambient Temperature	TO = 273 degrees (K)
Plunger Area	AP = 12 square inches
Lead Angle	AL = 30 degrees
Drum Radius	RO = 2 inches
Bearing Radius	RB = 1 inch
Frictional	MU = 0.05
Coefficients	MB = 0.05
Piston Weight	WP = 1.8 pounds
Drum Inertia	ID = 0.01 pound-inch-seconds square
Webbing Area	AW = 0.14 square inches
Webbing Length	LW = 18.00 inches
Material Coefficients	G1 = 64,000
	G2 = 64,000
	N1 = 6,400
	N2 = 6,400
Preload	FO = 5 pounds
Inertial Weight	WI = 50 pounds
Retraction Length	LI = 14.0 inches.

These reflect assumed diameters and lengths for a drum which must retract a strap 18 inches long. The material properties were also assumed prior to measured data availability.

The equations of motion require a time and temperature profile as input. Data were available from reports such as "Measurements of Pressure for the $Titl_x/KCLO_4$ System" by H. H. Chong and J. E. Gloub of Monsanto Research Corporation. An assumed temperature peak of 5000^{o} C in 0.005 seconds did not create a pressure as great as indicated on the one figure available. Although the peak temperature and time-to-peak were reasonable, the pressure was too small and it was then necessary to reexamine the input function. One method of improving the pressure response was to consider the pyrotechnic charge as being converted to a gas during the burning to create a more dense gas. With greater density and high temperature-time profile, the chamber pressure could be increased.

The initial computer runs were useful in finding diagnostic problems in the coding, but were of little value in generating a model with elements related directly to an operational piece of hardware. Revised initial volumes were assumed, piston areas changed, and material properties varied. It was apparent that dimensional data were required. Figures 42 and 43 are indicative of variations examined and show that some appreciation of the effects of parameter variations was possible during this phase.

REVISED INERTIA REEL MODEL

Two items of quantitative data were received from Pacific Scientific after the model had been made operational. The first was the test data of Figure 44 indicating the response of the reel to a pyrotechnic charge lifting a dead weight. This was a test environment as desired although the experimental design was still not known. The second data item was the configuration on the illustrated parts figure as shown in Figure 45. The figure does not contain any measurements, but the list accompanying the figure did call out a specific bolt size; therefore, it was possible to scale the figure to approximate lengths and diameters, and to calculate the lead angle. Also, it was necessary to incorporate two shafts into the model as well as the power spring that connects them. Assuming a 0.010-inch thickness power spring, curves relating drum rotation, power spring diameter on the drum and mandrel, and mandrel rotation were generated. These were necessary to include the effects of diameter changes during retraction.

As soon as the revisions had been made computer runs were made to determine the effects of the changes. As shown in Figure 46 the changes were significant. The new curves required changes in material

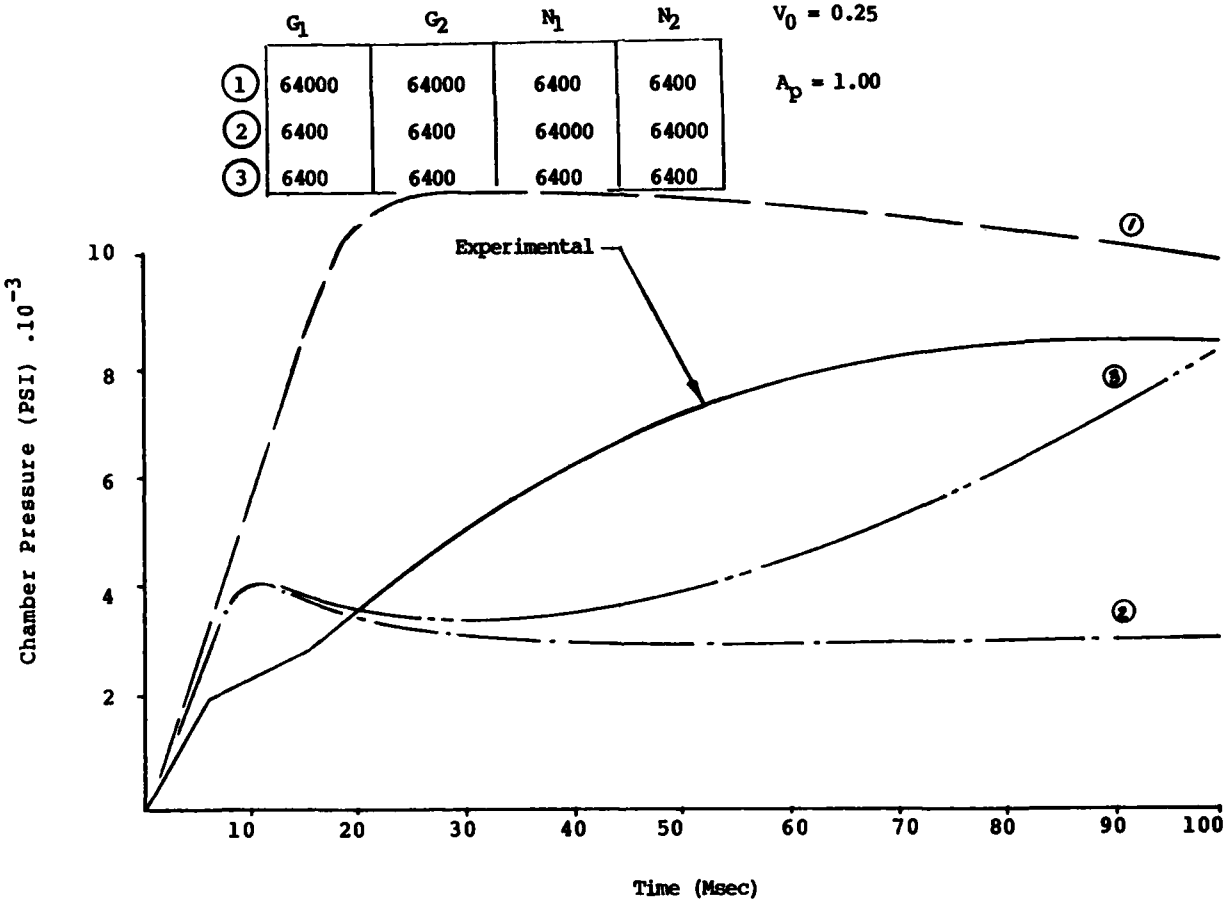

Figure 42 Chamber Pressure versus Time for Several Strap Material Properties Using Initial Reel Model.

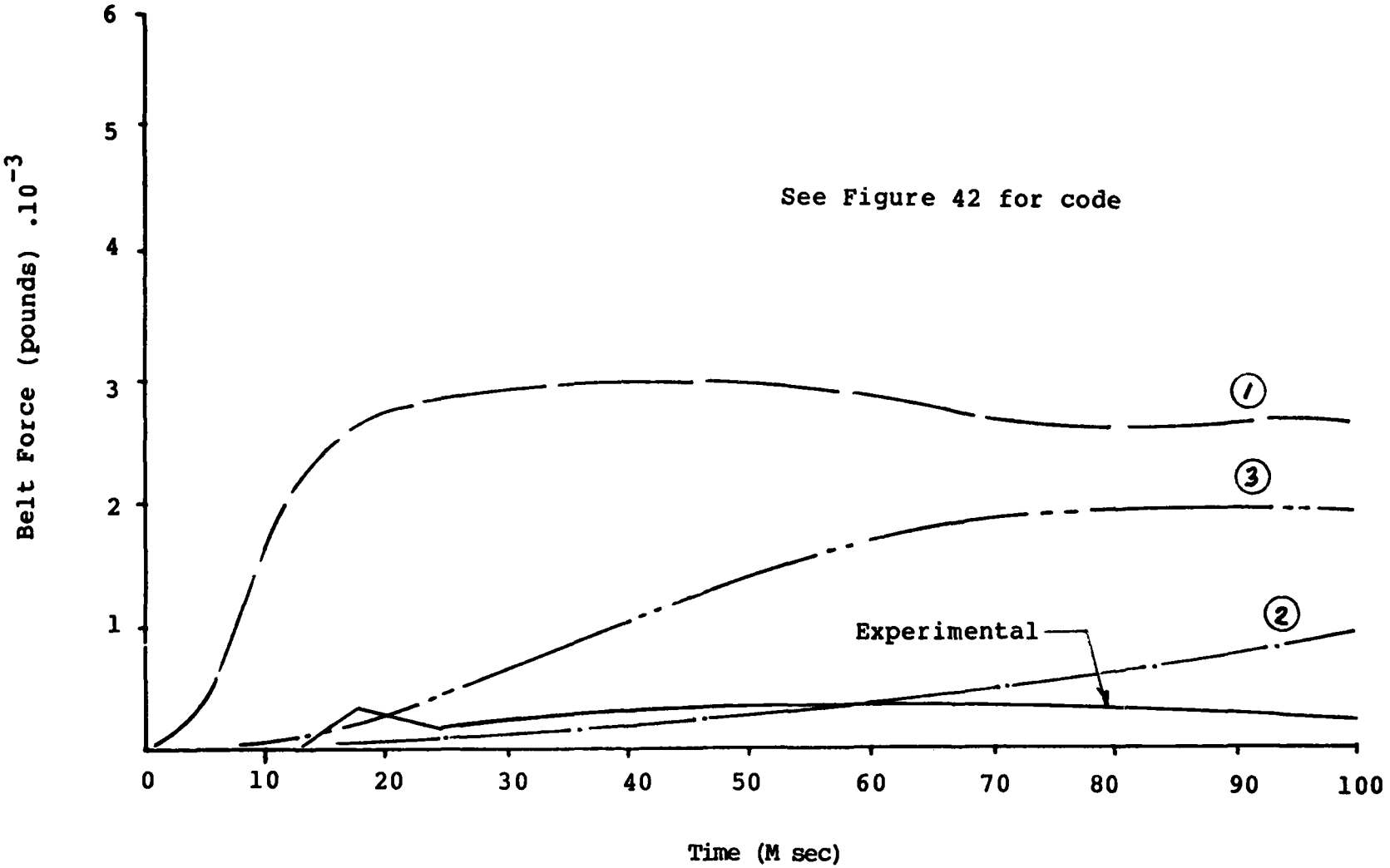

Figure 43 Belt Force versus Time for Several Strap Material Properties Using Initial Reel Model.

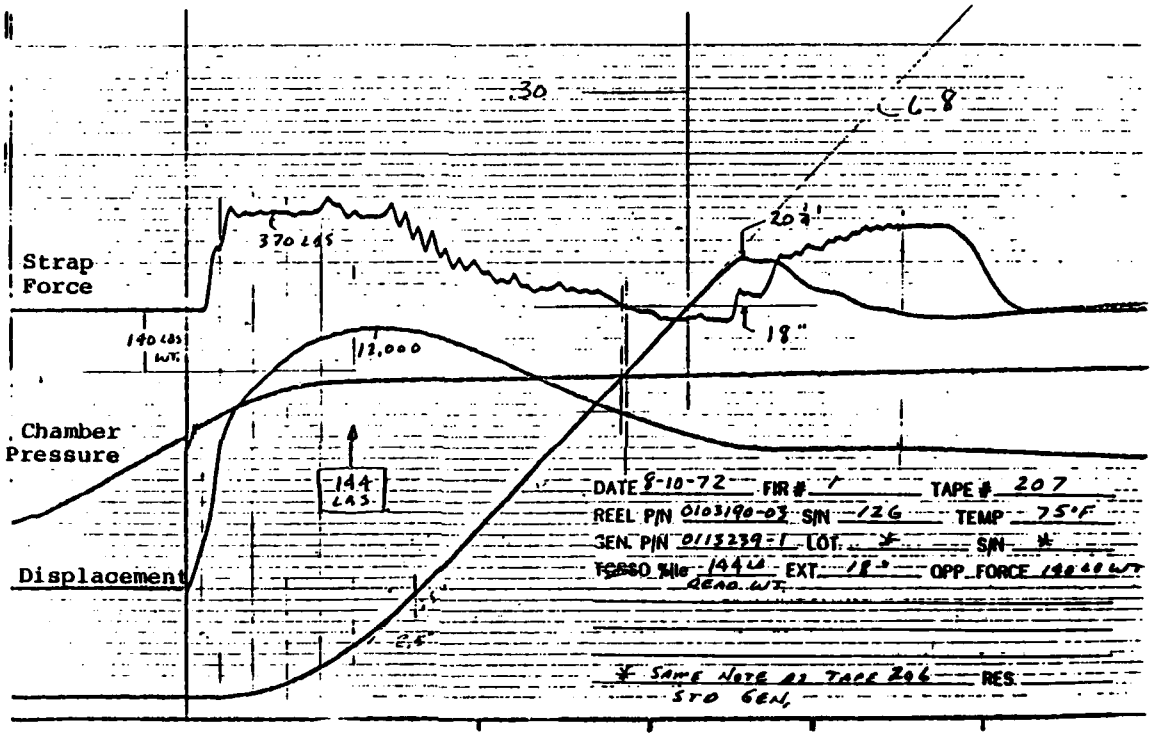

Figure 44 Experimental Data for Pyrotechnic Inertia Reel.

(As delivered by manufacturer)

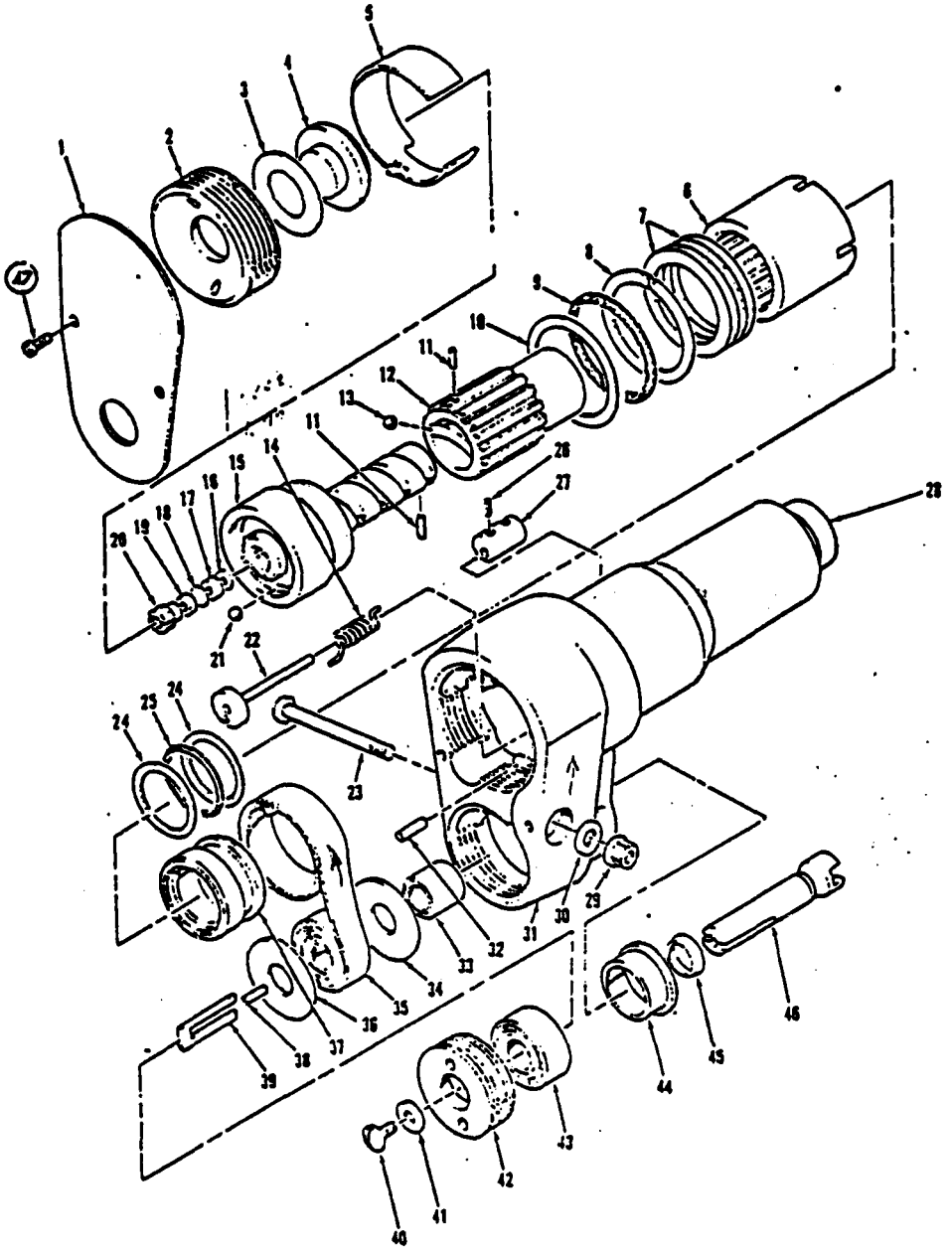

Figure 45 Illustrated Parts List.

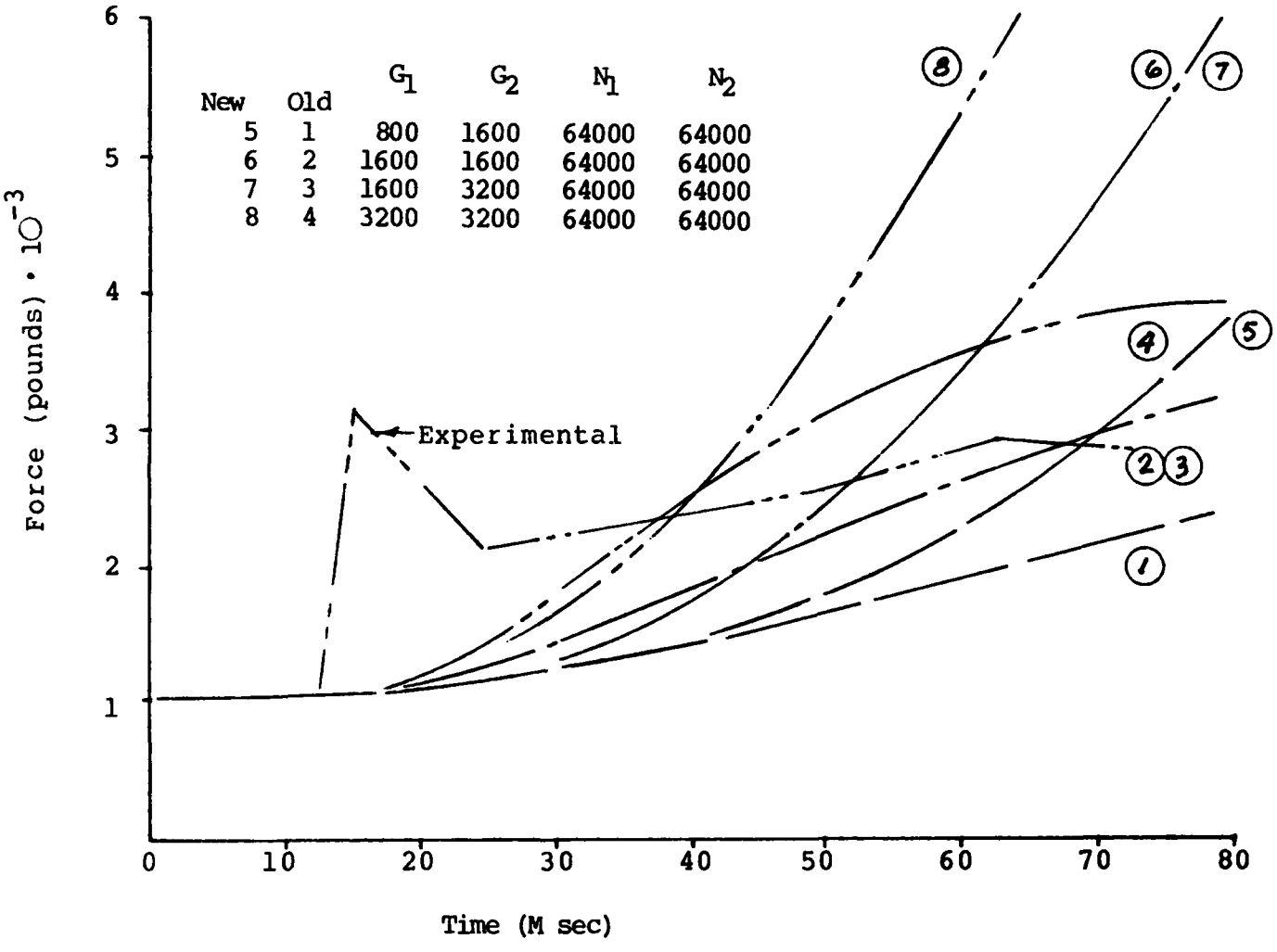

Figure 46 Force Response Curves for Revised Model versus Original Model.

coefficients and the temperature input in order to put the calculated chamber pressure, belt force, and mass acceleration at the approximate levels required.

During the same time period, discussions with Pacific Scientific indicated that the design incorporates characteristics which permit a high back pressure on the piston during its motion. The nature of the back pressure was not well defined although it was thought to be caused by fluid around the seals and pressure buildup through an orifice. Some time was spent attempting to quantitatively describe the phenomenon, but the number of unknowns made the problem too complex. It was apparent that the explanation would be creating more unknown parameters to be assumed. Therefore, it was assumed that the back pressure could be idealized as either a function of piston velocity or piston velocity squared. Although the exact nature of the flow around the piston is not known, it can be assumed to be:

$$p = p_o + KV_p \quad \text{or}$$

$$p = p_o + KV_p^2$$

where all of the unknowns are buried within the K value found to match the data.

The approach selected is contrary to the approach desired in that the quantitative relations buried in "K" are unknown. However, for any particular series of inertia reels, one with the same piston size, drum diameter, etc., one could assume that the back pressure relation would be reasonable. Hence, we are departing from being able to describe the kinetics of the reel by equations of equilibrium with dimensional data, and have yielded to a situation of too many unknowns. The result is a coefficient which is truly a model coefficient for that particular reel. The KV or KV^2 relation found is then used because it works, not because it is understood.

Many computer runs were made with the revised model. The required dimensional data came from the illustrated parts drawing, and material properties were being developed for the "standard" strap shown in the single set of dead weight test data available. Variations were made by assuming that two extremely different peak chamber temperatures would increase linearly with time. Variations in back pressure were also assumed by selecting many variations in KV and KV^2. The several curves generated are shown in Figures 47 and 48. From these results it was then possible to recognize variations required in both temperature and back pressure which would permit even better approximations to the measured data.

Investigations continued in model improvement since the fit could be improved by changing the temperature-time profile and changing the material properties. For example, the high frequency content on belt

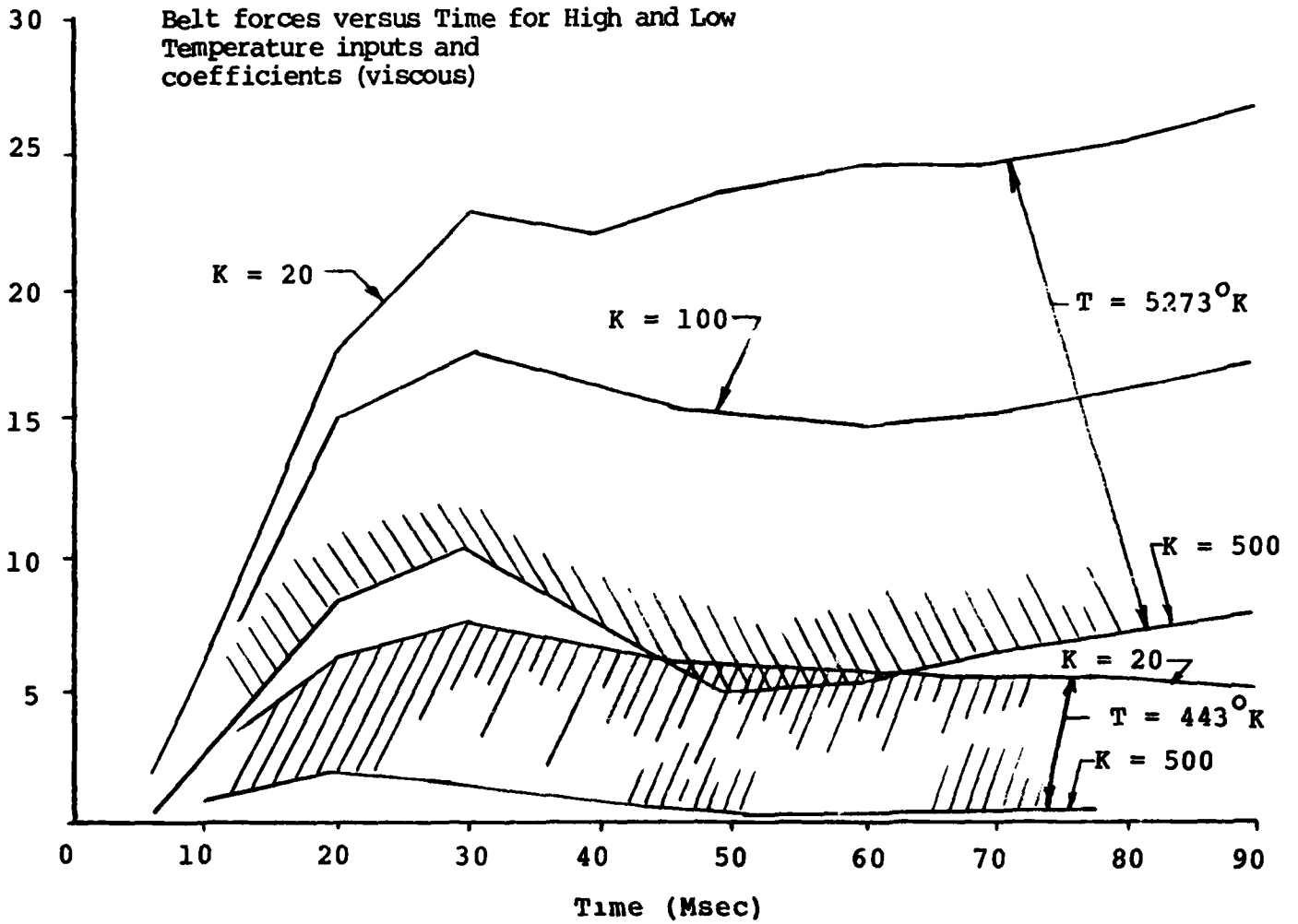

Figure 47 Revised Model Belt Force Envelopes for Back Pressure of KV Form.

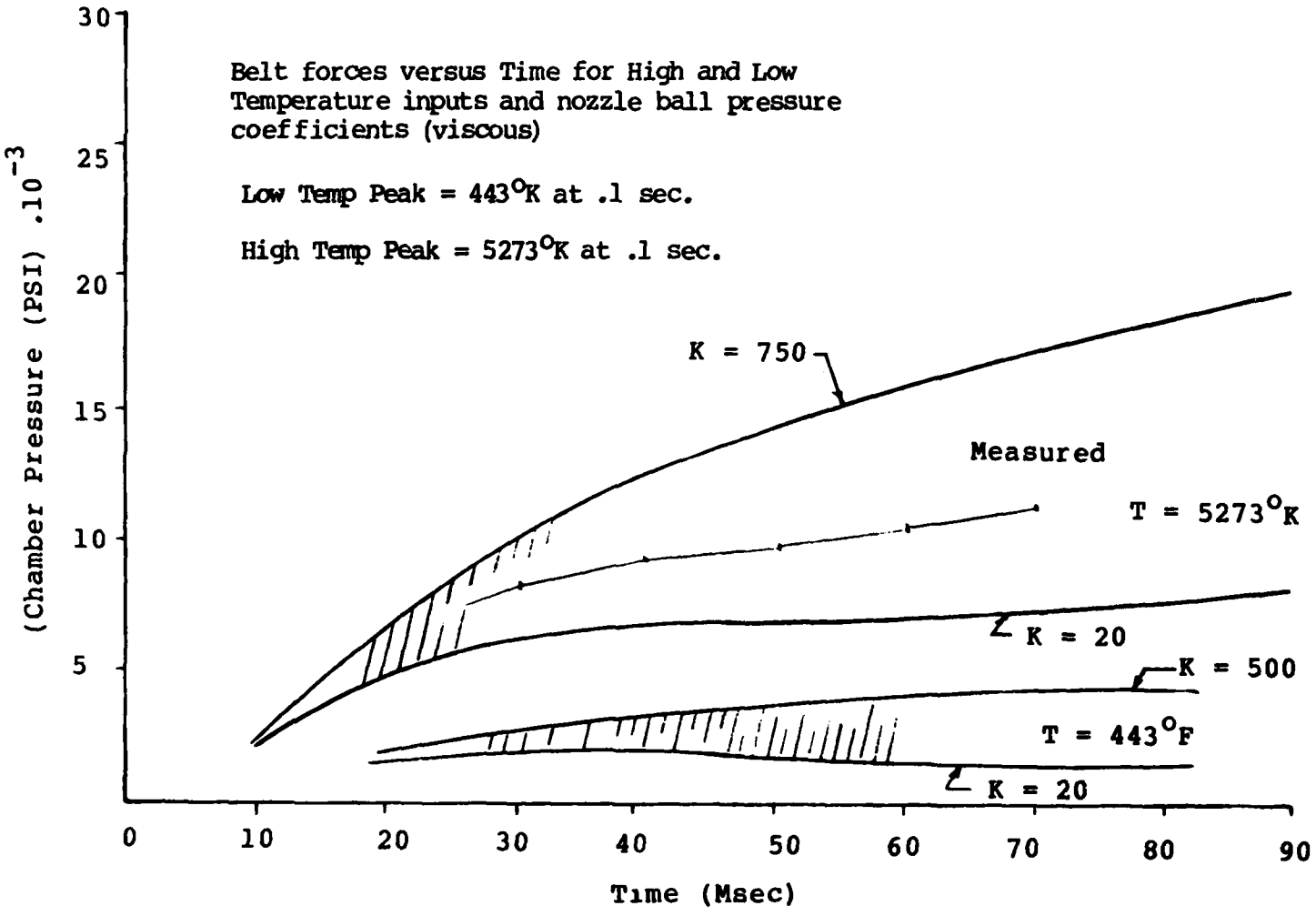

Figure 48 Revised Model Chamber Pressure Envelopes for Back Pressure of KV Form.

force output could only be duplicated by changing the material properties of the belt. At this point, a possible unique solution emerged to match chamber pressure, belt force, and belt travel. Peak chamber temperature and its time relation, and back pressure appeared to have effects which would permit, if not a unique solution, at least a narrow range of values which would create the desired responses. These hopes were short-lived.

A Pacific Scientific Inertia Reel appearing to match the one described in the illustrated parts figure was received for disassembly and inspection. The reel, specifically a device, (restraint harness take-up inertia-locking, powered-retracting meeting specification MIL-D-81514) was disassembled. The area diameters, and lengths were not exactly as scaled. This was to be expected. However, one major difference was that the lead angle shown on the illustrated parts list was a left-handed thread whereas the hardware was manufactured tc be a right-handed thread. Since the power spring could only retract in one direction, the assumption of a left-handed thread implied motion of a drum as dictated by the piston. If the lead angle is right-handed, the power spring attaches to the piston and the drum translates. Hence, those parts assumed to rotate translate, and those assumed to translate, rotate. The model had to be revised to incorporate dimensional changes, but the additional changes had not been anticipated.

The computer model was revised, coding changed, equations modified, and the revised model was exercised to try and bring the calculated responses up to the level of agreement with measured data that had been achieved prior to inspection of the hardware. The outputs generated did not compare favorably with the measured data, and, although it was possible to again conduct parameter variation studies, it was thought more prudent to question the measured data. Modeling was terminated until measured data on a documented test setup could be obtained.

PYROTECHNIC DEVICE TESTING, DATA COLLECTION AND ANALYSIS

Discussions with Pacific Scientific led to the evolution of a simplified testing program to collect data indicative of hardware response. As mentioned previously, it was desirable to eliminate as many unknowns as possible. Tests should be conducted with a reasonably inextensible strap, dead weight, a pyrotechnic charge, and a range of extensions.

The tests were to be conducted using a pyrotechnic charged reel retracting a dead weight of 144 pounds. Straps at the reel were to be Kevlar and a standard webbing material. The retraction distances were to be 4-1/2, 9, 12, and 18 inches.

The tests were conducted at Pacific Scientific using the test setup as shown in Figures 49, 50, and 51. The force in the strap was measured using a 0 to 500 pound transducer of ±2 percent accuracy. The chamber pressure was measured with a 0 to 20,000 psi transducer of ±2 percent accuracy, and a ±15 g acceleration with similar accuracy measured the acceleration of the dead weight.

The data collected during the tests are shown in Figures 52 and 53. These data are indicative of the tests conducted whether with Kevlar and Standard (Dacron WD 314) webbing. The results can be summarized as shown in the following table.

Table 11 Test Parameter Measured Versus Retraction Length

Table Number and Title	Retraction Length 4-1/2"	9"	12"	18"
Dead Weight Travel (inches)	5/8* / 0	1 3/4 / 4 1/4	7/9 3/8	18/17
Peak Pressure after Transient (pound per inch square)	5600/ 4600	5500/ 5000	5800/ 5400	9500/ 8400
Strap Velocity (inches per second)	0/0	1.1/ 1.3	2.0/ 2.9	6.2/ 5.9
Force Peak (pounds)	170/ 380	275/ 200	400/ 350	712/ 875
Time to Full Retraction (seconds)		0.35/ 0.50	0.53/ 0.48	0.33/ 0.40

*The upper figure is for the standard webbing, the lower for the Kevlar strap.

The results indicate that the device has the capability to retract a dead weight of 144 pounds over 18 inches. In doing so, the reel must wind up twice as much webbing at one-half the force level of the strap. The results also indicate that at retraction lengths of less than the maximum value, the reel cannot fully retract the dead weight.

Because of uncertainties in understanding the device's operation it is difficult to state exactly why the retraction becomes so

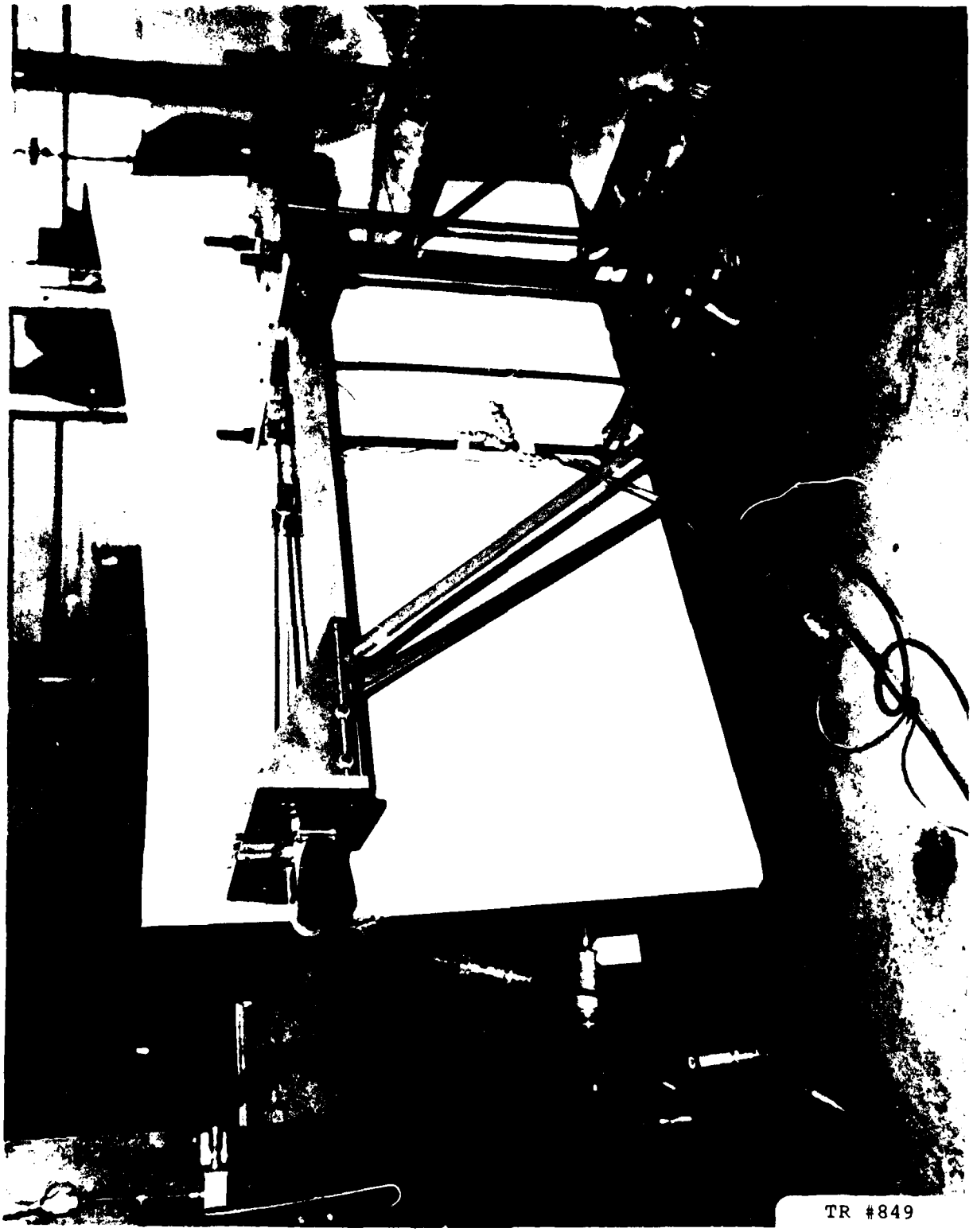

TR #849
Photograph #1

Figure 49. Test Set-up for Powered Retraction Tests.

TR #849
Photograph #2

Figure 50. Top View of Reflected Strap.

TR #849
Photograph #3

Figure 31. [illegible] Attachment.

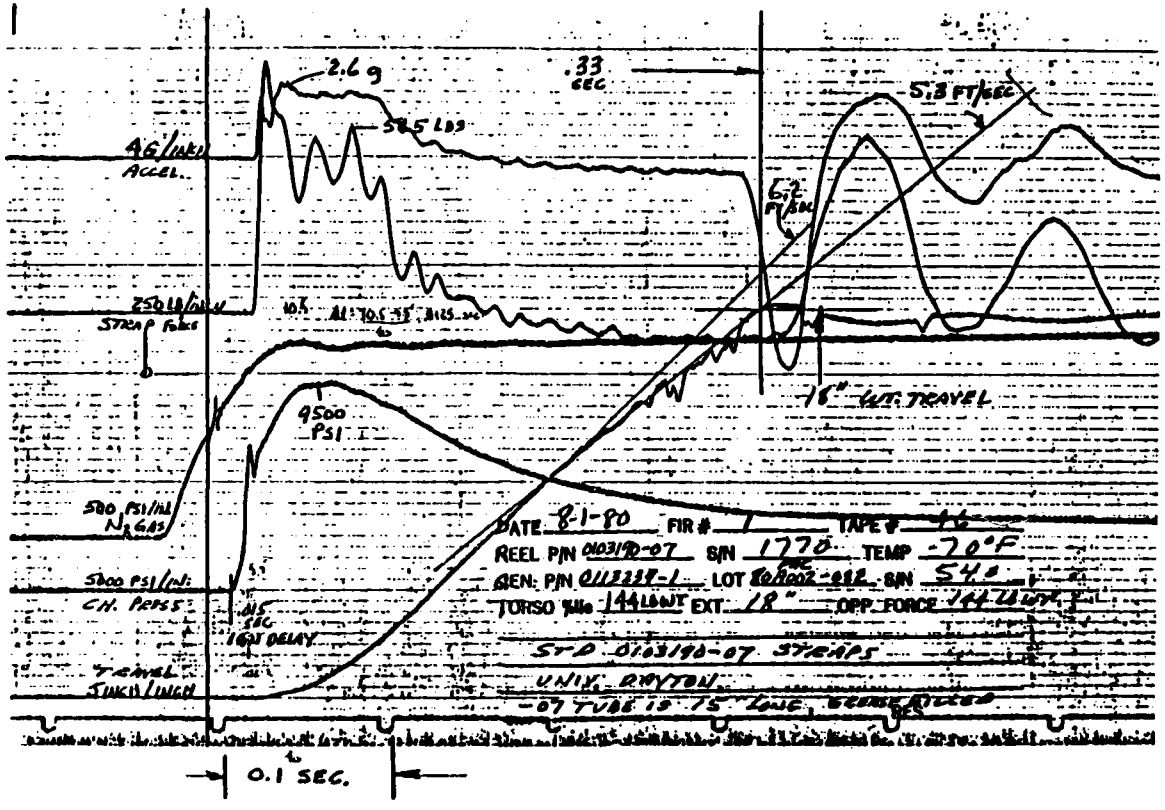

Figure 52 Inertia Reel Response Data for 18" Stroke Length.

(As delivered by manufacturer)

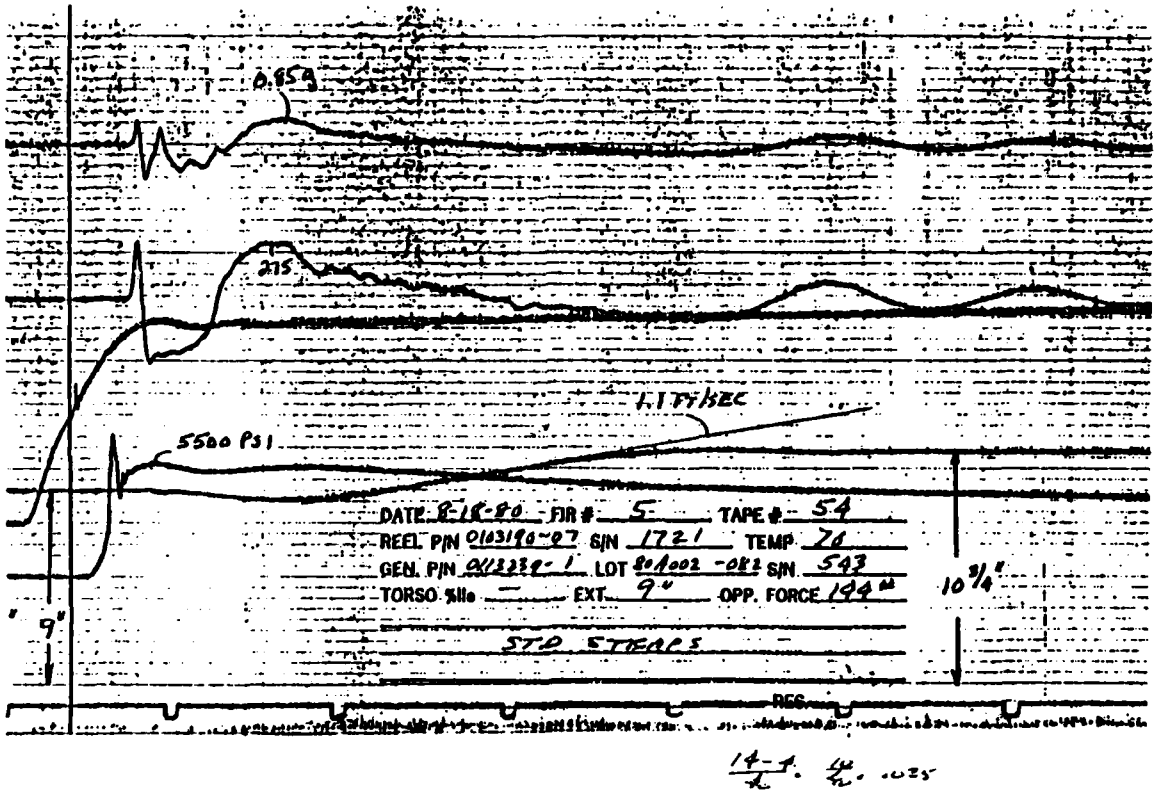

Figure 53 Inertia Reel Response Data for 9" Stroke Length.

(As delivered by manufacturer)

inefficient at the lesser retraction lengths. However, some observations can be made. As the retraction length is increased, the mandrel rotates clockwise as the webbing, which is attached to the mandrel, is extended from the reel. The mandrel is attached to the power spring which drives the arbor and screw assembly. The screw assembly rotates and drives the nut inward. The further the strap is pulled from within the device, the closer the nut is driven into a sleeve that restricts rotation of the nut. The end of the nut is positioned closer to the chamber containing the piston. This is necessary since the screw must be driven a greater distance as greater retraction is required. The nut is driven closer to the piston, as the webbing is withdrawn, and the volume between the two is decreased. This causes the pressure in the pyrotechnic compartment to build up more quickly since the initial volume is small, and with very little motion of the piston, the force in the strap acts to inhibit piston motion.

If the strap is retracted a small distance, the nut is separated from the piston by a significant distance creating a large volume. After the charge is fired, the piston is accelerated and the pressurized volume increases rapidly without any appreciable resisting force. Consequently, the pressure generated will decay more quickly and some of the energy is dissipated in accelerating a piston prior to creating a retraction force.

Another aspect to be considered, and seen in the data, is that since a standard material strap has viscoelastic properties, the strap elongates and compresses as it wraps around the mandrel. In the middle retraction lengths the travel of the dead weight is less with greater force developed. The strap material elongates more instead of being wound up and the energy is dissipated in stretching the material and compressing it on the mandrel. The more material on the mandrel the more work required to take out the "slack" before generating a force to overcome the inertia of the dead weight.

The measured data of Figures 52 and 53 are indicative of the actions described above. At the longer retraction length the charge is fixed and the pressure builds up to overcome some internal friction. At the point where the piston releases, the pressure spikes as the motion generates an increased volume. As the piston accelerates, the volume continues to increase, but the energy developed by the charge is capable of causing increased pressure. The pressure is increased also because the piston is acting against a screw assembly already restrained from rotating by an increasing strap force.

At the very short retraction length, the charge ignites and the piston is accelerated. As the gas is created and temperature increases, the volume increases to keep the pressure down and does so without being impeded by a resisting strap force. When the piston does contact the screw assembly, the pressure doesn't increase since

the force evidently goes into "winding up" the material on the mandrel or the energy available has been dissipated.

At this point, we questioned whether or not the model development should continue since the performance measured at the small stroke lengths was unacceptable. However, the need for the model remains in order to see whether or not the data can be fitted even approximately to aid in investigations to determine possible means of improving reel performance.

SECTION 5

RESTRAINT SYSTEM SCALING ANALYSIS

INTRODUCTION

The success of a protection system ultimately depends upon its capability to provide a tolerable human response from an environment which would have been intolerable without it. Evaluation of the performance of a protective system is far more difficult than might be suspected in that testing of a human in an intolerable environment is not permitted. Information on the performance of restraint systems are limited to accidents, where data are not collected, or from tests with human subjects at levels which are less than injurious. Consequently, surrogates are used to evaluate safety systems performance at injurious levels. These may be cadavers, anthropomorphic dummies, analytical models, or sub human. All have drawbacks and limitations. Only the use of a subhuman or a comparable primate model will be considered in this section.

Animals have been used to study injury potential in an acceleration environment for many years. The work of Kornhauser [11] illustrated the potential of using analog models of living systems to predict impulsive or long duration response similar to that of a spring-mass-damper system. This type of analogy has been used by many investigators to study scaling laws or laws of similitude as a means of inferring human tolerance. Unfortunately, it is not always possible to determine what the relationships between the species might be.

In the current effort the same problem is present but in a more complicated manner. If a restraint system is to be tested using a subhuman primate, the restraint must be tailored to fit the subject. But if the restraint is geometrically scaled, is the response linearly scaled? Even if the kinematic response does permit linear scaling, is the injury linearly scaled?

APPROACH TO PRIMATE SCALING

Restrained for the purposes of the initial portion of this investigation, subhuman primate is assumed to respond to a retraction environment in the same manner as the human. The torso is drawn back and the head and neck respond. Kinematically, the response is described in the same manner as the human, and therefore by the same model, as developed for the human. If the dimensional data and inertial data for the subhuman primate are available, prediction of torso and head and neck motion are possible. If the kinematics are found, then injury potential can be evaluated in terms of injury criteria models or injury data available for the animals. Using the

models evolved for a restrained human, the coefficients are adjusted to reflect the characteristics of the animals. Dimensions, inertial characteristics and injury criteria parameters can be easily adjusted. The problems remaining are the scaling of the restraint system and the environment.

The restraint system consists of a harness or belts made of a particular material and fabricated into a particular configuration. The straps are made from a material having a specific cross-sectional area. The area influences the response of the strap, and the width dictates the pressure at the surface of the body. The configuration is a geometrical arrangement of the straps or harness material over the torso. Duplication of the configuration implies having the same geometrical arrangement relative to the same anatomical landmarks on human or subhuman primate torsos. Hence, if the configuration is based upon a design suprasternal to distal length and shoulder width, then these dictate harness or strap length for both human and animal.

On the basis of the previous data presented, restraint configuration effects dominate over restraint material properties effects during retraction. Consequently, in scaling for subhuman primate tests, the configuration must first be considered. The subhuman primate and human are anatomically similar, but not necessarily geometrically similar. The angles formed by a restraint configuration on the human may not appear as the same angles on the animal. Since the harness rotates relative to the torso, in the human the same relative motion should exist on the animal. Therefore, it is assumed that a "scaled" harness will have a configuration established by locating the straps or harness material at the same location, relative to anatomical landmarks, as on the human.

After the configuration is defined, the specifics of the strap or harness material must be determined. Fortunately, since previous data indicate the importance of configuration over material properties, it is possible to consider first the practicalities. The straps must have adequate strength to create the retraction environment without failure. Secondly, the strap width must not create surface pressures which would cause injury. Based upon calculated tolerable chest surface pressures for the human of about 25 psi for a 10 g deceleration, this infers a surface area of about 8 square inches on a twenty-pound subhuman primate, or two 3/8" wide straps. For the types of materials tested this would imply a material thickness of only 0.033 inches to keep the stresses in a linear range.

A "scaled" harness can be fabricated from available materials, configured by anatomical similarity, and designed based upon strength considerations. The dynamic response of the torso due to the material properties must still be considered, but its effect, relative to the effect of the configuration is considered small.

The test subject is "scaled" dynamically by having dimensional and inertial characteristics from published literature. The harness or strap is scaled as discussed. The desired output or criterion parameter must also be scaled. Fortunately, this was accomplished as part of its development. The head injury criterion used is the maximum strain criterion (MSC) as established by Stalnacker several years ago. The criterion was developed by establishing a relation between injury observed and impedance characteristics measured. By conducting tests to establish impedance characteristics of a "skull" and "brain", it was possible to establish model characteristics which would duplicate the measured driving point mechanical impedance. Once model coefficients were found which duplicated external observations, it was a small step to relate the model kinematics to observed injury. This was accomplished by correlating model strain to observed levels of injury. Therefore, measured mechanical "properties" known to be related to external forces were used to calculate "tolerable" strain. Hence, for selected subhuman primates with impedance models, internal strains for known translational accelerations were found to agree with observed levels of injury. The level was then related to quantitative values of strain.

The use of the MSC model completes the whole body model necessary to study restraint system scaling. For a given restraint system, the configuration is anatomically scaled to locate straps at the correct position. The strap material is selected and scaled to provide adequate strength at a tolerable pressure. The environment is then varied to study its effect upon primate response.

DEVELOPMENT OF A PRIMATE MODEL

The completed human model was modified to predict the response of a seated, harnessed primate. Data for the model were taken primarily from AMRL-TR-78-7 "Refinement and Validation of a Three Dimensional Head-Spine Model" by Belytschko and Privitzer [13]. The report contains stiffness, strength and inertial characteristics for idealized human, baboon and rhesus monkey body segments. The data are related to spinal segments instead of the torso as a complete unit. Therefore, it was necessary to generate head, neck, and torso elements from the segment data. Since center of gravity locations, mass moments of inertia and mass were tabulated, it was possible to find the composite center of gravity and inertial characteristics. The values calculated are shown in Figure 54 and Table 9. The human data are shown for comparison with previously used data.

The tabulated data for the rhesus monkey were used to construct a rhesus model seated in the same orientation as had been used for the human model validation studies. The torso, neck, and head were oriented at the same angles relative to the horizontal and the restraint straps located at the same angle between top of shoulder and retraction point on the seat. The same viscoelastic webbing

	Y	Z	W	Ixx	Iyy	Izz
TORSO	9.835	26.481	42.458	16149.8	18087.5	5032.04
NECK	10.2	70.0	1.365	26.2	26.2	29.65
HEAD	10.04	79.765	5.612	447.86	404.4	338.5

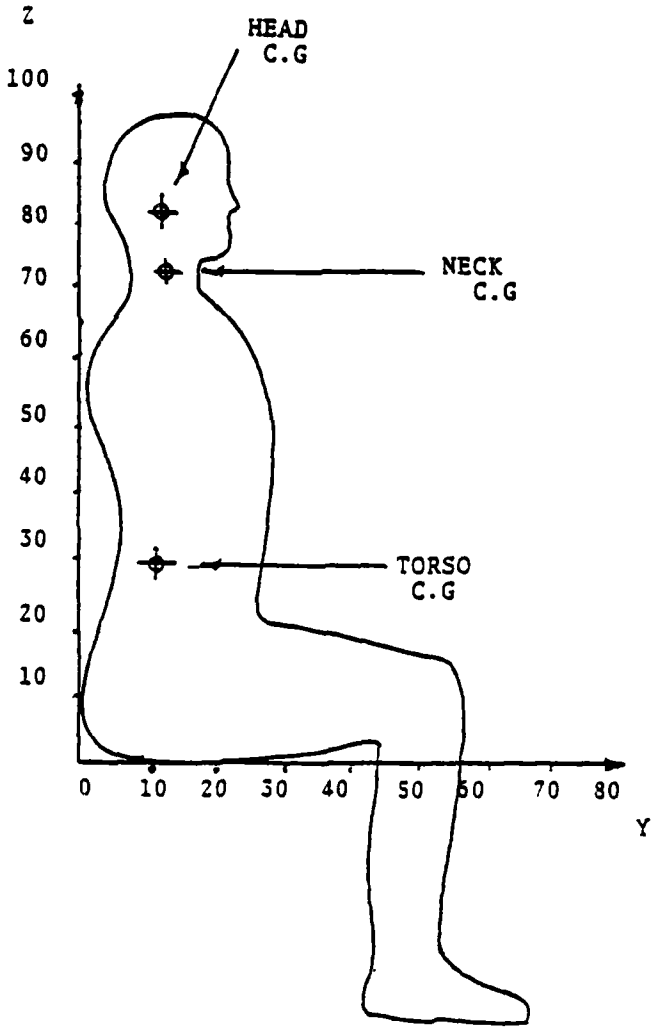

Figure 54 Human Dimensional Data.

TABLE 6

HUMAN AND PRIMATE DIMENSIONAL DATA

		$Y_{C.G}$	$Z_{C.G}$	W	Ixx	Iyy	Izz
HUMAN	TORSO	9.835	26.481	42.458	16150	18088	5032
	NECK	10.2	70.0	1.365	26.2	26.2	29.65
	HEAD	10.00	79.8	5.612	447.86	404.4	338.5
BABOON	TORSO		33.7	7.55	2054	2054	219
	NECK		63.2	0.14	0.39	0.39	0.63
	HEAD		69.248	0.9266	21.99	20.24	9.158
RHESUS	TORSO		18.7	4.03	526.274	526.274	71.5629
	NECK		39.0	0.078	0.145	0.145	0.45
	HEAD		44.88	0.652	7.465	7.465	7.465

ALL UNITS - INCH - POUND - SECONDS

properties were used along with the same harness coefficients except that the harness force displacement curves were modified to reflect a scale change. Since there are no data on a rhesus harness, the "slack" in the harness was assumed to be approximately proportional to the ratio of seated torso heights. Hence, instead of a 2.6 inch maximum harness rotational displacement, only 1.3 inches was used.

The primary unknowns were the coefficients necessary to represent the head and neck joint resistances. Although vertebral element data were available, it was desirable to have coefficients taken from experimentally observed head and neck motion of a rhesus. Such data were available from research conducted on Contract F33657-68-1353 with the Aerospace Medical Research Laboratory. The unpublished data, were collected by photographically observing the head response of rhesus monkeys during force and aft vibrations. Over the frequency range of 3 to 30 Hz, two peaks in the transmissability curves for translation and rotation were found. The one, at about 4.5 Hz, was believed to be translational due to neck/shoulder joint motion. The second, at about 21.0 Hz, was thought to be the rotational response about head/neck joint. The effort resulted in the deviation of damping ratios for both joints. Using the known masses, mass moments of inertia, and center of gravity lengths, stiffness and damping coefficients for both joints were calculated.

The values used were:

K_H = 114.9 inch pounds/radian

C_H = 0.01 inch pounds/sec/radian

K_N = 28.1 inch pounds/radian

C_N = 0.105 inch pounds/sec/radian

These assumed a head rotational natural frequency of 21.0 H_z with a damping ratio of 0.01 and a translational natural frequency of 4.5 Hz with a damping ratio of 0.45.

All of the coefficients assumed and calculated are shown below as taken from the tabulated computer routine input.

TABLE 10 - RHESUS INPUT DATA

	HEAD	NECK	BRAIN	CHEST WALL
WEIGHT	1.438	0.172	1.197	0.222
LENGTH REQUIRED	1.600	1.800	2.180	(NOT REQUIRED)
MASS MOMENT OF INERTIA	0.00660	0.000128	(NOT REQUIRED)	
DAMPING COEFFICIENT	0.010	0.105	1.000	0.253
STIFFNESS COEFFICIENT	114.9	28.1	10000.	333.0,-138.7
(ALL UNITS, INCH-POUND-SECONDS-RADIAN.)				

The chest wall model parameters were selected using data available from Beckman [14], "Thoracic Force-Deflection Studies in Living and Embalmed Primates". Force-deflection curves for rhesus monkeys were available for chest impacts at up to 65 feet per second. The initial dynamic stiffness was approximately 333 pounds/inch with the force gradually curving over to a 150 pound peak at approximately 1.8 inches of deflection. These were duplicated by the nonlinear stiffness capability of the model.

ANALYSIS OF RHESUS RETRACTION MODEL DATA

The rhesus model was first used to examine response to the same input as used in the human validation study. The input and strap length were then varied to examine the effects of some preliminary changes which could guide future scaling changes. The results in terms of strain are shown in Figure 53.

The first observation is that for the rhesus, tested with a "scaled" harness and using the same input as a known easily tolerable human test. The strain is a little over 0.001 which is about two orders of magnitude below the tolerable limit of 0.098. By increasing the acceleration input by a factor of six, the peak strain is 0.0075 or still less than one tenth of tolerable. However, at such high acceleration inputs, the torso is separated from the seat pan and computer results are invalid beyond that point.

For comparison, the same figure indicates the human response as predicted for the original input acceleration and one of six times greater magnitude. For the human, the original input acceleration generates a strain of only 0.0005, but the greater acceleration input creates a strain, 0.0043, in excess of the toler-able value of 0.0033. For the human at the higher input acceleration, the torso separates from the seat pan as did the rhesus torso .

The two comparisons demonstrate the difficulty of scaling. For the human, an input at or near tolerable causes whole body response that is indicative of the torso being pulled out of the seat. The rhesus "test" at a level where the torso is pulled from the seat is still well below any tolerance limit for the rhesus based upon strain.

The curves presented indicate that the human response is impulsive, and that the response occurs well after the input pulse. For the rhesus at the lower input acceleration, this appears to be true but not necessarily at the higher input. In order to make the response impulsive, the restraint strap was lengthened by a factor of ten. The response curve indicates that for an input at the higher level the peak output strain is delayed and reduced prior to torso-seat separation. Hence, for a condition where the peak response is

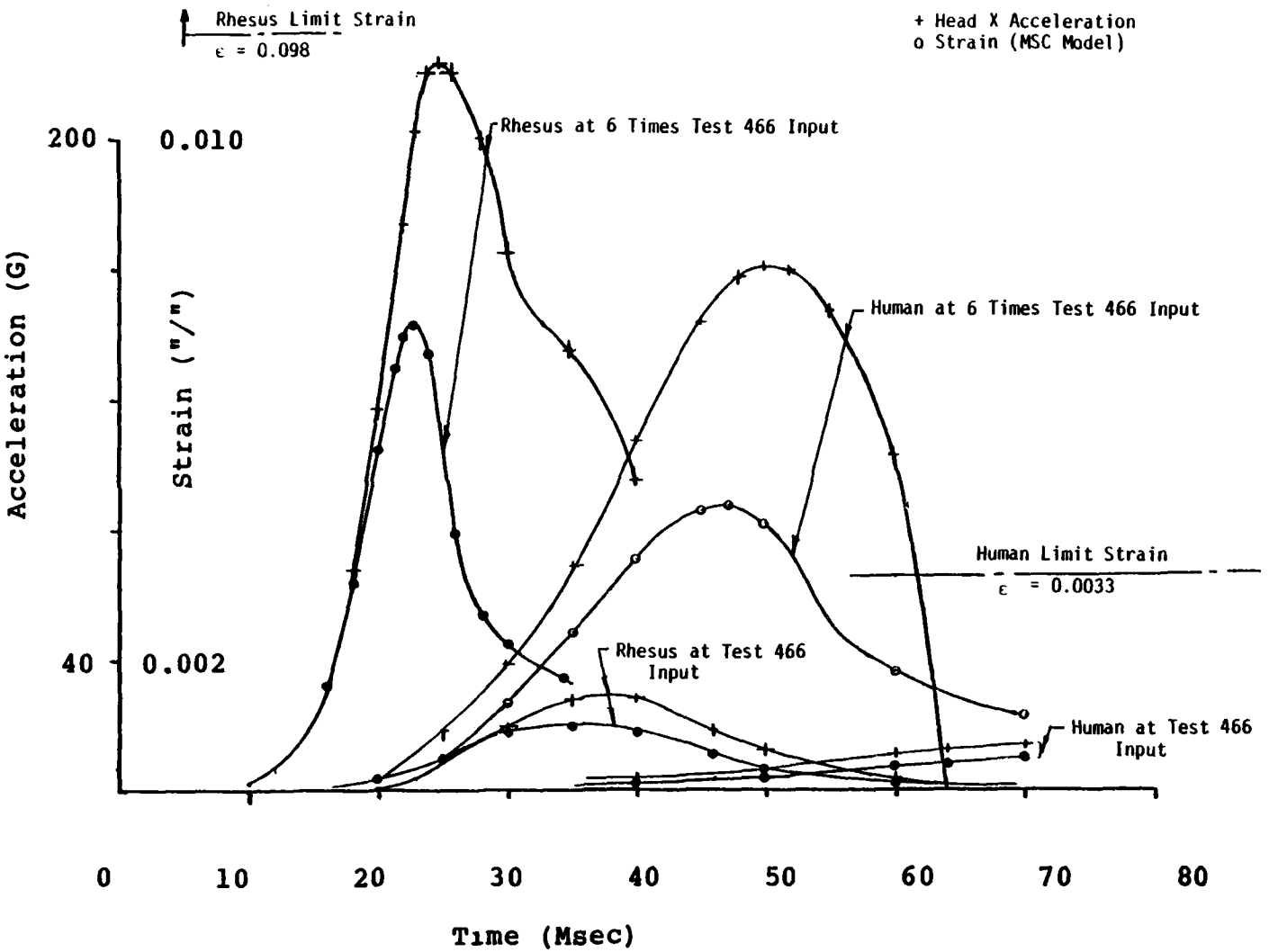

Figure 55 Human and Rhesus Predicted Response Curves.

dictated by overall response similar to the lower input human response, the strain is still one-thirtieth of tolerable as compared with one-seventh for the human.

For the high, but tolerable, input the rhesus output has strap forces of about 500 pounds generating nearly 60 psi surface pressure and head and neck joint forces of approximately 250 pounds and 70 pounds shear and axial, respectively. Although there are no injury criteria known for comparison, these values in comparison with human tolerance data seem quite high. This indicates that although the primary injury criterion has not been exceeded, other output parameters available infer that a different injury mechanism may have been critical.

From a practical viewpoint, the testing of a rhesus monkeys, even if the injury mechanism were linearly related to the human, would be exceedingly difficult. In order to insure impulsive response, the "softening" of the system by such means as the lengthening of the strap creates an unusual configuration. The model assumed has a strap of 9 feet and yet the response was still not clearly impulsive. If the acceleration were raised to reach tolerable strain, assuming linearity, the peak would have to be increased by a factor of 78 (2579G). These indicate that the test setup required to test a rhesus in a retraction environment could not be accomplished in any existing test device.

RESTRAINT SYSTEM SCALING GUIDELINES

The original intent of this segment of the research was to evolve guidelines which could be used in scaling a restraint system to the environment in order to evaluate the protective capability of the restraint. In order to accomplish this, a model was created capable of using subhuman primate data as input for both kinetic and injury prediction. The injury criterion selected was maximum strain since data were available from subhuman primate tests which related strain to injury for dynamic environments. Predictions generated by the rhesus monkey model indicate that achieving the head acceleration tolerance limit is very questionable since other injury parameters could be exceeded well before the maximum strain value has been achieved. Consequently, it appears that guidelines for the study of restraint harness and environment scaling as required for retraction studies are pointless with the current criterion. The primate will "fail" due to other factors for which there are no established limits.

However, a method can be established which will assist in future efforts. The steps are:

(1) Establish injury criteria levels for the primate for the following parameters:

(a) Head and chest translational and rotational accelerations.

(b) Head and neck shear, axial and bending moments, and

(c) Belt surface pressures.

2) Develop a harness configuration with anatomical similarity as mentioned previously. The harness material and strap sizes are dictated by strength and pressure requirements.

(3) Conduct tests using the harnessed primate in the type of environment desired to collect force, acceleration, and photographic data to isolate harness characteristics in terms of force-displacement.

(4) Establish primate geometric and inertial values necessary for the computer routine.

(5) Use impulsive input accelerations to generate response curves for each of the parameters listed under (1).

(6) Increase input amplitude to determine which parameter (s) reach tolerance limits first.

(7) Examine injury parameters first exceeded to determine frequency response characteristics. Was response indicative of impulsive response?

(8) Examine response of same injury parameters as predicted by human model for same harness configuration.

(9) Compare responses to determine compatability of kinetics. Is the response of the subhuman primate similar, impulsive, or long duration, to the kinetics of the human?

(10) If both are kinetically similar then the input used for the primate model is a valid input to be used during testing of the primate. If the computed results are not similar, then the input must be changed either to create an impulsive response, or the strap and the harness changed to achieve similarity.

(11) Once kinetic similarity has been achieved for the injury parameter selected, then harness configuration changes can be studied using a primate for the input acceleration wave form found. Significant harness configuration changes would have to be examined by returning to step (2) and re-examining changes that occur during testing of the physical system.

The method established is a combination of modeling and testing as dictated by the results of the human test result for one harness. For those tests, maximum strain was an impulsive response for both human and subhuman primate, but injury could not be achieved during tests because of the tolerance level of the primate. Therefore, in setting up a program with a primate, it is necessary to start with the primate using assumed step (1) criteria, and conduct computer studies to determine the response. Once injury for a parameter is reached by a particular impulsive acceleration input, it is then possible to study the human response and determine whether or not kinetically similar responses are applicable or realistic. For the data previously studied, the rhesus response in terms of limiting strain would have been an extreme input. The input for the human would have been unrealistic, and harness or strap changes would not have created kinetic similarity.

It is obvious from the steps evolved that injury criteria for the subhuman primate was of primary importance. If tolerable levels for selected parameters are not available, it is inappropriate to conduct any analysis or testing. It is unfortunate that the one criterion selected does not appear to be the most critical for the primate. When the other criteria are available, additional progress can be made in this area.

RESTRAINT SYSTEM SCALING ANALYSIS SUMMARY

The tools for examining scaling effects have been established. Data are available relative to physical response but not injury response. With additional injury criteria, animal studies can be undertaken to scale a harness using a scaled environment. Unfortunately, if maximum strain is indicative, the relation between dynamic similarity and injury similarity is not linear. Therefore, it may be impractical and/or impossible to scale the primate to simulate the human response.

SECTION 6

RESTRAINT SYSTEMS EVALUATION

INTRODUCTION

Evaluation is defined as a systematic approach to establishing the value of a system relative to particular criteria. A systematic approach will be established by listing and discussing the elements of this system, and the criterion is established as body retraction without injury in a minimum time.

SYSTEM ELEMENTS

The elements of the system are:

1) Pyrotechnic inertia reel
2) Restraint retraction strap
3) Restraint harness
4) Seat Belt
5) Chest Wall
6) Head and Neck
7) Torso
8) Thighs

The latter four are all characteristics of the human and are not under the control of an evaluator. For a given percentile man, the inertial characteristics of the body segments are estimated values. The coefficients of joint stiffness and damping as well or diminsional data are available. Whether or not the characteristics are truly representative of the human is a problem beyond the scope of this effort.

PYROTECHNIC INERTIA REEL

The pyrotechnic inertia reel, as the source of the retraction environment, should be well understood. Unfortunately, it is not. The steps necessary for evaluation of the reel are outlined in Section 4. What is needed, however, is a model that provides an acceptable correlation between predicted and measured performance. At the outset of this research effort it was hoped that a model having elements related to the physical hardware could be developed so that the effects of piston size, lead angle, and pyrotechnic charge could be evaluated. That stage was never reached, and hence, an inertia reel model is not available.

Tests are still required for selected stroke lengths and dead weights using belt materials that permit isolation of material

property effects. What additional measurements should be made have not been established at this time. Perhaps the future will provide an explanation of the phenomenon. In the interim, it will be necessary to use models currently available which only "model" the performance.

By using test data as presented in Section 4 it is possible to "fit" the data using selected time-temperature profiles and arbitrary "K" values for viscous or hydrodynamic drag forces. Values can be selected to provide the desired strap force and rigid body motion using the available material properties for the webbing. The analytical model is then the best possible available for system evaluation.

RESTRAINT MATERIALS

The materials to be used as restraint material should be evaluated over a range of strains and strain rates. The ranges of strain, strain rate, and stress levels to be used are:

strain: up to 0.100 inch per inch

strain rate: from static to 10 inch per inch per second

stress: up to 15000 psi

Using stress and strain normalizes the force and elongation and lets the evaluator establish his own coupon length, gage length, and belt size as applicable to his test device. The belt can be of any arbitrary length, width and thickness, theoretically, as long as the material type is established. Testing over the ranges of strain, strain rate, and stress as listed above should provide data applicable to usage by aircrew personnel in a retraction environment. Some discretion is necessary, of course, in that significant deviations in belt size from what would be thought as a "nominal" belt size would be tested to determine whether or not thickness, width, or length effects exist. However, for belts of the sizes currently used, the levels given are sufficient to include those anticipated for human retraction systems. Measurements beyond those levels will probably be near failure or at least in a non-linear range where prediction models will be difficult to evolve.

The data should be collected using strain gages and force cells having accuracies in the 3 to 5 percent of full scale range. This should not be difficult to achieve and yet is consistent with the inherent variability of the subject being tested. Results collected using greater accuracy indicate that strains vary by as much as 10 percent at a given stress for identical samples at fixed strain rates.

RESTRAINT HARNESS

The restraint harness configuration is too complex to analyze rigorously but not impossible to evaluate using test hardware available. The restraint harness acts as a series of tension elements seeking an equilibrium configuration during the initial phase of the retraction. In order to evaluate the harness it is necessary to test it using the rigid torso model first. By using the harnessed rigid torso in the BPRD it is possible to study the response of the harness on a non deforming body. The force and accelerations measured provide the kinetics to define torso motion. Photographic data provide the kinematics of the harness, or specifically the Koch fitting, as it travels up the chest. The force, measured, and displacement, observed, provide the configuration change force-displacement to be matched. The same harness is then used to test humans with the same instrumentation and photographic data collection system. The difference between harness kinetics observed with the human and that of the rigid torso is established as the effect of the thighs or whatever body segment can be realistically assumed to create the difference.

In evaluating the harness it is necssary to use discretion in stating what causes the significant differences. Since the type of harness to be used is an unknown, only the procedure can be outlined. Obviously, if the harness has a primary load path across the pelvis instead of around the thigh, this is possible to recognize from the photographic data. The test data used in this study indicated thigh compression as the primary difference between rigid and non rigid body response. This may not be applicable for other harness designs.

Chest elasticity should also be considered. The location of the chest relative to the applied force is such that the strap force is directed more along the spinal axis rather than normal to the chest. This is somewhat corroborated in that the model chest stiffness required to match the data must have a value greater than even the "dynamic" stiffness of the chest reported in the referenced biomechanics papers. It seems reasonable that the strap rotates the clavicle more than the chest. This may not be true for the next harness.

Once this process has been completed, the model representing the harnessed human can then be used in conjunction with restraint strap and inertia reel models to examine system response at higher retraction speeds and selected displacements.

SEAT BELTS

Lap belts do not significantly influence the response of the retracted human at tolerable levels according to the computer analyses accomplished during this effort. Lap belt models were not necessary

originally in that the torso motion did not "load" the lap belt. However, at large retraction velocities, the lower torso is rotated into the lap belt creating large forces. Should the system design rely upon lower torso motion, the lap belt would greatly influence the response and its effect should be evaluated.

Since the lap belt is a material being subjected to an environment similar to the shoulder straps, although at a less severe level, the procedures for determining its properties are the same as discussed for the straps. The belt does require one additional action experimentally. That is, the lap belt should also be instrumented. Existing data do not reflect lap belt loads primarily because they weren't significant. However, they may be significant for the next generation design particularly since published survivable lap belt loads at the pelvis are higher than those at the chest.

SYSTEM SYNTHESIS

The elements discussed are synthesized into the restraint system. The pyrotechnic model, restraint materials, harness, lap belt and human models, are all synthesized into the developed computer routine of Section 3. The routine was designed to accept coefficients from each of the elements. The pyrotechnic model will have interface values of strap force and strap motion, the restraint material is defined by four material properties, and its length, and cross-sectional area. The lap belt, although only a stiffness and damping coefficient currently, can easily be changed to the four element model representation. The torso harness is described by stiffness coefficients evolved from torso tests. The human model with head, neck, torso, and injury prediction capability is not altered unless a different percentile man is desired or a segment angular attitude is required.

Once the system is quantitatively defined, tests should be conducted using human test subjects on the BPRD at sub injurious levels. This will require prior testing using the rigid torso to verify systems response. A series of tests using selected retraction distances and piston pressures, as previously conducted, would be required. Assuming the test results for the rigid torso are acceptable, human tests should follow. Assuming these are also acceptable, the restraint systems model should then be exercised to study responses at more severe retraction levels.

FINAL EVALUATION

In addition to the terms contained in the definition of evaluation at the beginning of this section, another desirable aspect of evaluation is to have alternative solutions to a problem. This is true in retraction systems evaluation. Although we want to evaluate

relative to minimum retraction time at tolerable limits, the tolerable limits are relative to whomever selects them. However, given that a tolerance limit is established, one system's performance can be compared with that of another in operating within that limit regardless of whether or not the limit is correct. The baseline data have been established. Data are available for a system with a PCU-15/P harness with lap belt. Additional data can be collected and performance calculations compared with those of this particular system. A decision can be made as to which system is better in terms of how much faster the occupant can be retracted without exceeding the tolerance limit.

The steps required to evaluate a powered inertia reel and the model study that was restraint system can be enumerated.

(1) Establish the injury criterion. The model study that was accomplished during this research indicated that neck injury is the critical criteron. Whether neck shear or axial force is used is left up to the evaluator at this point. The study also showed that it is reasonable to omit the head injury maximum strain criteron (MSC).

(2) Conduct inertia reel tests to determine an analytical model that predicts strap forces and the correct belt displacements.

(3) Conduct material properties tests for the restraint straps and determine the coefficients for the four element fluid model.

(4) Conduct experiments using a rigid manikin torso to determine the harness coefficients for a rigid torso.

(5) Conduct experiments using human subjects to determine the interaction effects between harness and torso/thigh elements.

(6) Use the developed restraint systems model to calculate performance at extreme torso haulback conditions.

(7) Compare retraction performance with that of other alternate systems or variations of the same system.

(8) Select the "best" system.

The steps above represent a systematic approach to evaluate the powered inertia reel and restraint system relative to a specified criterion. The steps require testing, modeling, and more testing. Human tests are required. As the data base is increased, thigh

elasticity, chest wall effects, and other significant parameters may be incorporated into the torso model. If the human model and the synthesized protection system model can be shown to provide acceptable predictions, design changes to protection systems components can be predicted analytically and verified by minimal testing with human subjects.

SECTION 7

CONCLUSIONS AND RECOMMENDATION

The primary objective of the research was to develop a mathematical analog of the human body and restraint system such that the model could be used to analytically determine optimum material properties for given operational conditions. During the process of evolving these, experimental test hardware and test methods were to be fabricated and developed in order to be capable of establishing the validity of the models.

The pyrotechnic inertia reel was to be modelled by using data from controlled experiments conducted by a reel manufacturer. A reel was available for disassembly, inspection and measurement. It was not possible to accurately model the reel. Although the inertia reel performance can be modeled by an analytical representation of pistons, arbors, springs, mandrels[2] and belts the analog still needs arbitrary constants and assumed flow characteristics to predict performance approximately.

Belt mechanical properties were established for three standard Air Force webbing materials by assuming a viscoelastic representation. Examination of existing webbing materials test data collected at various strain rates indicated the desirability of using a four element fluid viscoelastic representation. Test hardware were designed and fabricated to conduct tests with samples at lengths, strains and strain rates, indicative of those developed during retraction. Coefficients for all three materials were found which can approximated the dynamic stress-strain cnaracteristics over the linear range of the material.

Human torso response was derived by conducting a series of experiments using a rigid torso simulator and by examining data from previous human tests. In order to eliminate torso compressibility, a rigid torso device was designed, fabricated and tested. The torso represented that of a 95th percentile aircrewman in mass, center of gravity location, mass moment of inertia in pitch, and approximate shoulder and chest contour. Tests in the BPRD were conducted using the rigid torso, tin man, in order to isolate the effects of the BPRD retraction cable and harness kinetics on a rigid torso. Instrumentation was available to provide cable force, chest accelerations, seat pan and seat back forces as functions of time. Photographic data were available to observe the motions of the harness. An analytical model of the restrained torso model was later expanded to reflect head and neck elements, a head injury model, (the maximum strain criteria level) chest elasticity and restraint elements. The coefficients were established by matching the measured accelerations, forces and displacements of head, chest and harness as applicable.

Once the model was finalized for a 50th percentile human, input variations were studied to examine predicted performance. It was found that the maximum strain criteria limit of the head injury model was not reached for BPRD input waveforms before neck force or head translational acceleration limits are reached. The peak force limit would theoretically be reached at about 1.5 times the current testing capability of the BPRD. Change of restraint webbing material properties changed peak neck and head response by about 10 percent. Additional studies of means to improve performance indicated that a crotch strap would be beneficial. The harness tested developed significant slack when the aircrewman was leaning forward. This, in conjunction with belt motion due to thigh elasticity, created considerable delay in torso retraction.

A body response analog was used with rhesus monkey data to examine the possibility of conducting scaled experiments. Although a methodology was presented as a means of studying future scaling experiments, the analytical studies conducted indicated that additional injury criteria will probably be necessary. The head injury maximum strain limit for a rhesus was so great that other mechanisms of failure will probably be reached first.

Based upon the results of the research effort, it was possible to establish an evaluation procedure to be used for future restraint systems. The evaluation requires establishment of injury criteria, testing of the system with the rigid torso, computer modeling, testing with humans, additional modeling, and then studies using the model with maximum capability inputs. The results can then be compared with other baseline data to select the best system.

CONCLUSIONS

(1) The pyrotechnic inertia reel is not a simple piston, screw thread, nut, and rotating shaft device. Measured dimensions and assumed temperature-time profiles do not generate the measured performance. There are evidently other mechanisms operating that were not isolated during the analysis conducted, a more rigorous analysis is required.

(2) Standard belt materials can be approximated over the linear range of stress-strain by a four element viscoelastic fluid model. Techniques are available to hand calculate the coefficients but use of a computer routine is necessary for complex inputs to a belt.

(3) Limited calculations indicate that the effects of material changes on the response of a retracted human are in the range of 10 percent. This is in terms of head response and maximum strain at tolerable input levels.

(4) An analytical model of a restrained human has been evolved which is capable of providing outputs for comparison with most of the injury criteria available. The model generates head, neck, chest, and torso accelerations, velocities, and displacements. Forces and moments at all joints are available; strap loads and seat pan loads are calculated. Maximum strain of the MSC model is also provided.

(5) Analysis of human response for retraction conditions similar to those produced by the BPRD indicates that the human and restraint system respond as low frequency systems driven by an impulsive input. The stiffness of the chest wall assumed is high enough that it does not enter significantly into the response. Belt material properties do not appreciably influence the response. Lap belt stiffness has little effect on torso response. The addition of a crotch strap analog has a significant effect.

(6) Rhesus monkey data were used to create an analog of a seated subhuman in a restraint harness. The model was used with BPRD input waveforms at 3 and 6 times the original magnitudes to examine theoretical response. The output, in terms of MSC strains are well below tolerance limits for a rhesus monkey. The strains are so low, in relation to the allowable, that it is even more doubtful than with the human that MSC strain is important. Without additional rhesus injury data, it is not possible to determine injurious environments, and, therefore, restraint scaling cannot proceed. A methodology was presented for future research.

(7) Restraint systems evaluation techniques have been improved through the efforts of this research. The approach taken has established a procedure (requiring a rigid torso) which can be followed to evaluate the elements of the system as well as the system as a whole. By using experimental results, incorporating them within the model, conducting more experiments, incorporating these results, and then validating with low level human test; it is possible to generate a systems model which can be used to predict human response for a particular harness. The harness elements can be changed, the input changed, elements added; the effects can be calculated for comparison with injury criteria.

RECOMMENDATIONS

(1) Additional research into pyrotechnic inertia reel performance is required. Since the reel creates the input to the harnessed human, and is itself influenced by the force generated, it is critical that the phenomenon be better understood. As a portion of a larger program only a given amount of time and effort was allocated to it. The nature of its operation evidently requires more investigation than was provided.

(2) The webbing material properties were found using test equipment

that dictated calculation of a test artifact due to grip design. Although the data did indicate that the artifact could be calculated and removed, because of the test design, the experiments should be repeated. An extensometer, optical gage or some other device capable of accurately measuring large strains at high strain rates should be used with the same test design to verify the results.

(3) Studies should be initiated to utilize the harnessed human analog. Specifically, there are data available for humans tested with a lap belt/shoulder harness restraint system. The sequence of tests conducted in Section 3 should be replicated to evaluate this system. This will add to the desired restraint systems data base while improving confidence in the predictive capability of the model.

4. Studies should be initiated to utilize a negative g strap with the harness configuration tested. The limited predictions generated for harness improvement indicate that the best way to improve retraction time with the harness, and remain tolerable, is to remove the slack in the harness when the aircrewman is leaning forward. Another concept would be to make the negative g strap also retracted and locked by an inertia reel.

(5) Additional effort will be necessary in proving or disproving the feasibility of scaling. The analytical tool is available, but tolerance criteria are not. Since the MSC model did not prove to be the indicator of injury, the means of using available primate injury data was lost. Since it appears that this is true for the human also, injury criteria such as neck shear and axial force for the primate will be necessary in the future.

6. The harnessed human analog should be exercised with the ejection environment imposed on the retraction sequence as it exists or is desired to exist. The program was written to accept accelerations vertically as well as horizontally through the seat belt attachments. This capability was never used, and hence, additional problems are awaiting solution.

REFERENCES

1. Flugge W., 1967, Viscoelasticity, Blaisdell Publishing Company.

2. Nielsen, Lawrence, E., 1965, Mechanical Properties of Polymers, Reinhold Publishing Corporation, New York.

3. Gross, Bernhard, 1952, Mathematical Structure of the Theories of Viscoelasticity, Publications De L'Institute National De Technologie, Paris.

4. Carr, Richard W. and Singley, George T., 1975 "Advanced Restraint Systems for Army Aircraft", in Aircraft Crash Worthiness, ed. Saczalski, Kenneth, Singley, George T., Pilkey, W.O., and Huston, Rl L., University Press of Virginia, Charlottesville, pp. 365-397.

5. Patrick, L.M., Mertz, H.J., Kroell, C.K. and 1967, Cadaver, Knee, Chest and Head Impact Loads, Proceedings of the Eleventh Stapp Conference.

6. Hertzberg, H.T.E., Daniels, G.S., and Churchill, E., 1950, Anthropometry of Flying Personnel--1950, WADC Technical Report 52-321, Wright Air Development Center, Wright Patterson AFB, Ohio, September 1952.

7. Kaleps, Ints., 1975 Thoracic Responses During Blunt Impact, in Aircraft Crash Worthiness, ed. Saczalski, Kenneth, Singley, George T., Pilkey, W.O., and Huston, R.L., University Press of Virginia, Charlottesville, pp. 365-397.

8. Patrick, L.M., Kroell, C.K. and Mertz, H.J., 1967, Forces on the Human Body in Simulated Crashes. Proceedings of the Ninth Stapp Conferences.

9. Phillip, N. S., Analysis and Measurement of Helmeted Aircrewman Response Resulting from Birdstrike, AMRL-TR-79-75, Aerospace Medical Research Laboratory, Wright Patterson Air Force Base, Ohio, January 1980.

10. Chong, C.H.H., and Glaub, J.E., Measurements of Pressure for the $TiH_x/KClO_4$ System, MLM-2507, Monsonto Research Corporation, Mound Facility, Miamisburg, Ohio, April 1978.

11. Kornhauser, M. and Gold, A., "Application of the Impact Sensitivity Method to Animate Structures", Impace Acceleration Stress Sympoium, Publication 977, NAS-NRC, November 1961.

12. Stalnaker, R.L. and Mc Elhaney, J.H. "Head Injury Tolerance for Linear Impacts by Mechanical Impedance Methods," ASME Paper 70-WA/BHG-4, October 1971.

13. Belytschko, T. and Privitzer, E., Refinement and Validation of a Three-Dimensional Head-Spine Model, AMRL-TR-78-7, Aerospace Medical Research Laboratory, Wright Patterson Air Force Base, August 1978.

14. Beckman, D.L., Palmer, M.F., and Roberts, V.L. "Thoracic Force-Deflection Studies in Living and Embalmed Primates, ASME Paper 70-BHF-8, May, 1970.

APPENDIX A

```
          ESTABLISH [illegible] TEMPERATURE INPUT
            CON(PS,TO,[illegible])
            CON([illegible],MU,G3,WP,ZO,ZW)
            CON(LW,AG,[illegible],F)
            CON(W2,[illegible],[illegible],P,T30)
            PAR(G1,G2,N1,N2)
            PAR(BACK)
F1        = N1/G2+N1/G1+N2/G2
P2        = (N1*N2)/(G1*G2)
D2        = (G1*N2)/G2
Q1        = N1
          CALCULATE ACCELERATION OF THE PLUNGER
T_N       = SIN(A1)/COS(A1)
2DXP      = (ONE-TW)-THETE)/MPUR
WO        = (WO*VO)/17?.
WPY       = (GLP/453.6)*(T/T30)
WPYO      = FSW(T-T30,WPY,WPY,GLP/453.6)
ONE       = (WPY/WO)*((FO*VO*TE)/(TO*(VO+(AP*XP))))*AP-FB*AP
FB        = PO*3.1*K*1DXP
PROSS     = (ONE+PB*AP)/AP
TWO       = AP1*FS*.5
THETE     = MU*AP
FOU       = (AP/3.+P2*(AP**2/3.))
1DXP      = INT(2DXP,0.)
XP        = INT(1DXP,0.)
NP1       = (COS(A1)+MU*SIN(A1))/(SIN(A1)*FO-MU*FB*COS(A1))
NP2       = NP1/(FO*TAN)
          CALCULATE BELT FORCE
2DXF      = (1./(P2*TW))*(Q1*(1DXW-1DXI)+Q2*(2DXW-2DXT))-DIFF
DIFF      = (P1*1DXF)/P2+XF/P2
1DXF      = INT(2DXF,0.)
XF        = INT(1DXF,FO/AW)
FS        = XF*AW
          CALCULATE INERTIAL MASS ACCELERATION
2DXI      = (FS-FO)/(WT/32.)
1DXI      = INT(2DXI,0.)
XI        = INT(1DXI,0.)
          CALCULATE SLEEVE MOTION
2DXS      = 2DXP/TAN
1DXS      = 1DXP/TAN
XS        = INT(1DXS,0.)
          CALCULATE WEBBING MOTION
2DXW      = 2DXS*(.3+.0273*XS)+1DXS*1DXS*.0273
1DXW      = .3*1DXS+.0273*XS*1DXS
XW        = .3*XS+.0137*XS*XS
STRAIN    = (XW-XI)/LW
          INPUT TEMPERATURE
T         = 50.*1000.*T+273.
DT        = .001
          FIN(T,.1)
          OUT(T,2DXP,1DXP,XP, , )
          OUT( ,2DXW,1DXW,XW, , )
          OUT( ,2DXI,1DXI,XI, , )
```

APPENDIX B

```
      RESPONSE OF SEATED TORSO LAP BELT SHOULDER HARNESS MOD
      CON(XLO,YLO,CS,CB,MU,IO)
      CON(THEO,X10,Y10)
NA    = CON(13.0)
NB    = CON(2.0)
      PAR(2DTHE)
      PAR(KS,KB,WT,WL,L1,L2)
      CALCULATE ACCELERATIONS
MT    = WT/386.
2DXL  = (ONE+TWO-THREE-FOUR-FIVE)/((WL+WT)/386.)
ONE   = (MT*L1*SIN(THE))*(2DTHE-MU*1DTHE*1DTHE)
TWO   = (MT*L1*COS(THE))*(1DTHE*1DTHE-MU*2DTHE)
THREE = MU*(WL+WT)
FOUR  = KS*(COS(THU)-MU*SIN(THU))
FIVE  = KB*(COS(THB)-MU*SIN(THB))
1DXL  = INT(2DXL,0.)
XL    = INT(1DXL,XLO)
2DTHE = IMP(2DTHE,TEN+AA*2DXL)
1DTHE = INT(2DTHE,0.)
THE   = INT(1DTHE,THEO)
SIX   = KS*(COS(1.5708-(THU+THE)))*L2
SEVEN = L1*COS(THE)*(WT+2.0*MT*L1*SIN(THE)*1DTHE*1DTHE)
NINE  = SIN(THU)*COS(THE)+COS(THU)*SIN(THE)
TEN   = (SIX-SEVEN+KS*L1*NINE)/(IO+MT*L1*L1)
AA    = L1*MT*SIN(THE)/(IO+MT*L1*L1)
      EVALUATE NEEDED TERMS
LT    = L1+L2
2DXO  = FUN(NA,T)
1DXO  = INT(2DXO,0.)
XO    = INT(1DXO,0.)
1DX1  = INT(2DXO,0.)
X1    = INT(1DX1,X10)
2DYO  = FUN(NB,T)
1DYO  = INT(2DYO,0.)
YO    = INT(1DYO,0.)
1DY1  = 1DYO
Y1    = INT(1DY1,Y10)
1DYL  = INT(2DYO,0.)
YL    = INT(1DYO,YLO)
LB    = SQRT(XLO*XLO+YLO*YLO)
LS    = SQRT(XTA*XTA+YTA*YTA)
XTA   = XLO+LT*COS(THEO)-X10
YTA   = Y10-(YLO+LT*SIN(THEO))
XSO   = XLO+LT*COS(THEO)
XS    = INT(1DXS,XSO)
YSO   = YLO+LT*SIN(THEO)
XTO   = XLO+L1*COS(THEO)
YTO   = YLO+L1*SIN(THEO)
FS    = KS*DELS+CS*DELSD
DELS  = SQRT((XS-X1)*(XS-X1)+(YS-Y1)*(YS-Y1))-LS
DELSD = ((XS-X1)*(1DXS-1DX1)+(YS-Y1)*(1DYS-1DY1))/(DELS+LS)
Z     = LT*SIN(THE)*2DTHE-LT*COS(THE)*1DTHE*1DTHE
2DXS  = 2DXL-Z
1DXS  = INT(2DXS,0.)
```

```
2DYS    = LS*COS(THE)*2DTHE+L2*SIN(THE)*1DTHE*1DTHE
1DYS    = INT(2DYS,0.)
YS      = INT(1DYS,YS0)
FB      = KB*DELB+CB*DELBD
DELB    = SQRT((XL-X0)*(XL-X0)+(YL-Y0)*(YL-Y0))-LB
DELBD   = ((XL-X0)*(1DXL-1DX1)+(YL-Y0)*(1DYL-1DY1))/(DELB+LB)
FTX     = (-WT/386.)*2DXT-FS*COS(THU)
2DXT    = 2DXL-L1*SIN(THE)*2DTHE-L1*COS(THE)*1DTHE*1DTHE
1DXT    = INT(2DXT,0.)
XT      = INT(1DXT,XT0)
THU     = ATN(Y1-YS,XS-X1)
2DYT    = L1*COS(THE)*2DTHE+L1*SIN(THE)*1DTHE*1DTHE
1DYT    = INT(2DYT,0.)
YT      = INT(1DYT,YT0)
FTY     = FS*SIN(THU)-WT-(WT/386.)*2DYT
THB     = ATN(YL-Y0,XL-X0)
DT      = .001
          FIN(T,.1)
          OUT(T,2DXL,1DXL,XL,FB,FS)
          OUT( ,2DTHE,1DTHE,THE,THU,THB)
          OUT( ,DELB,DELBD,DELS,DELS0, )
          PLO(T,FS,FB,XL,THE)
          PLO(T,2DXL,1DXL,2DTHE,1DTHE)
          PLO(T,2DXT,2DYT,THB)
          END
```

APPENDIX C

```
                REFRACTION DUE TO CABLE/STRAP/HARN WITH HEAD
                CON(XLO,YLO,CS,CB,MF,IO)
                CON(THEO,X10,Y10,L3)
                CON(KS,KB,WT,WL,L1,L2)
                CON(LC,AC,LST,AST,LHA,AHA)
                CON(G1,G2,N1,N2,JERK)
                CON(LN,WN,IN,LH,WH,IH)
                CON(THHO,THNO,FSO,KT,CT,WUP)
                CON(KN,CN,KH,CH)
NA          =   CFN(2.0)
NB          =   CFN(2.0)
NC          =   CFN(8.)
ND          =   CFN(2.0)
                PAR(2DTHE)
                PAR(2DTHH)
                PAR(2DTHN)
                PAR(2DXS)
                PAR(KH1,KH2,KH3)
                CALCULATE ACCELERATIONS
DTMIN       =   .0005
MN          =   WN/386.
MH          =   WH/386.
MT          =   WT/386.
MU          =   MF
2DXL        =   ((ONE+TWO-THREE-FOUR-FIVE)/((WL+WT)/386.))
ONE         =   (MF*L1*SIN(THE))*(2DTHE+MU*1DTHE*1DTHE)
TWO         =   (MF*L1*COS(THE))*(1DTHE*1DTHE-MU*2DTHE)
THREE       =   MU*(WT+WL)
FOUR        =   FS*(COS(THU)-MU SIN(THU))+MU*FNY+FNX
FIVE        =   FB*(COS(THB)+MU*SIN(TH3))
1DXL        =   INT(2DXL,0.)
XL          =   INT(1DXL,XLO)
2DTHE       =   IMP(2DTHE,TEN+AA*2DXL)
1DTHE       =   INT(2DTHE,0.)
THE         =   INT(1DTHE,THEO)
SIX         =   FS*LT*SIN(THU+THE)
SEVEN       =   L1*WT*COS(THE)
EIGHT       =   (MH+MN*.5)*LN*LT*T1+MH*LH*LT*T2-(WN+WH)*LT*COS(THE)-NE
T2          =   SIN(THH-THE)*1DTHH*1DTHH-COS(THH-THE)*2DTHH
T1          =   SIN(THN-THE)*1DTHN*1DTHN-COS(THN-THE)*2DTHN
NINE        =   -CT*(1DTHE)-KT*(THE-THEO)+MLO
TEN         =   (SIX-SEVEN+EIGHT+NINE)/(IO+MT*L1*L1)
MLO         =   WH*(LN*COS(THNO)+LH*COS(THHO))+MLO1
MLO1        =   WN*LN*0.5*COS(THNO)+WT*L1*COS(THEO)+MLO2
MLO2        =   (WH+WN)*LT*COS(THEO)-FSO*SIN(THUO+THEO)*LT
AA          =   (L1*MT+(MH+MN)*LT)*SIN(THE)/AB
AB          =   IO+MT*L1*L1+(MH+MN)*LT*LT
                EVALUATE NEEDED TERMS
LT          =   L1+L2
2DXO        =   FUN(NA,T)
1DXO        =   INT(2DXO,0.)
XO          =   INT(1DXO,0.)
3DX1        =   DER(T,2DX1,-JERK)
2DX1        =   FUN(NC,T)
```

```
1DX1    = INT(2DX1,0.)
X1      = INT(1DX1,X10)
2DY0    = FUN(NB,T)
1DY0    = INT(2DY0,0.)
Y0      = INT(1DY0,0.)
2DY1    = FUN(ND,T)
1DY1    = INT(2DY1,0.0)
Y1      = INT(1DY1,Y10)
1DYL    = INT(2DY0,0.)
YL      = INT(1DY0,YL0)
LB      = SQRT(XL0*XL0+YL0*YL0)
XS0     = XL0+LT*COS(THE0)
YS0     = YL0+LT*SIN(THE0)
XT0     = XL0+L1*COS(THE0)
YT0     = YL0+L1*SIN(THE0)
3DFS    = ((A1*(1DXS-1DX1)+B1*(2DXS-2DX1)+C1*(3DXS-3DX1))/G3)-NX
NX      = (D1*FS+E1*1DFS+F1*2DFS)/G3
2DFS    = INT(3DFS,0.)
1DFS    = INT(2DFS,0.)
FS      = INT(1DFS,FS0)
XH1     = FS/KH1
XH2     = 1.0+(FS-50.)/KH2
XH3     = 2.5+(FS-175.)/KH3
XHC0    = FSW(XH1-1.040,TRUE,TRUE,FALSE)
KHA     = LSW(XHC0,KH1,KHB)
XHCA    = FSW(XH2-2.6,TRUE,TRUE,FALSE)
KHB     = LSW(XHCA,KH2,KH3)
XHA     = FSW(XH3-2.6,XH2,XH2,XH3)
A1      = Q0C*Q1ST*Q0H
B1      = Q0H*Q0C*Q2ST+Q0H*Q1C*Q1ST
C1      = Q0H*Q1C*Q2ST
D1      = LST*Q0H*Q0C/AST
E1      = Q1ST*(Q0H*(LC/AC)+Q0C*(LHA/AHA))+E2
E2      = Q0H*(LST/AST)*((P1ST*Q0C)+Q1C)
F1      = Q0H*Q2ST*(LC/AC)+Q0H*(LST/AST)*(Q0C*P2ST+Q1C*P1ST)+F2
F2      = (LHA/AHA)*(Q0C*Q2ST+Q1C*Q1ST)
G3      = Q1C*(Q0H*P2ST*(LST/AST)+Q2ST*LHA/AHA)
Q0C     = KS*LC/AC
Q1C     = CS*LC/AC
Q1ST    = N1
Q2ST    = N1*N2/G2
P1ST    = N1/G2+N1/G1+N2/G2
P2ST    = (N1*N2)/(G1*G2)
Q0H     = KHA*LHA/AHA
Z       = LT*SIN(THE)*2DTHE+LT*COS(THE)*1DTHE*1DTHE
2DXS    = IMP(2DXS,2DXL-Z)
1DXS    = INT(2DXS,0.)
XS      = INT(1DXS,XS0)
3DXS    = DER(T,2DXS,0.)
2DYS    = LT*COS(THE)*2DTHE-LT*SIN(THE)*1DTHE*1DTHE
1DYS    = INT(2DYS,0.)
YS      = INT(1DYS,YS0)
          CALCULATE THE EFFECT OF THE HEAD AND NECK
2DTHH   = IMP(2DTHH,2DTHA)
```

```
2DTHA  = (1./(IH+1.*MH*LH*LH))*(HA+HB+HC+HD+HE)
HA     = -(CH*(1DTHH-1DTHN)+KH*((THH-THH)-(THN-THNO)))+MHO
MHO    = WH*LH*COS(THHO)
HB     = -MH*LH*LN*COS(THH-THN)*2DTHN
HC     = -MH*LH*LN*SIN(THH-THN)*1DTHN*1DTHN
HD     = -WH*LH*COS(THH)
HE     = LH*MH*(2DXS*SIN(THH)-2DYS*COS(THH))
1DTHH  = INT(2DTHH,0.)
THH    = INT(1DTHH,THHO)
2DTHN  = IMP(2DTHN,2DTHB)
2DTHB  = (1./(IN+MH*LN*LN+MN*LN*LN*.25))*NS
NS     = NE+NF+NG+NH+NI+NJ
NE     = -(CN*(1DTHN-1DTHE)+KN*((THN-THNO)-(THE-THEO)))+MNO
MNO    = (MH*LN+WN*LN*.5)*COS(THNO)+MNO1
MNO1   = WH*LH*COS(THHO)
NF     = -HA
NG     = -MH*LH*LN*COS(THH-THN)*2DTHH
NH     = MH*LH*LN*SIN(THH-THN)*1DTHH*1DTHH
NI     = -(MN*LN*.5+WH*LN)*COS(THN)
NJ     = (MH*LN+MN*LN*.5)*(2DXS*SIN(THN)-2DYS*COS(THN))
1DTHN  = INT(2DTHN,0.)
THN    = INT(1DTHN,THNO)
2DXNU  = 2DXS-LN*SIN(THN)*2DTHN-LN*COS(THN)*1DTHN*1DTHN
2DYNU  = 2DYS+LN*COS(THN)*2DTHN-LN*SIN(THN)*1DTHN*1DTHN
FHX    = MH*(2DXNU-LH*1DTHH*1DTHH*COS(THH))-FHX1
FHX1   = LH*2DTHH*SIN(THH)*MH
FHY    = WH+MH*(2DYNU-LH*1DTHH*1DTHH*SIN(THH))+FHY1
FHY1   = MH*LH*2DTHH*COS(THH)
2DXN   = 2DXS-LN*2DTHN*SIN(THN)*.5-LN*1DTHN*1DTHN*COS(THN)*.5
2DYN   = 2DYS+LN*2DTHN*COS(THN)*.5-LN*1DTHN*1DTHN*SIN(THN)*.5
FNX    = FHX+MN*2DXN
FNY    = FHY+MN*2DYN+WN
FB     = KB*DELB+CB*DELBD
DELB   = SQRT((XL-XO)*(XL-XO)+(YL-YO)*(YL-YO))-LB
DELBD  = ((XL-XO)*(1DXL-1DXO)+(YL-YO)*(1DYL-1DYO))/(DELB+LB)
FTX    = (WT/386.)*2DXT+FS*COS(THU)+FNX
FTXS   = MT*2DXTS+FS*COS(THU)+FNX
2DXTS  = -L1*SIN(THE)*2DTHE-L1*COS(THE)*1DTHE*1DTHE
2DXT   = 2DXL-L1*SIN(THE)*2DTHE-L1*COS(THE)*1DTHE*1DTHE
1DXT   = INT(2DXT,0.)
XT     = INT(1DXT,XTO)
THJ    = ATN(Y1-YS,XS-X1)
THUO   = ATN(Y10-YSO,XSO-X10)
2DYT   = L1*COS(THE)*2DTHE-L1*SIN(THE)*1DTHE*1DTHE
1DYT   = INT(2DYT,0.)
YT     = INT(1DYT,YTO)
FTY    = -FS*SIN(THU)+WT+(WT/386.)*2DYT+FNY
THB    = ATN(YL-YO,XL-XO)
NORM   = FB*SIN(THB)+WL+FTY+WUP
         CALCULATE ACCELEROMETER OUTPUT
2DXA   = 2DXT+L3*COS(THE)*2DTHE-L3*SIN(THE)*1DTHE*1DTHE
2DYA   = 2DYT+L3*SIN(THE)*2DTHE+L3*COS(THE)*1DTHE*1DTHE
2DXAC  = 2DXA*SIN(THE)-2DYA*COS(THE)
2DYAC  = -2DXA*COS(THE)-2DYA*SIN(THE)
```

```
DT      = .001
          FIN(T,0.08)
          OUT(T,2DXL,1DXL,XL,FB,FS)
          OUT(NORM,XHA,2DFS,1DFS,NEXT,X1)
          OUT( ,2DXA,2DYA,2DXAC,2DYAC,XH1)
          OUT(X1A,YL,DELB,DELBD,FNX,FNY)
          OUT(FHX,FHY,THN,THH,THE)
          OUT(XSO,YSO,FTX,FTY,TEN,MLO)
          OUT(2DTHA,2DTHN)
          PLO(T,FS,FB,XL,THE)
          PLO(T,2DXL,1DXL,2DTHE,1DTHE)
          PLO(T,2DXT,2DYT,THB,NORM)
          PLO(T,2DXA,2DYA,2DXAC,2DYAC)
          END
```

APPENDIX D

```
      RETRACTION DUE TO CABLE/STRAP/HARN WITH HEAD (RHESUS)
      CON(XLO,YLO,CS,CB,MF,IO)
      CON(THEO,X10,Y1C,L3,L4)
      CON(KS,KB,WT,WL,L1,L2)
      CON(LC,AC,LST,AST,LHA,AHA)
      CON(G1,G2,N1,N2,JERK)
      CON(LN,WN,IN,LH,WH,IH)
      CON(THHO,THNO,FSO,KT,CT,WLP)
      CON(KN,CN,KH,CH)
      CON(MFR,C2R,KBR,LREF)
      CON(WCW,CCW,KCW1,KCW2)
NA    = CON(2.0)
NB    = CON(2.0)
NC    = CON(8.)
ND    = CON(2.0)
      PAR(2DTHE)
      PAR(2DTHH)
      PAR(2DTHN)
      PAR(2DXS)
      PAR(KH1,KH2,KH3)
      CALCULATE ACCELERATIONS
DTMIN = .0005
MN    = WN/386.
MH    = WH/386.
MT    = WT/386.
MCW   = WCW/386.
MU    = MF
2DXL  = ((ONE+TWO-THREE-FOUR-FIVE)/((WL+WT)/386.))
ONE   = (MT*L1*SIN(THE))*(2DTHE+MU*1DTHE*1DTHE)
TWO   = (MT*L1*COS(THE))*(1DTHE*1DTHE-MU*2DTHE)
THREE = MU*(WT+WL)
FOUR  = FS*(COS(THU)-MU*SIN(THU))+MU*FNY+FNX
FIVE  = FB*(COS(THB)+MU*SIN(THB))
1DXL  = INT(2DXL,0.)
XL    = INT(1DXL,XLO)
2DTHE = IMP(2DTHE,TEN+AA*2DXL)
1DTHE = INT(2DTHE,0.)
THE   = INT(1DTHE,THEO)
SIX   = FS*LT*SIN(THU+THE)
SEVEN = L1*MT*COS(THE)
EIGHT = (MH+MN*.5)*LN*LT*T1+MH*LH*LT*T2-(WN+WH)*LT*COS(THE)-NE
T2    = SIN(THH-THE)*1DTHH*1DTHH-COS(THH-THE)*2DTHH
T1    = SIN(THN-THE)*1DTHN*1DTHN-COS(THN-THE)*2DTHN
NINE  = -CT*(1DTHE)-KT*(THE-THEO)+MLO
TEN   = (SIX-SEVEN+EIGHT+NINE)/(IO+MT*L1*L1)
MLO   = WH*(LN*COS(THNO)+LH*COS(THHO))+MLO1
MLO1  = WN*LN*0.5*COS(THNO)+WT*L1*COS(THEO)+MLO2
MLO2  = (WH+WN)*LT*COS(THEO)-FSO*SIN(THUO+THEO)*LT
AA    = (L1*MT+(MH+MN)*LT)*SIN(THE)/AB
AB    = IO+MT*L1*L1+(MH+MN)*LT*LT
      EVALUATE NEEDED TERMS
LT    = L1+L2
2DXO  = FUN(NA,T)
1DXO  = INT(2DXO,0.)
```

```
XO      = INT(1DXO,C.)
3DX1    = DER(T,2DX1,-JERK)
2DX1    = FUN(NC,T)
1DX1    = INT(2DX1,0.)
X1      = INT(1DX1,X10)
2DYO    = FUN(NE,T)
1DYO    = INT(2DYO,C.)
YO      = INT(1DYO,0.)
2DY1    = FUN(NC,T)
1DY1    = INT(2DY1,0.3)
Y1      = INT(1DY1,Y1O)
1DYL    = INT(2DYO,C.)
YL      = INT(1DYO,YLO)
LH      = SQRT(XLO*XLO+YLO*YLO)
XSO     = XLO+LT*COS(THEO)
YSO     = YLO+LT*SIN(THEO)
XTO     = XLO+L1*COS(THEO)
YTO     = YLO+L1*SIN(THEO)
3DFS    = ((A1*(1DXCW-1DX1)+B1*(2DXCW-2DX1))/(G3))+NX1
NX1     = ((C1*(3DXCW-3DX1))/(G3))-NX
NX      = (D1*FS+E1*1DFS+F1*2DFS)/G3
2DFS    = INT(3DFS,0.)
1DFS    = INT(2DFS,0.)
FS      = INT(1DFS,FSO)
XH1     = FS/KH1
XH2     = 0.52+(FS-50.)/KH2
XH3     = 1.3+(FS-175.)/KH3
XHCO    = FSW(XH1-0.520,TRUE,TRUE,FALSE)
KHA     = LSW(XHCO,KH1,KH3)
XHCA    = FSW(XH2-1.3,TRUE,TRUE,FALSE)
KHA     = LSW(XHCA,KH2,KH3)
XHA     = FSW(XH3-1.3,XH2,XH2,XH3)
A1      = QOC*Q1ST*QOH
B1      = QOH*QOC*Q2ST+QOH*Q1C*Q1ST
C1      = QOH*Q1C*Q2ST
D1      = LST*QOH*QOC/AST
E1      = Q1ST*(QOH*(LC/AC)+QOC*(LHA/AHA))+E2
E2      = QOH*(LST/AST)*((P1ST*QOC)+Q1C)
F1      = QOH*Q2ST*(LC/AC)+QOH*(LST/AST)*(QOC*P2ST+Q1C*P1ST)+F2
F2      = (LHA/AHA)*(QOC*Q2ST+Q1C*Q1ST)
G3      = Q1C*(QOH*P2ST*(LST/AST)+Q2ST*LHA/AHA)
QOC     = KS*LC/AC
Q1C     = CS*LC/AC
Q1ST    = N1
Q2ST    = N1*N2/G2
P1ST    = N1/G2+N1/G1+N2/G2
P2ST    = (N1*N2)/(G1*G2)
QOH     = KHA*LHA/AHA
Z       = LT*SIN(THE)*2DTHE+LT*COS(THE)*1DTHE*1DTHE
2DXS    = IMP(2DXS,2DXL-Z)
1DXS    = INT(2DXS,0.)
XS      = INT(1DXS,XSO)
3DXS    = DER(T,2DXS,0.)
2DYS    = LT*COS(THE)*2DTHE-LT*SIN(THE)*1DTHE*1DTHE
```

```
1DYS    = INT(2DYS,0.)
YS      = INT(1DYS,YSO)
          CALCULATE THE EFFECTSOF THE CHEST WALL
2DXCW   = ((-FS*SIN(THE+THU)-KCW1*(XCW-XT))/(MCW))+NY1
NY1     = ((-KCW2*(XCW-XT)*(XCW-YT)-CCW*(1DXCW-1DXT))/(MCW))
1DXCW   = INT(2DXCW,0.)
XCW     = INT(1DXCW,XTO)
2DXCW   = DER(T,2DXCW,0.)
          CALCULATE THE EFFECT OF THE HEAD AND NECK
2DTHH   = IMP(2DTHH,2DTHA)
2DTHA   = (1./(IH+1.*MH*LH*LH))*(HA+HB+HC+HD+HE)
HA      = -(CH*(1DTHH-1DTHN)+KH*((THH-THHO)-(THN-THNO)))+MHO
MHO     = WH*LH*COS(THHO)
HB      = -MH*LH*LN*COS(THH-THN)*2DTHN
HC      = -MH*LH*LN*SIN(THH-THN)*1DTHN*1DTHN
HD      = -WH*LH*COS(THH)
HE      = LH*MH*(2DXS*SIN(THH)-2DYS*COS(THH))
1DTHH   = INT(2DTHH,0.)
THH     = INT(1DTHH,THHO)
2DTHN   = IMP(2DTHN,2DTHB)
2DTHB   = (1./(IN+MH*LN*LN+MN*LN*LN*.25))*NS
NS      = NE+NF+NG+NH+NI+NJ
NE      = -(CN*(1DTHN-1DTHE)+KN*((THN-THNO)-(THE-THEO)))+MNO
MNO     = (WH*LN+WN*LN*.5)*COS(THNO)+MNC1
MNO1    = WH*LH*COS(THHO)
NF      = -HA
NG      = -MH*LH*LN*COS(THH-THN)*2DTHH
NH      = MH*LH*LN*SIN(THH-THN)*1DTHH*1DTHH
NI      = -(WN*LN*.5+WH*LN)*COS(THN)
NJ      = (MH*LN+MN*LN*.5)*(2DXS*SIN(THN)-2DYS*COS(THN))
1DTHN   = INT(2DTHN,0.)
THN     = INT(1DTHN,THNO)
2DXNU   = 2DXS-LN*SIN(THN)*2DTHN-LN*COS(THN)*1DTHN*1DTHN
2DYNU   = 2DYS+LN*COS(THN)*2DTHN-LN*SIN(THN)*1DTHN*1DTHN
2DYH    = 2DYNU+LH*2DTHH*COS(THH)-LH*1DTHH*1DTHH*SIN(THH)
2DXH    = 2DXNU-LH*2DTHH*SIN(THH)-LH*COS(THH)*1DTHH*1DTHH
2DXBI   = 2DXH*COS(THH-THHO)+2DYH*SIN(THH-THHO)
1DXBI   = INT(2DXBI,0.)
XBI     = INT(1DXBI,0.)
2DXB    = (1./MBR)*(-CBR*(1DXB-1DXBI)-KBR*(XB-XBI))
1DXB    = INT(2DXB,0.)
XB      = INT(1DXB,0.)
STR     = (XB-XBI)/LREF
FHX     = MH*(2DXNU-LH*1DTHH*1DTHH*COS(THH))-FHX1
FHX1    = LH*2DTHH*SIN(THH)*MH
FHY     = WH+MH*(2DYNU-LH*1DTHH*1DTHH*SIN(THH))+FHY1
FHY1    = MH*LH*2DTHH*COS(THH)
2DXN    = 2DXS-LN*2DTHN*SIN(THN)*.5-LN*1DTHN*1DTHN*COS(THN)*.5
2DYN    = 2DYS+LN*2DTHN*COS(THN)*.5-LN*1DTHN*1DTHN*SIN(THN)*.5
FNX     = FHX+MN*2DXN
FNY     = FHY+MN*2DYN+WN
FB      = KB*DELB+CB*DELBD
DELB    = SQRT((XL-XO)*(XL-XO)+(YL-YC)*(YL-YO))-LB
DELBD   = ((XL-XO)*(1DXL-1DXO)+(YL-YO)*(1DYL-1DYO))/(DELB+LB)
```

```
FTX     = (WT/386.)*2DXT+FS*COS(THU)+FNX
FTXS    = WT*2DXTS+FS*COS(THU)+FNX
2DXTS   = -L1*SIN(THE)*2DTHE-L1*COS(THE)*1DTHE*1DTHE
2DXT    = 2DXL-L1*SIN(THE)*2DTHE-L1*COS(THE)*1DTHE*1DTHE
2DXC    = 2DXL-L4*SIN(THE)*2DTHE-L4*COS(THE)*1DTHE*1DTHE
1DXT    = INT(2DXT,0.)
XT      = INT(1DXT,XTO)
THU     = ATN(Y1-YS,XS-X1)
THUO    = ATN(Y1O-YSO,XSO-X1O)
2DYT    = L1*COS(THE)*2DTHE-L1*SIN(THE)*1DTHE*1DTHE
2DYC    = L4*COS(THE)*2DTHE-L4*SIN(THE)*1DTHE*1DTHE
1DYT    = INT(2DYT,0.)
YT      = INT(1DYT,YTO)
FTY     = -FS*SIN(THU)+WT+(WT/386.)*2DYT+FNY
THB     = ATN(YL-YO,XL-XO)
NORM    = FB*SIN(THB)+WL+FTY+WUP
          CALCULATE ACCELEROMETER OUTPUT
2DXA    = 2DXC+L3*COS(THE)*2DTHE-L3*SIN(THE)*1DTHE*1DTHE
2DYA    = 2DYC+L3*SIN(THE)*2DTHE+L3*COS(THE)*1DTHE*1DTHE
2DXAC   = 2DXA*SIN(THE)-2DYA*COS(THE)
2DYAC   = -2DXA*COS(THE)-2DYA*SIN(THE)
DT      = .001
          FIN(T,0.08)
          OUT(T,2DXL,1DXL,XL,FB,FS)
          OUT(NORM,XHA,2DFS,1DFS,NEXT,X1)
          OUT( ,2DXA,2DYA,2DXAC,2DYAC,XH1)
          OUT(X1A,YL,DELB,DELBD,FNX,FNY)
          OUT(FHX,FHY,THN,THH,THE,STR)
          OUT(XSO,YSO,FTX,FTY,TEN,MLO)
          OUT(2DTHA,2DTHN,2DXH,2DYH,XCW,XT)
          PLO(T,FS,FB,XL,THE)
          PLO(T,2DXL,1DXL,2DTHE,1DTHE)
          PLO(T,2DXT,2DYT,THB,NORM)
          PLO(T,2DXA,2DYA,2DXAC,2DYAC)
          END
```


☆U.S. GOVERNMENT PRINTING OFFICE: 1983—659-005/2030


4-
DT